Controlling the Self-Assembly of Synthetic Metal-Coordinating Coiled-Coil Peptides

by

Kimberly A. Scheib

B.S. Biochemistry & Biology, University of Pittsburgh at Johnstown, 2016

Submitted to the Graduate Faculty of the

Dietrich School of Arts and Sciences in partial fulfillment

of the requirements for the degree of

Master of Science

University of Pittsburgh

2019

UNIVERSITY OF PITTSBURGH

DIETRICH SCHOOL OF ARTS AND SCIENCES

This thesis was presented

by

Kimberly A. Scheib

It was defended on

April 8, 2019

and approved by

Lillian T. Chong, Associate Professor, Department of Chemistry

Stephen G. Weber, Professor, Department of Chemistry

Thesis Advisor: W. Seth Horne, Associate Professor, Department of Chemistry

Controlling the Self-Assembly of Synthetic Metal-Coordinating Coiled-Coil Peptides

Kimberly A. Scheib, M.S.

University of Pittsburgh, 2019

A distinct gap between the fields of peptide-based supramolecular assemblies and metal-organic frameworks (MOFs) exists. Despite recent efforts to explore this area of materials, many metal-directed peptide-based assemblies remain unpredictable, necessitating deeper study to establish robust design principles with which functional materials may be built. The profound unpredictability is not surprising, since peptide-based building blocks are more complex than others which have achieved success in organic and inorganic materials chemistry. The present study attempts to expand and solidify basic design rules for self-assembling metal-directed peptide-based architectures by first exerting control over the assembly of a serendipitously discovered supramolecular lattice. Recent published work has shown coiled-coil peptides containing one or more unnatural solvent-exposed terpyridine (Tpy) side chains can self-assemble to form supramolecular networks in the presence of copper (II) ion. Unexpected was the involvement of glutamic acid (Glu) side chains in the coordination motif (Tpy-Cu^{2+}-Glu). Here, we seek to exert better control over these materials through systematic placement of both Tpy and Glu residues. Results are presented for six designed sequences, including one that manifests a hexagonal net rare in the materials literature. Collectively, these results demonstrate the power of harnessing peptide folding and metal coordination as driving forces for the formation of predictable supramolecular architectures.

Table of Contents

List of Tables

List of Figures

List of Schemes

1.0 Introduction

1.1 Protein-Based Materials

Proteins by nature are complex molecules built from simple building blocks. Beyond their central role as functional agents enabling life, protein-based bulk materials found widespread use in the forms of fabrics derived from animals (wool) or insects (silk). These natural materials are robust yet biodegradable and find application in countless industries; however, harvesting materials from living organisms is sometimes regarded as inefficient and/or ethically questionable, resulting in a demand for cheap synthetic alternatives. While analogous synthetic materials are achievable from organic polymers, synthetic protein-based materials remain in the spotlight since they are amenable to modification, biodegradable, and in some cases, very close mimics of harvested materials.

Protein-based materials can go farther than synthetic bulk fabrics and have been expanded to nanomaterials with a variety of functions. For example, protein-based nanomaterials are small enough to physically disrupt the membranes of pathogens, giving them antimicrobial activity.[1] Likewise, protein nanomaterials can have different electronic and optical properties compared to their bulk counterparts, which allows them to detect molecules and even single atoms with high sensitivity and specificity, making them useful for chemical sensing and separation.[2] Lastly, protein-based materials can be utilized to deliver drugs to the cytoplasm, since they can be biologically active and trigger natural processes.[3] All of the applications of protein-based nanomaterials mentioned above are made possible thanks to the ability of these materials to be

tuned at the nanoscale. That is, small changes in molecular makeup can be implemented to cause a dramatic change in the structure and function of the material.

Formation of protein-based nanomaterials is driven by the intrinsic ability of proteins to fold into secondary structures (i.e. α-helices and β-strands) which self-associate through defined noncovalent interactions to form quaternary assemblies (i.e. β-sheets and coiled coils). Assembly driven by β-sheet stacking in nature yields β-amyloid fibers which are known to play a significant role in neurodegenerative diseases.[4-8] Extensive study of amyloid structures has elucidated specific motifs which favor assembly, inspiring materials chemists to engineer amyloids for a variety of functions including CO_2 capture,[9] nanocoatings, scaffolds, sensors, adhesives, and others comprehensively reviewed by Knowles.[10-11]

Supramolecular assemblies based on a helical secondary structure are found in nature as well. Tropomyosin is an α-helical coiled coil protein found within a groove along the surface of actin filaments and is an integral part of muscle contraction and other cellular processes, such that it occurs as a large number of isoforms.[12-13] The α-helix is a well characterized secondary structure and α-helical coiled coils can be engineered with specific function in mind thanks to the well precedented design rules which have accumulated over the last few decades.[4, 14-17] Thus, coiled coils are of specific interest to materials chemists looking to use proteinaceous building blocks and will be further discussed in Section 1.3.

In contrast to assemblies formed through association of monomers that contain a single type of secondary structure, many functional supramolecular protein complexes in nature are formed through the defined assembly of more complex tertiary folds. Such protein complexes are involved in the electron transport chain, DNA transcription, homeostasis, and other biological processes,[18] and have inspired chemists to engineer and refunctionalize natural proteins with

discrete assembly modes via head-to-head, head-to-tail, or sticky end interactions which spontaneously self-assemble (Figure 1).[4, 7, 19-21]

Figure 1. Discrete Protein Assembly Modes
Proteins can be engineered to spontaneously assemble into fibers via (A) head-to-head and tail-to-tail, (B) head-to-tail, or (C) sticky end interctions.

1.2 Metalloprotein-Based Materials

A plethora of naturally occurring proteins contain one or more metal coordinating sites on their surfaces or sequestered in cavities. These coordination sites have been found to have specific functions, including the facilitation of folding and catalysis. Understanding and harnessing the power of metalloproteins is an important step on the path to developing *de novo* enzymes, which promises to revolutionize synthetic and medicinal chemistry.[22]

Inspired by the self-assembly of metal-organic frameworks (MOFs), Tezcan and co-workers sought to develop protein-metal supramolecular assemblies by designing coordination sites on the surfaces of non-metal coordinating proteins via specific mutations.[23] Histidine (His)

and cysteine (Cys) are canonical metal-coordinating residues often found in zinc finger motifs.[24] They designed MBPC-1, a metal-coordinating variant of cytochrome *cb*$_{562}$ (Figure 2).

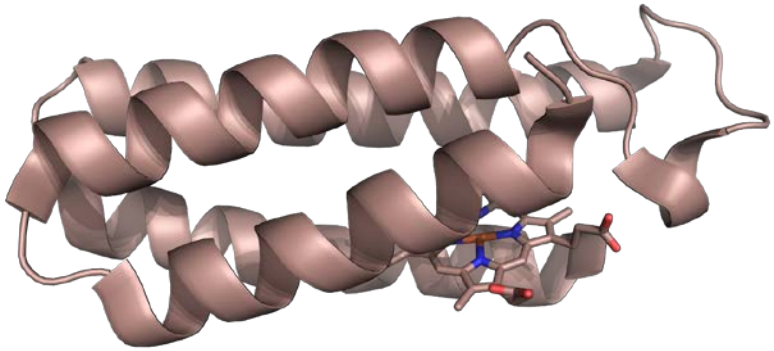

Figure 2. Structure of Parent Cytochrome *cb*$_{562}$
Tezcan, *et al*. incorporated a cytochrome *c*-type heme linkage into *E. coli* cytochrome *b*$_{562}$ resulting in cytochrome *cb*$_{562}$, which was used as the parent structure for MBPC-1. PDB ID: 2BC5[27]

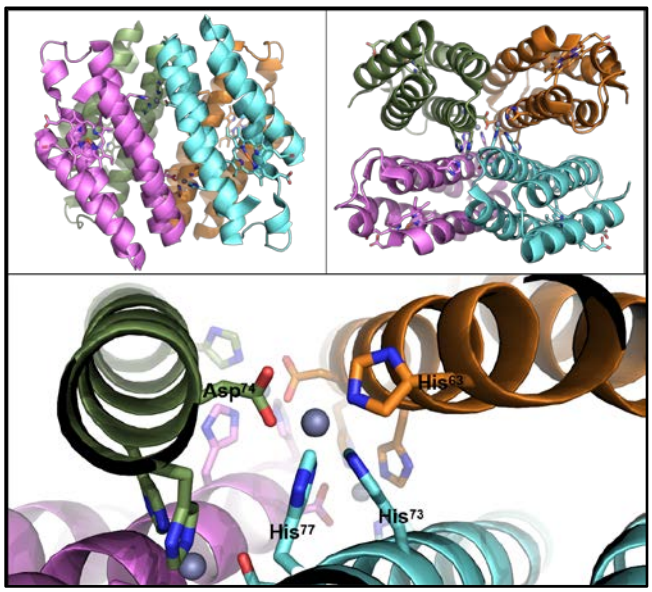

Figure 3. MBPC-1 Coordinating Zinc (II) Ion
Side view (top left) and top view (top right) of a single asymmetric unit which contains four unique chains that are associated through metal coordination of Zn^{2+} (bottom) and protein-protein interactions (PPIs) (not shown). PDB ID: 2QLA[25]

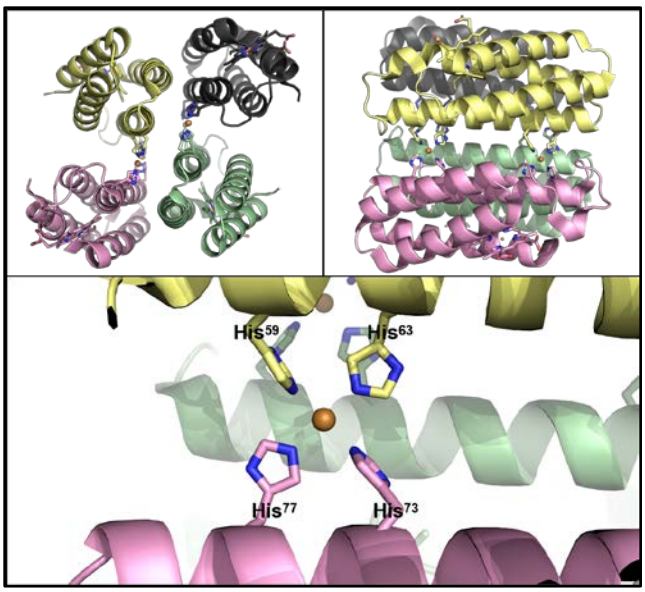

Figure 4. MBPC-1 Coordinating Copper (II) Ion
Top view (top left) and side view (top right) of a single asymmetric unit that contains four chains associated through His coordination of Cu^{2+} (bottom) and PPIs (not shown). PDB ID: 3DE8[26]

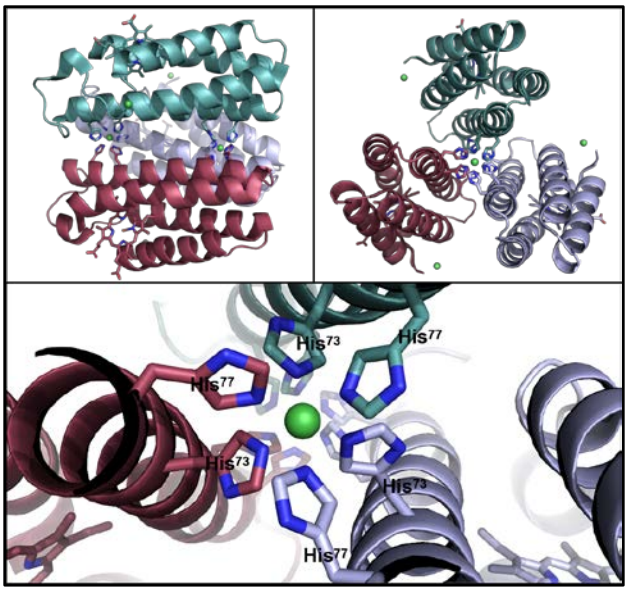

Figure 5. MBPC-1 Coordinating Nickel (II) Ion
Side view (top left) and top view (top right) of three asymmetric units which coordinate Ni^{2+} ions via three-fold symmetry (bottom). Protein-protein interactions not pictured. PDB ID: 3DE9[26]

MBPC-1 formed a supramolecular assembly involving zinc (Figure 3),[25] copper (Figure 4),[26] and nickel[26] (Figure 5) each with its own respective metal-driven assembly mode which did not form in the absence of coordinating metal.

Though the assemblies were proven to be metal-driven, an extensive network of protein-protein interaction (PPI) was found between the interfaces of the protein monomers,[25] prompting further investigation into the significance of PPI-driven assembly. They engineered MBPC-2, which displayed the primary metal-coordinating motif closer to the N-terminus of the helix compared to its predecessor. The supramolecular assembly formed by MBPC-2 in the presence of zinc involved a tetrahedral coordination of four His residues,[28] differing from that of MBPC-1, which coordinated zinc with three His residues and one aspartic acid (Asp) residue (Figure 3).[25] In all MBPC assemblies, arginine (Arg)-Asp salt bridges constituted the majority of the PPI (Figure 6). Upon removing these salt bridges, the previously established assemblies of both MBPC-1 and MBPC-2 became less favored. Thus, they concluded that the Arg-Asp salt bridges, and more generally PPI, play a significant role in the formation of their supramolecular assemblies.[28]

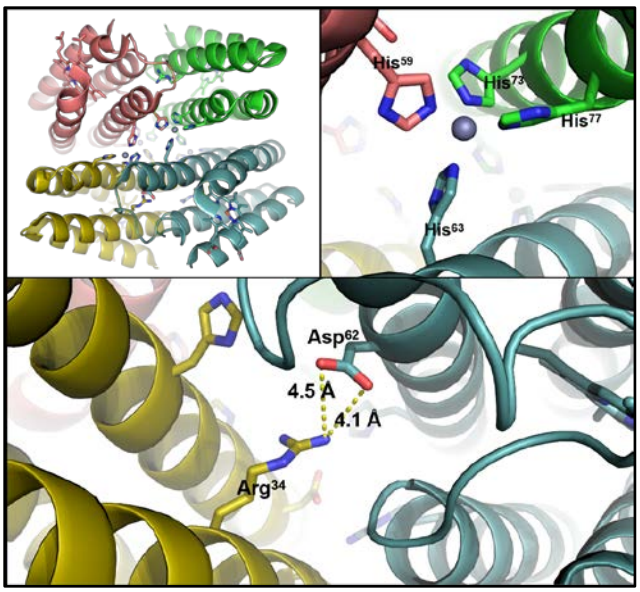

Figure 6. MBPC-2 Coordinating Zinc (II) Ion
Top view of a single asymmetric unit (top left) formed by four unique chains which are associated via His-Zn^{2+} coordination (top right) and salt bridges (bottom). PDB ID: 3C62[28]

Following the successful implementation of "metal-directed protein self-assembly (MDPSA)"[23] using canonical coordinating motifs, Tezcan, *et al*. continued their investigation by switching to non-canonical coordinating residues. They incorporated phenanthroline (phen) on the surface of cyt cb_{562} (dubbed MBP-Phen1$_3$) and examined the resulting supramolecular assembly with nickel (Figure 7). Interestingly, the coordination of the nickel (II) ion was unsaturated, since it was sequestered in a hydrophobic pocket that allowed for interaction with only one His residue and one phen residue.[29] This result is significant since rationally designing an unsaturated metalloprotein is likely a crucial step on the path to creating a catalytically functional synthetic enzyme.

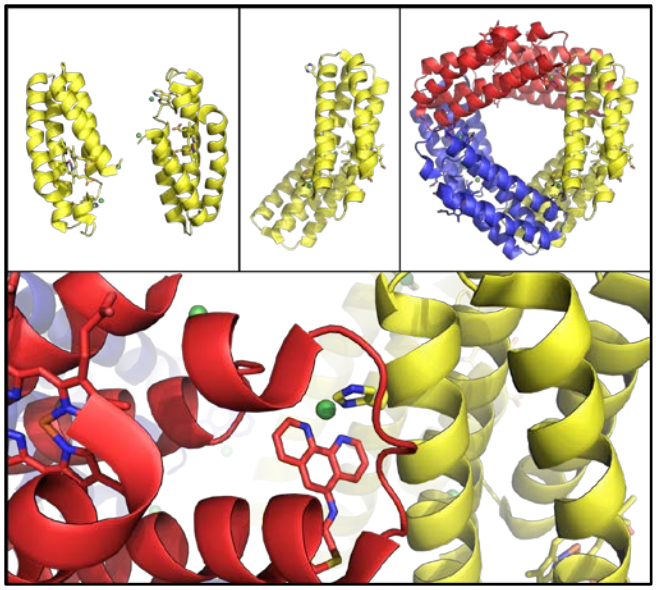

Figure 7. MBP-Phen1$_3$ Coordinating Nickel (II) Ion
(Top left and top middle) A single asymmetric unit containing two MBP-Phen1$_3$ molecules which assmbled into a supramolecular triangle via C3 symmetry (top right) with unsaturated coordination of nickel (II) ion (bottom). PDB ID: 3FOP[29]

Understanding how natural metal-coordinating motifs on proteins evolved is a good place to start for designing functional coordination spheres in synthetic proteins. Thus, Tezcan, *et al.* established "metal templated interface redesign (MeTIR)" to replicate a hypothetical evolutionary pathway.[23, 30] In this work, they modeled metal-binding protein evolution with MBPC-1 using RosettaDesign[31] to optimize the PPIs induced after metal-directed self-assembly, and engineered two variants, RIDC-1 and RIDC-2, both of which complemented the metal-binding pocket of MBPC-1 with more favorable PPIs than those discovered in the original structure. Through these experiments, they concluded that single mutations in primary protein sequence is enough to induce the evolution of a specific metal-binding protein complex.[30]

1.3 Peptide-Based Materials

While proteins have made some interesting and useful materials, there is a distinct size threshold at which they become a challenge to study. Many proteins can be expressed and harvested in large quantities from prokaryotic systems, but these techniques are limited by the 22 canonical amino acids. Incorporation of noncanonical amino acids in expressed proteins quickly becomes a nontrivial task as the number of unnatural residues increases, but many labs continue to use amber and ochre codons and post-purification modifications to incorporate unnatural side chains into large proteins for study.[29]

In contrast, synthetic proteins allow for maximal incorporation of noncanonical amino acids but are plagued by laborious synthesis, complicated purification, and low yield due to numerous tandem reactions. These problems can be ameliorated by instead targeting synthetic peptides, which are shorter, and as a result, can be prepared in higher yields with fewer complications. Synthetic peptides can fold into an array of different secondary and tertiary structures; however, the diversity of folds accessible is limited by short sequence length. An advantage of simplified folding motifs, however, is simplified design principles for their construction. Furthermore, peptides are more amenable to fine tuning than proteins, as single mutations can have more pronounced effects on the structure, and unnatural residues can be incorporated anywhere in the sequence.

Self-assembling peptides rely on folding-directed assembly just as proteins do, but their shorter length limits the local folding motifs available to the monomer. Despite this issue, synthetic peptides have found widespread use in supramolecular materials. Ideally, every amino acid in the sequence should contribute to secondary structure and therefore self-assembly. Many self-assembling β-sheet peptides have been studied[32] as antibacterial agents,[1] responsive hydrogels,[33]

and nanofibers.[34] Additionally, collagen and other polyproline structures have been extensively studied as robust peptide-based nanomaterials.[35-37] Likewise, α-helices have found some success in materials chemistry. Helices can form from peptides with as few as seven amino acids,[38] yet can span dozens of residues uninterrupted.[39] From a materials perspective, the most notable feature of α-helices is their propensity to form coiled coils.

Coiled coil chemistry is a well-established field with design rules for creating a plethora of multimeric states.[15] Not all coiled coils result from the assembly of α-helices, but only α-helical coiled coils are discussed herein. Coiled-coil-forming α-helices are characterized by a heptad repeat pattern of hydrophobic (H) and polar (P) amino acids. Multiple heptad patterns exist, but the most common is HPPHPPP, which defines an amphiphilic helix with hydrophobic residues arrayed in a stripe on one face. Oligomerization state and arrangement of helices in the quaternary structure are dictated by which specific residues occupy the hydrophobic positions within the heptad as well as flanking interactions between polar residues. This is best illustrated through a helical wheel diagram (Figure 8). The coiling of the coil is a result of the display of hydrophobic side chains every 3.5 residues (positions *a* and *d*) and the turn of the helix which occurs every 3.6 residues.[15]

The rules of coiled coil design have been established through decades of research by many peptide chemists and was comprehensively reviewed by Woolfson.[15] At their most fundamental, the design trends indicate that oligomerization state is dictated primarily by side chain identity at positions *a* and *d*, at which β-branched side chains are best accommodated by higher order oligomerization states (Table 1). Many coiled-coil designs include complementary salt bridges between positions *e* and *g* on adjacent strands,[41-43] while residues in positions *b*, *c*, and *f* vary more widely.

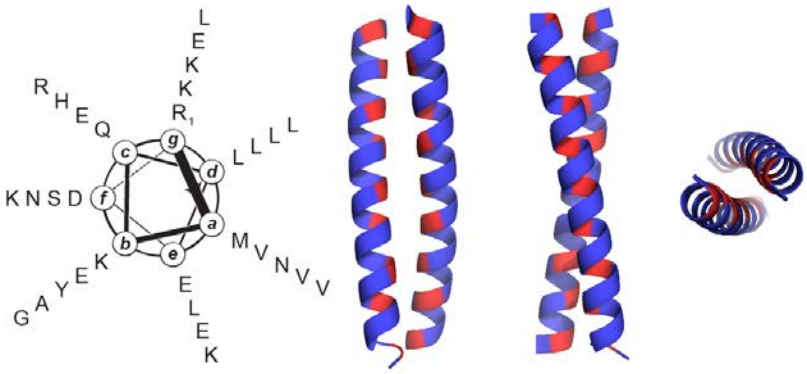

Figure 8. GCN4: A Coiled Coil Dimer
(Left) Helical wheel diagram allows for facile visualization of side chain display on the surface of a single α-helix. (Center) GCN4 leucine zipper as an example of a coiled-coil peptide dimer. Hydrophobic residues are highlighted in red to illustrate winding of core residues (positions *a* and *d*) in the fold. (Right) Top view of dimer illustrates coiling of chains to accommodate hydrophobic core. PDB ID: 4DMD[40]

Table 1. Preferred Amino Acids at the *a* and *d* Sites of Known Coiled-Coil Structures[15]

	Most preferred amino acids	
Structural type	*a*	*d*
Parallel two-stranded	Asn > Val > Leu > Ile (1.77)	Leu > Met
Parallel three-stranded	Ile > Val > Leu (1.91)	Leu > > Ile
Parallel four-stranded	Met ≈ Ile > Val > Leu > Ala	Met > Ile > Gln
Parallel five-stranded	Leu > Ile	Met > Gln > Thr > Val
Antiparallel two-stranded	Leu ≈ Ile	Leu

SOCKET analysis of residue frequency at sites *a* and *d* in published coiled-coil structures in the PDB as of April 2001 where residues with frequency 2 or higher were automatically added to the list. Values in parentheses indicate residues which fell below the threshold but the author felt they were worth mentioning.[15, 44] Reprinted from *Advances in Protein Chemistry*, **70**, Woolfson, Derek N., "The Design of Coiled-Coil Structures and Assemblies," 79-112, Copyright (2005), with permission from Elsevier.

As a result of the established trends in their sequence-structure relationship, coiled-coil peptides have been used by many research groups to create peptide-based supramolecular assemblies, among which Woolfson's work stands out. His first notable foray into the field of coiled-coil materials came before his review of coiled coil design in 2005 as a pair of "self-

assembling fiber (SAF)" peptides which were designed to form sticky-ended heterodimers when mixed together. The association was monitored by circular dichroism (CD) scans. Each single strand did not show significant coiled-coil character, but when mixed together in equal concentrations and allowed to "mature" for one hour, the molar ellipticity at 208 nm and 222 nm increased dramatically, indicating that a profound coiled coil architecture had formed (Figure 9).[45] Additionally, SEM and TEM images of the fibers were captured, revealing that fibers formed up to 70 nm wide with lengths in the tens of micrometers (images not shown).[45]

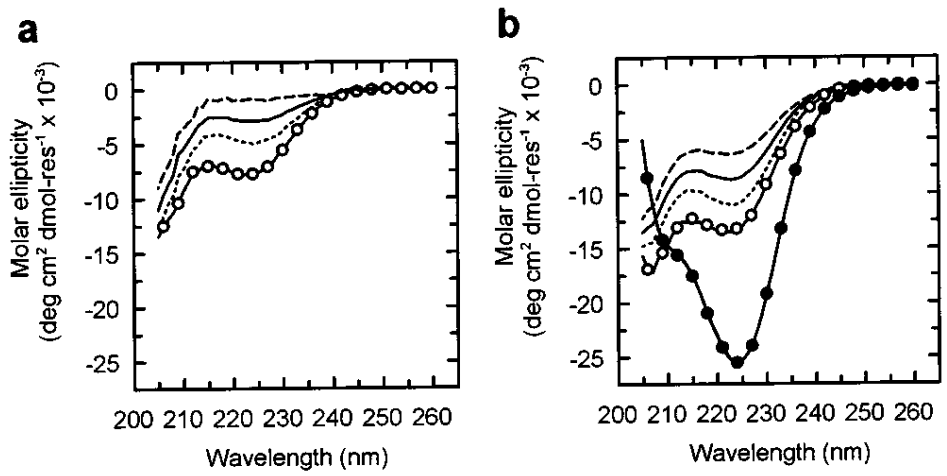

Figure 9. CD Scans of SAF-p1 and SAF-p2 association[45]

Individual scans of SAF-p1 (– –), SAF-p2 (- -), their average (—), and initial scan of a 1:1 mixture of the two peptides (○) show no significant coiled coil character (**a**), while coiled coil character is observed after 1 h of "maturation" (●)(**b**). The authors note that the noticeably small minimum at 208 nm compared to that at 222 nm is likely due to the scattering of light upon fibril aggregate formation, and that the solution was slightly cloudy after maturation. Adapted with permission from Pandya, M.; Spooner, G.; Sunde, M.; Thorpe, J.; Rodger, A.; Woolfson, D. *Biochem*. **2000,** *39* (30), 8728-8734. Copyright (2000) The American Chemical Society.[45]

Woolfson's work with SAF peptides was later expanded through redesigns that allowed for branching,[46-47] kinking, waving,[47] and functionality.[48]

Since Woolfson's SAF peptides were published, many groups have studied coiled coils at length. Coiled coils have been engineered with pH, salt, and temperature sensitivity (some which

cause an α-to-β shift in secondary structure), disulfide bond induced stability, "small molecule induced self-assembly," and various other properties that contribute to supramolecular assembly, as reviewed by Klok in 2010.[49]

More recently, Horne and co-workers defined a water-soluble supramolecular assembly built from coiled-coil peptide dimers which were perpendicularly covalently crosslinked. They found that their assemblies could persist in solution and were amenable to separation through gel-permeation chromatography, and that the rigidity of the linkers with which the coiled coils were connected had a significant effect on apparent assembly size (*n*) (Figure 10).

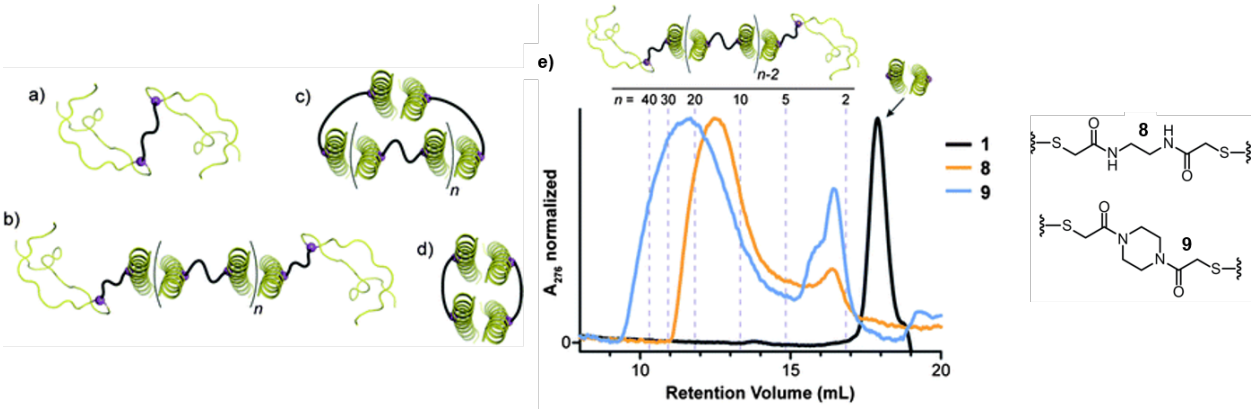

Figure 10. Self-Assembly Modes of GCN4-Derived Monomers[50]
Monomeric linked subunits (**a**) can associate linearly (**b**), cyclicly (**c**), or as a dimer (**d**). Gel-permeation experiments performed on samples of GCN4 single dimer (**1**) and two cross-linked samples with different linkers (**8**) and (**9**) show that a variety of oligomer states are formed and are affected by linker identity. Adapted with permission from Staples, K.; Oshaben, K.; Horne, W.S. *Chem. Sci.* **2012,** *3* (12), 3387-3392. Copyright (2012) The Royal Society of Chemistry.

Furthermore, they found that oligomer state can be controlled by mixing different ratios of parent peptide **1** with peptides **8** and **9** (data not shown).[50]

1.4 Metal-Directed Peptide-Based Materials

At the forefront of metal-directed materials research are metal-organic frameworks (MOFs).[2, 51-55] Inspired by their natural counterparts, zeolites, MOFs are rationally designed frameworks composed of metal ions coordinated to organic linker molecules and can be functionalized for a variety of applications, including as sensors for detecting explosives,[56-58] small molecules in enantiospecific fashion,[59] and hazardous metal ions,[60-61] many with convenient luminescent readouts.[2] Additionally, MOF catalysts have enjoyed recent attention,[62] especially those that can perform complex one-pot reactions.[63-64] Furthermore, the sensitivity and selectivity of MOFs allow their effective use as sorbents for chemical separations.[65]

MOFs and peptide-based materials are similar in that they are modular and self-assembling. It stands to reason that the organic nature of peptides would enable them to be used as the linkers in a MOF. Peptides participating in a MOF would self-assemble with orthogonal driving forces, peptide folding and metal coordination, to create a new type of material: one that is peptide-based and metal-directed. The marriage of these two fields is relatively new, but there is some literature precedent from recent years.

Besenius and coworkers designed temperature-controlled, gold-mediated peptidic fibers from amphiphilic monomers. The monomers were designed to associate via aurophilic interactions between closed shell gold metal centers, as well as π-π stacking interactions between adjacent phenylalanine (Phe) side chains. PEG-like tails were attached to the end of each gold ion to facilitate solubility in water (Figure 11, top left). Small assemblies formed at 5°C, as indicated by CD minima at 219 nm and 250 nm (Figure 11, top right). As temperature increased, minima became more intense, indicating higher order oligomer states were forming. At 60°C, they were surprised to see that the CD signature had dramatically shifted (Figure 11, top right). Upon

investigating with TEM, they found that at higher temperatures, the gold amphiphiles coiled around each other to form wider fibers (Figure 11, bottom).[66]

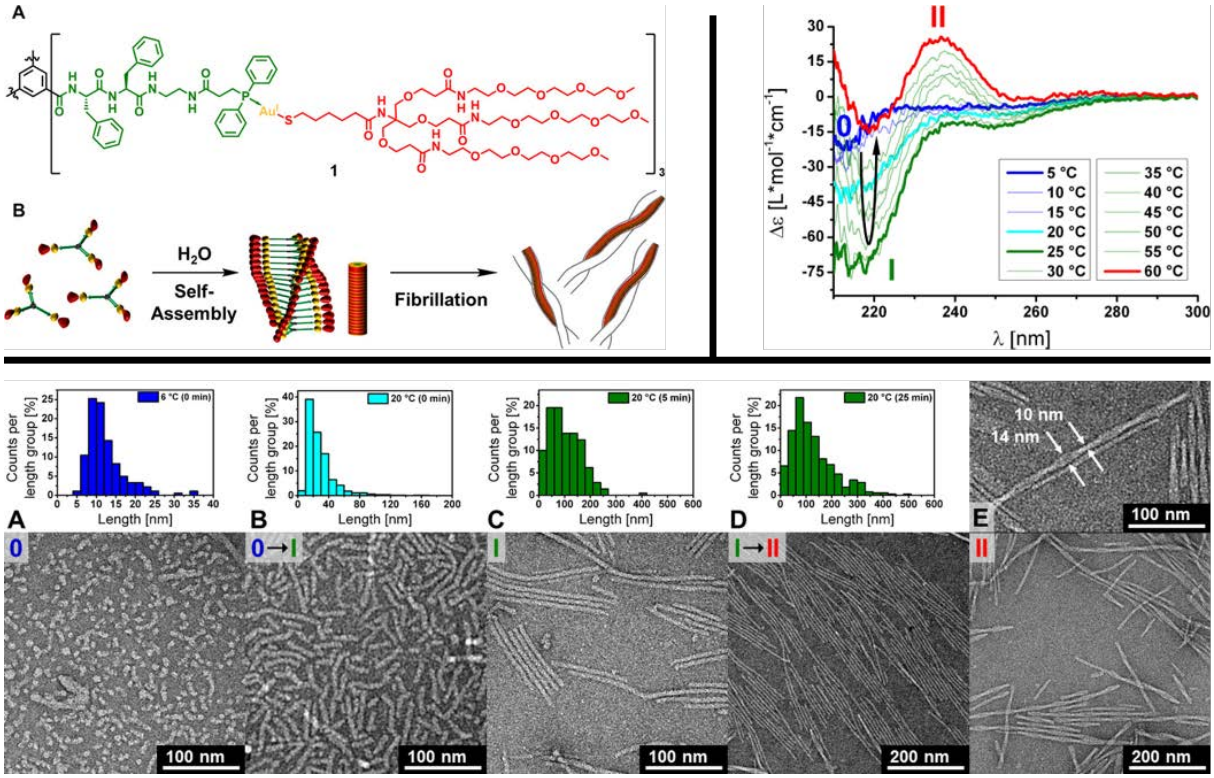

Figure 11. Assembly of Au^{I}-Metallopeptides[66]

(Top left) Amphiphilic monomers built from bi-Phe peptide with PEG-like tail (A) stack through aurophilic interactions to form single fibers which coil together to form superfibers (B). (Top right) CD data show stepwise ordered assembly as a function of temperature, and two discrete supramolecular structures are characterized. (Bottom) Fiber formation as a function of time and temperature with associated TEM images. Reproduced with permission from Kemper, B.; Zengerling, L.; Spitzer, D.; Otter, R.; Bauer, T.; Besenius, P. *J. Am. Chem. Soc.* **2018,** *140* (2), 534-537. Copyright (2018) The American Chemical Society.

Arguably, Besenius' aurophilic peptide bundles more closely resemble MOFs than metallopeptides, but they are interesting for two reasons. First, assembly I shows a distinct CD signature with minima at 219 nm and 250 nm, which may correlate to this specific structure, or derivatives of it. Whether the CD signature changes if a different bipeptide or PEG-like tail were used may establish guidelines for building similar assemblies. Second, the supercoiling of the fibers which created assembly II is remarkably similar to the natural supercoiling of peptide α-

helices. The PEG-like tails were intended to increase solubility in water but ended up playing a second role in assembly II formation. Elucidating the interactions which caused this assembly would likely enable control over it.

A notable early example of *de novo* metallopeptide design came in 1990, when Ghadiri and colleagues used metal binding to stabilize a previously established[67] α-helical fold, by inserting Cys and His residues at *i* and *i*+4 positions near the C-terminus. According to their CD data, one such peptide was 54% helical in the absence of metal and up to 90% helical in the presence of cadmium ion.[68] Later, they engineered a 15-residue peptide with a bipyridine moiety at the N-terminus which associated into a three-helix bundle in the presence of bivalent transition metal cations. The 15-residue peptide monomers were too short in length to promote the formation of a stable coiled-coil trimer in the absence of metal.[69] Soon after, Sasaki, *et al*. explored a similar concept.[70-71]

Since the publication of Ghadiri's and Sasaki's metal-stabilized coiled coils, many metal-directed self-assembling peptides have been studied.[72] Gilmartin, *et al*. thoroughly investigated the electrochemistry of pyridine-displaying small peptides (1-10mers) which coordinated platinum and copper ions,[73] and synthesized pyridine-containing trimers and bipyridine-containing hexamers which assembled in the presence of copper (II) or iron (II) ions.[74] Additionally, Stupp designed short peptides which self-assemble in the presence of bivalent metal cations including calcium, magnesium, and barium.[75-78] All of these assemblies were built from peptides which had no notable secondary structure until they coordinated a metal ion.

Conversely, peptides which participate in orthogonal assembly modes, as many modern MOFs and other self-assembling polymers do,[79] have found limited success. Klok, *et al*. was one of the first groups to explore the relationship between quaternary structure and metal-directed

assembly. They synthesized *de novo* peptides based on a previously reported coiled-coil[80] with an added terpyridine (Tpy) moiety at the N-terminus. Consequently, the peptides folded as dimers and tetramers in the presence of iron (II) ion. Results for larger order aggregates were positive but ambiguous.[81]

More recently, Horne, *et al*. have explored the orthogonal assembly of metal-coordinating coiled-coil peptides by incorporating unnatural Tpy side chains which were intended to bis-coordinate bivalent transition metal ions in aqueous solution.[82] These peptides were similar to their previous study of covalently perpendicularly linked coils, in that the intercoil assembly occurs perpendicular to the helical axis.[50] Originally, the three peptides were designed to fold as a dimer, trimer, and tetramer, respectively. The intended quaternary oligomerization states were specified by precedented hydrophobic cores and stabilized by flanking polar residues which participated in salt bridges and no off-target oligomer states were observed (Figure 12).

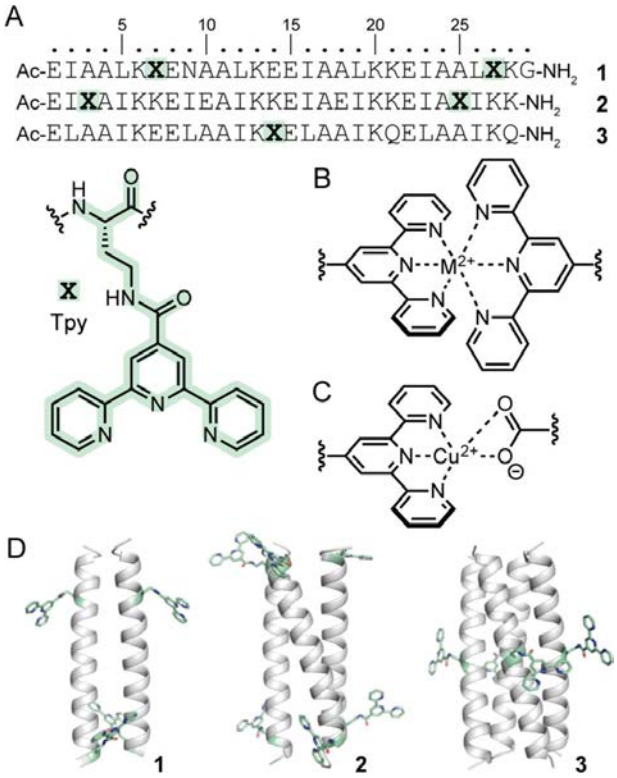

Figure 12. Series of Metal-Coordinating Coiled-Coil Peptides Examined by Horne, *et al*.[82]
(A) Sequences of which coded for (**1**) dimeric, (**2**) trimeric, and (**3**) tetrameric oligomerization states, and were designed to coordinate bivalent metal ions in a bis-Tpy (X) fashion (B). (C) Observed coordination mode of Cu^{2+}. (D) Coiled coil oligomer states observed for each peptide. Adapted with permission from Tavenor, N. A.; Murnin, M. J.; Horne, W. S. *J. Am. Chem. Soc.* **2017**, *139* (6), 2212-2215. Copyright (2017) The American Chemical Society.

Upon examining the resulting crystal structures, it became apparent that no bis-Tpy coordination of copper had occurred. Instead, only heteroligand coordination of copper involving Tpy and carboxylate, either from buffer component or Glu, were present.[82] Two crystal forms were found for the dimeric peptide. In the first, intercoil assembly was driven by a network of citrate molecules which associated to bring the coils together linearly (Figure 13, left). The other crystal form observed for the dimeric coiled coil associated via Tpy-Cu^{2+}-$Glu^{14/22}$ coordination and assembled linearly (Figure 13, right).

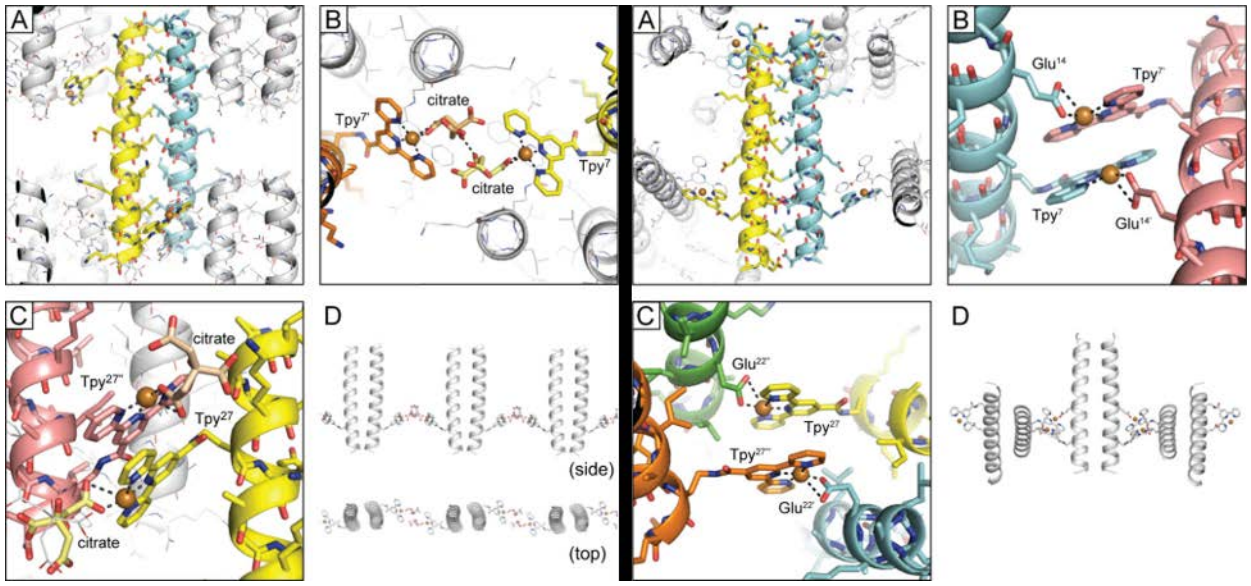

Figure 13. Metal-Directed Self-Assembly of a Dimeric Coiled Coil[82]

Left: Crystal form *a* (A) A single dimeric coiled coil in the context of the crystal structure. (B) Observed coordination of copper (II) ion included a network of citrate molecules from the crystallization buffer, and (C) heteroligand coordination with free citrate molecules. (D) Linear assembly of coiled coils as a result of the heteroligand coordination network shown in (B).

Right: Crystal form *b* (A) A single dimeric coiled coil in the context of the crystal structure. (B) and (C) Observed coordination of copper (II) ion by Tpy and Glu residues. (D) Linear assembly of coiled coils as a result of the heteroligand coordination of copper.

One crystal structure for the trimeric coiled coil was observed, for which the metal-directed assembly was dominated by Tpy-Cu^{2+}-Glu^{22} coordination in lieu of the desired bis-Tpy configuration. In addition, well defined Tpy-Tpy stacking interactions were observed, resulting in an ordered, square-looking lattice (Figure 14). Lastly, one crystal structure of the tetrameric coiled coil was observed, which consisted of a packed assembly of the tetramers via Tpy-Cu^{2+}-$Glu^{1/7}$ coordination (Figure 15).

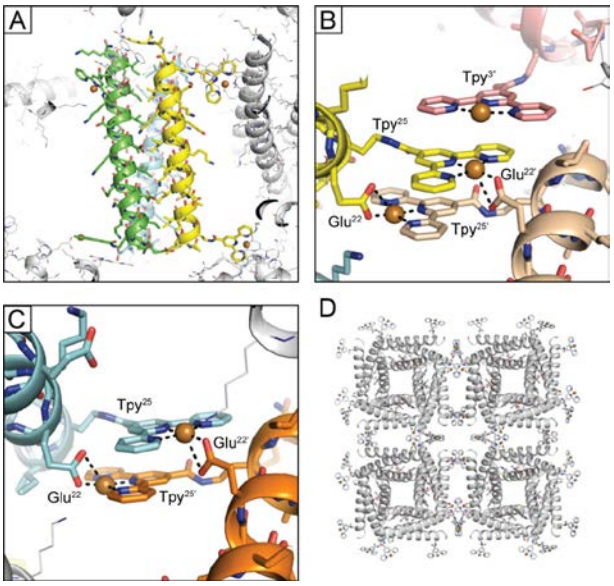

Figure 14. Metal-Directed Self-Assembly of a Trimeric Coiled Coil[82]

(A) A single trimeric coiled coil in the context of the crystal structure. (B) and (C) Observed intercoil interactions include Tpy-Cu^{2+}-Glu^{22} and Tpy stacking. (D) Square-looking assembly of coiled coils as a result of the heteroligand coordination of copper and the Tpy stacking interactions. Adapted with permission from Tavenor, N. A.; Murnin, M. J.; Horne, W. S. *J. Am. Chem. Soc.* **2017**, *139* (6), 2212-2215. Copyright (2017) The American Chemical Society.

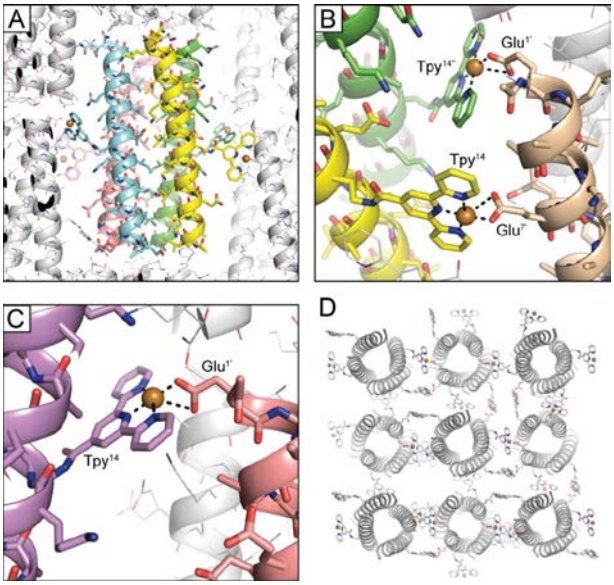

Figure 15. Metal-Directed Self-Assembly of a Tetrameric Coiled Coil[82]

(A) A single tetrameric coiled coil in the context of the crystal structure. (B) and (C) Observed Tpy-Cu^{2+}-$Glu^{1/7}$ coordination. (D) Packed assembly of coiled coils as a result of the heteroligand coordination of copper. Adapted with permission from Tavenor, N. A.; Murnin, M. J.; Horne, W. S. *J. Am. Chem. Soc.* **2017**, *139* (6), 2212-2215. Copyright (2017) The American Chemical Society.

While the heteroligand coordination of copper was unexpected, the authors note that it is literature precedented.[83-84] The copious incorporation of Glu side chains in the peptide sequences were intended to stabilize the quaternary structure through salt bridges but had the unintentional side-effect of participating in metal coordination. Such coordination of copper was unpredictable, therefore, there is room for improvement on the design principles used to build these metal-driven peptide-based supramolecular materials.

1.5 Project Objectives

The goal of the present study is to exert control over the Tpy-Cu^{2+}-Glu coordination observed by Horne and Tavenor,[82, 85] and use metal-driven assembly to build predictable, novel lattices out of coiled-coil peptide building blocks. Our central hypothesis is that removal of all but one Glu residue in each peptide sequence would allow for only a single coordination mode of copper in the resulting crystal structure. To this end, we replaced Glu residues with their amide counterpart, Gln, as it is the most chemically similar of the canonical amino acids.

We first targeted the assembly of the tetramer described by Horne, *et al*., since the observed lattice (packed) was most similar to the expected one (open). We hypothesized that restricting the coordination mode of copper with a single Tpy and Glu would result in increased ease of crystallization and more robust crystals. Furthermore, we attempted to probe the effect of Tpy/Glu location on the resulting assembly. The tetrameric series herein provided some useful insights on coil stability and resulted in the revision of the design principles.

Next, we applied our revised design principles to two trimers described by Horne and Tavenor.[82, 85] Of these two trimers, one produced diffraction quality crystals and one did not. The

trimer which produced the crystal structure in *JACS* was designed to coordinate in an offset, parallel fashion, while the other trimer was designed to build an open hexagonal lattice upon coordination. We sought to design a trimer which would coordinate and assemble in an antiparallel fashion, build an open hexagonal lattice, and form robust diffraction quality crystals.

Collectively, this study attempts to further solidify our design principles for metal-directed self-assembling peptide-based supramolecular materials, and elucidate novel architectures assembled from these building blocks. Success of this study would establish a springboard from which a variety of metal-directed peptide-based materials may stem, hypothetically limited only by the act of conceiving them.

2.0 Experimental

2.1 Materials

All Fmoc-protected amino acids were purchased from NovaBiochem or Chem Impex, and the resin was purchased from NovaBiochem. HPLC grade solvents were purchased from Fisher Scientific, and organic reagents were purchased from Sigma Aldrich, Acros Organics, or Fisher Scientific. Stocks of peptides **1** and **7** were inherited from Nathan Tavenor (PhD, University of Pittsburgh, 2017). Crystallization reagents, preformulated screens, 24-well hanging and sitting drop trays, cover slips, and tools were purchased from Hampton Research.

2.2 Synthesis

2.2.1 4-Carboxy-Terpyridine Synthesis

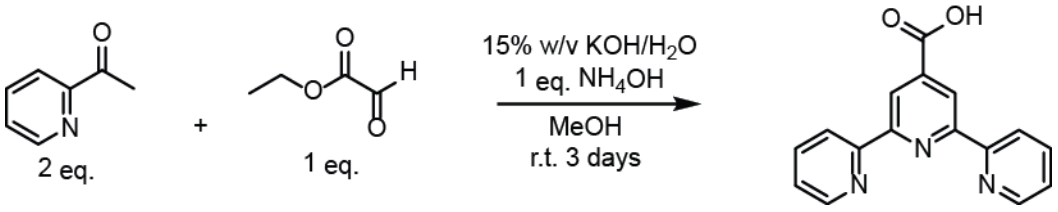

Scheme 1. 4-Carboxy-Terpyridine Synthesis

4'-Carboxy-2,2':6',2"-terpyridine (4-carboxy Tpy) was synthesized on a 30 mmol scale and purified as previously described by Stublla, *et al.*[86] (Scheme 1). First, 2-acetylpyridine and ethyl

2-oxoacetate were added to 100 mL MeOH in a round bottom flask, and stirred for 5 min. Meanwhile, a separate solution of ammonium hydroxide in 15% w/v KOH/water was prepared in an ice bath. The KOH solution was added to the reaction vessel, and the solution turned yellow. The flask was sealed with a rubber septum and parafilm, vented with a needle, and allowed to stir at room temperature for three days. Over the course of the reaction, the solution changed colors in the following order: translucent yellow, orange, brown, green with white suspension, then light brown with white suspension.

The emulsion was vacuum filtered and washed with 100 mL choloroform followed by 100 mL of chilled 50/50 v/v MeOH/water solution. At this point the filtrate was a light pink. The solid was suspended in 100 mL 80/20 MeOH/water solution, sonicated until translucent and acidified to pH 2.19 with 1 M HCl, after which a white precipitate formed. Finally, the mixture was vacuum filtered, washed with chilled water, placed on a high-vacuum system overnight, and then lyophilized. The reaction yielded approximately 23% compared to the reported 54%.[86] Product structure was confirmed via ^{1}H and ^{13}C NMR (Bruker 500 MHz, DMSO-d_6) (Appendix A) and high resolution mass spectrometry (Thermo ESI-QExactive) (Appendix B).

2.2.2 Peptide Synthesis

Peptides were synthesized by Fmoc solid phase methods on NovaPEG Rink Amide resin. Coupling reactions consisted of 5 eq Fmoc-protected amino acid, 6 eq DIEA, and 4 eq HCTU in NMP, and were performed at 70°C in a CEM MARS microwave with 2 min ramp to temperature, 4 min hold at temperature, and 5 min cooldown. Fmoc deprotection reactions proceeded with stirring in 20% 4-methylpiperidine in DMF solution at 80°C with 2 min ramp, 2 min hold, and 5 min cooldown. Resin was washed three times with DMF after each coupling and deprotection

reaction. The first amino acid was double coupled to the resin, after which coupling and deprotection cycles were performed until all 28 residues were attached. Peptides were capped on resin with a solution of 8:2:1 DMF/DIEA/acetic anhydride at room temperature for 20 min, then washed for two minutes three times each with DMF, DCM, and MeOH and placed on a vacuum desiccator overnight.

2.2.3 Alloc Deprotection

Each peptide contained one orthogonally Alloc-protected 2,4-diamino-L-butyric acid (Dab) residue which allowed for separate coupling of 4-carboxy Tpy to the peptide while on resin. Alloc deprotections were performed under inert atmosphere (Ar) in dry DCM with catalytic tetrakis(triphenylphosphine)palladium(0) and triphenyl silane as previously described by Grieco, *et al*. (Scheme 2).[87]

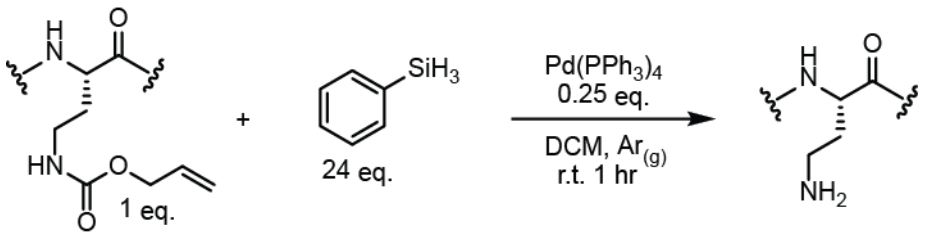

Scheme 2. Alloc Deprotection of Dab Side Chain

First, the resin was swelled in dry DCM, bubbled with argon, and treated with excess triphenyl silane for about 10 min. In a separate vessel, $Pd(PPh_3)_4$ was dissolved in dry DCM. The catalyst solution was then added to the solvated resin, and the reaction proceeded for about an hour with occasional manual agitation and addition of dry DCM to ensure all resin was solvated. In

most cases, the reaction turned from bright yellow to burnt orange due to the poisoning of the catalyst over time. Next, reaction vessels were drained and washed three times each for three minutes with DCM and DMF followed by three five-minute washes with 0.02 M sodium dithiocarbamate in DMF with stirring. Finally, the resin was washed three times for three minutes with DMF.

2.2.4 4-Carboxy Tpy Coupling

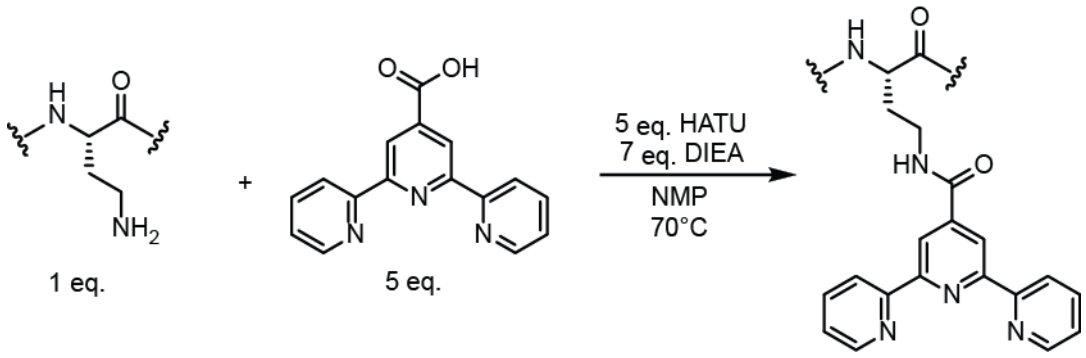

Scheme 3. Coupling of 4-Carboxy Tpy to Dab Residue

After Alloc deprotection of the Dab side chain, 4-carboxy Tpy was activated with DIEA and HATU in NMP and coupled at 70°C in the CEM MARS microwave with stirring for 2 min ramp, 4 min hold, and 5 min cooldown times respectively (Scheme 3). After coupling, the resin was washed three times for 30 sec with DMF, then DCM, and MeOH for 3 min. Dried resin was placed in a vacuum desiccator overnight.

2.2.5 Peptide Cleavage

Two cleavage cocktails were used during peptide preparation. Cocktail 1: 90% TFA; 3% water; 3% EDT; 3% anisole; 1% TIS. Cocktail 2: 95% TFA; 2.5% water; 2.5% TES. Cocktail 1 gave the highest yield of recovered protein. The aggressive scavengers were necessary to prevent hypothesized reattachment of the peptide to the resin. In one parallel experiment, cocktail 1 yielded at least twice as much crude peptide as cocktail 2. Cleavage cocktails were mixed then carefully added to dry resin in fritted polypropylene syringes. Syringes were capped and a back pressure was applied to allow for expansion. Reactions proceeded for four hours at room temperature with gentle agitation (rocking).

Subsequently, cleavage mixtures were ejected into clean polypropylene tubes and the remaining resin was rinsed with fresh cleavage cocktail. Combined product mixtures were dried under $N_{2(g)}$ stream, then a large excess of chilled diethyl ether was added to the tube, resulting in formation of a white precipitate. Ether suspensions were centrifuged at 6000 rpm for 2 min, and supernatants were decanted and later neutralized and discarded. Crude solid product was dried under $N_{2(g)}$ stream then solvated in a small amount of MeCN. Finally, water was added to the solution to an approximate final ratio of 30/70 MeCN/water.

2.2.6 Peptide Purification

Crude product solutions were analyzed using a Hitachi LaChrom Elite analytical HPLC with a diode array detector. Initial reversed phase chromatography experiments used a steep gradient of solvent B (0.1% TFA in MeCN) in solvent A (0.1% TFA in water), and gradients were optimized for each peptide. Phenomenex Luna (100 Å, C18, 3 μm, 150 x 4.6 mm) and Jupiter (300

Å, C18, 3 μm, 150 x 4.6 mm) columns, and a flow rate 1.0 mL/min were used for the analyses. HPLC experiments were monitored at 220 nm, 280 nm, and 310 nm, and resolved peaks were manually collected for mass analysis on a Bruker ultrafleXtreme MALDI-TOF mass spectrometer. Matrices used for MALDI included CHCA, sinapinic acid, and SDHB, and ionization efficiencies of the matrices depended on peptide sequences.

At the outset of the study, solid crude reaction mixtures were dissolved in 30% solvent B in solvent A, and crude chromatograms showed an extra peak containing the mass of product plus TFA. We hypothesized that the Tpy side chain was forming a TFA complex which had a longer retention time. To test this hypothesis, crude reaction mixtures were reconstituted and dissolved in 30% pure MeCN in pure water. The resulting chromatogram lacked the suspected peptide-TFA complex peak, and subsequent experiments were adapted to use TFA-free solvents for the stock solutions prepared for injection.

After gradient optimization on the analytical scale, preparative reversed phase HPLC was performed on a Hitachi LaChrom Elite Preparative HPLC with a standard UV detector, monitored at 220 nm. Phenomenex Luna PREP (100 Å, C18, 10 μm, 250 x 21.2 mm, AXIA™ Packed) and Jupiter PREP (300 Å, C18, 10 μm, 250 x 21.2 mm) columns were used with a flow rate of 15 mL/min. Resolved peaks were automatically collected, and pure fractions were combined after mass analysis and lyophilized. Lyophilized peptides were concentrated, and purity was confirmed via MALDI-TOF (Table 2 and Appendix C) and analytical HPLC (Figure 16).

Table 2. MALDI-TOF Characterization of Each Peptide

Peptide	Ion Identity	Calculated m/z	Observed m/z
1	$[M+Na]^{1+}$	3328.848	3328.007
2	$[M+Na]^{1+}$	3324.912	3324.286
3	$[M+Na]^{1+}$	3324.912	3324.298
4	$[M+Na]^{1+}$	2982.783	2982.093
5	$[M+Na]^{1+}$	3210.869	3210.178
7	$[M+Na]^{1+}$	3560.912	3560.193
8	$[M+H]^{1+}$	3187.879	3188.170
9	$[M+Na]^{1+}$	3210.869	3210.599

Some peptides formed aggregates in solution, complicating purification. Initial analytical chromatograms of crude sample showed a single product-containing peak, but over time a second product-containing peak appeared in increasing concentration at a later retention time. Aggregate formation was circumvented by reconstituting the crude sample and re-dissolving in at least 1 M guanidine hydrochloride in 30% MeCN solution. The resulting chromatograms had only a single peak which contained the desired product.

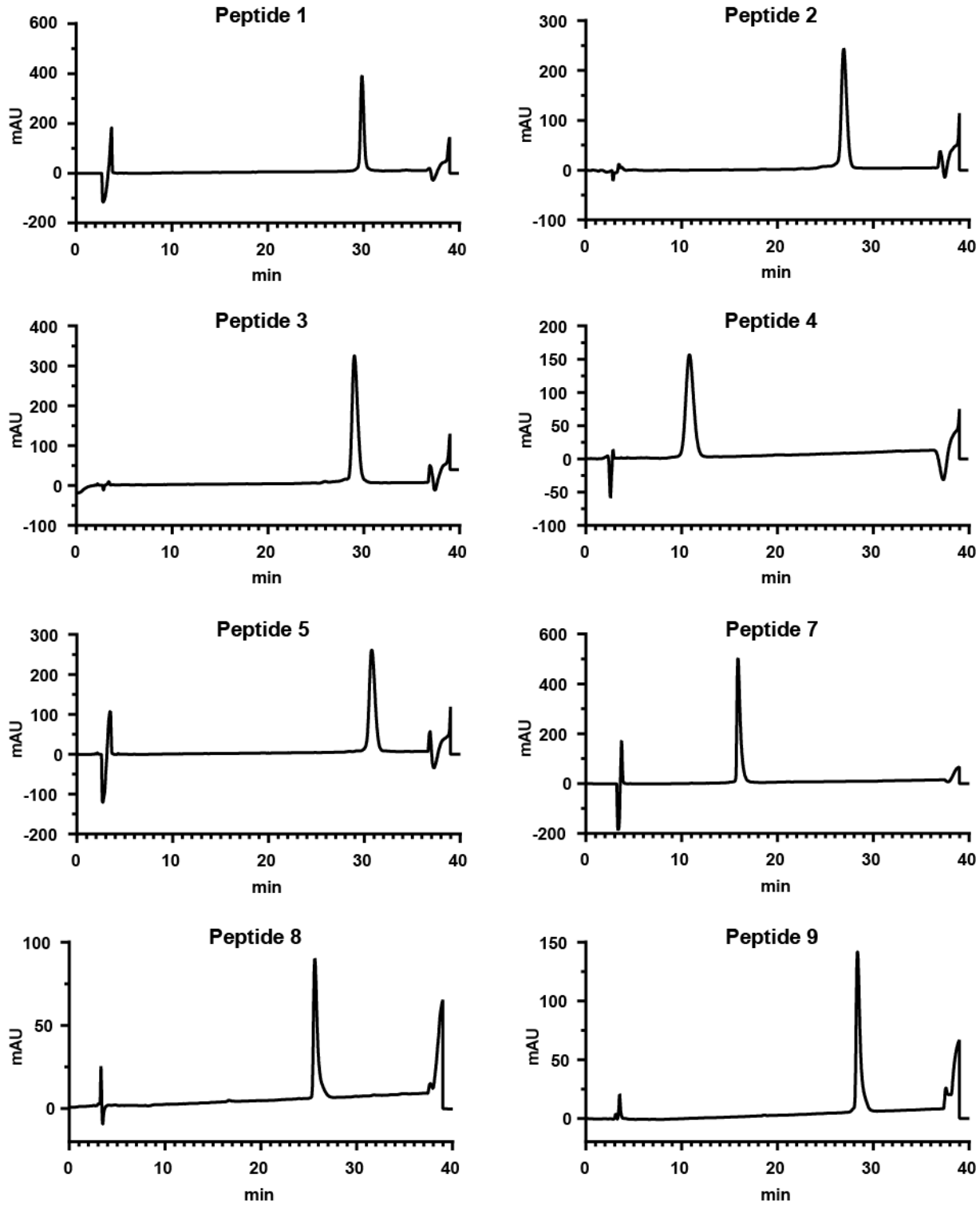

Figure 16. Analytical Chromatograms of Purified Material

Reversed phase analytical HPLC was performed on purified peptides using gradients of solvent B (0.1% TFA in MeCN) in solvent A (0.1% TFA in water): **1**: 30-45%; **2**: 32-40%; **3**: 32-40%; **4**: 60-70%; **5**: 36-46%; **7**: 35-55%; **8**: 37-47%; **9**: 37-49%. No experiments were performed on peptide **6**. Columns used for **1-5**: Phenomenex Luna 100 Å, C18, 3 μm, 150 x 4.6 mm; **7-9**: Phenomenex Jupiter 300 Å, C18, 3 μm, 150 x 4.6 mm.

2.3 Characterization

2.3.1 Concentration Quantificiation

Peptide stock solutions were diluted with 6 M guanidine hydrochloride and subjected to UV analysis for quantification using an Olis HP 8452 diode array UV spectrophotometer and Beer's Law, where the molar absorptivity of the Tpy side chain at 310 nm was 8400 ± 200 M^{-1} cm^{-1} as calculated by Tavenor.[85]

2.3.2 Circular Dichroism

CD scans of peptide solutions (300 μL, 100 μM in 10 mM HEPES pH 7.1 buffer) were recorded using an Olis DSM17 circular dichroism spectrophotometer. Scans were performed at 25°C with 2 nm bandwidth and 5 s integration time at each wavelength from 200 nm to 260 nm. Measurements were baseline corrected against a buffer blank measured in the same experiment, and scans were smoothed using GraphPad Prism 7.[88]

Thermal denaturation experiments were subsequently performed on the same samples with monitoring at 222 nm and 260 nm with 2 nm bandwidth, 5 s integration time, and a 5 min equilibration at every fourth temperature between 2°C and 98°C, inclusively. Measurements were baseline corrected against the buffer blank measured in the CD scan experiment. Melting temperatures were calculated using GraphPad Prism 7 and fitted with equations as described by Shortle, *et al*.[89]

2.3.3 X-Ray Crystallography

Peptides were subjected to vapor diffusion crystallization trials using the Hampton Research Index Screen (HR2-144) which consists of 96 unique buffer formulations. Once peptides were quantified using UV spectroscopy, they were reconstituted and dissolved in pure water (18MΩ conductance) to the desired concentration. Aliquots of peptide stocks were combined with aliquots of mother liquor and copper (II) chloride salt solution (1:1:1) to form the drop, which was sealed in either hanging drop or sitting drop fashion.

X-ray diffraction data were collected using Cu/Kα radiation on a Rigaku diffractometer (FR-E generator, VariMax optics) with a Saturn 944 CCD or R-Axis HTC Image Plate detector. Data were processed using d*TREK and structures were solved by molecular replacement using Phaser.[90] The search model used was a modified version of PDB ID: 5U5B (peptide **6**) with truncated ends and two mutations (X3R and X25R). Refinement was performed with assistance from Dr. W. Seth Horne using Phenix[91] and Coot.[92] Data collection and refinement statistics for all crystal forms are in Table 3. Models were generated with educationally licensed PyMOL for analysis.

Table 3. X-Ray Data Collection and Refinement Statistics

Data Collection	**9***a*	**9***b*	**8***a*
Cryo-protection	none	30% glycerol	none
Unit cell dimensions (Å, °)	a = 51.0, b = 79.3, c = 48.8 $\alpha = \beta = \gamma$ = 90	$a = b$ = 27.6, c = 125.6 $\alpha = \beta$ = 90, γ = 120	$a = b$ = 39.7, c = 42.0 $\alpha = \beta$ = 90, γ = 120
Space group	$P2_12_12$	$P6_422$	H3
Resolution (Å)	41.54–2.50 (2.59–2.50)	31.41–2.40 (2.49–2.40)	26.61–2.30 (2.38–2.30)
Total observations	26,729	20,663	5,748
Unique observations	7,260	1,398	1,094
Redundancy	3.7 (3.4)	14.8 (10.1)	5.3 (3.8)
Completeness (%)	99.9 (98.4)	100 (94.5)	100 (100)
I/σ	18.0 (11.6)	19.4 (3.6)	16.3 (2.4)
R_{merge} (%)	5.7 (8.1)	9.3 (42.3)	7.0 (36.9)
Refinement			
Resolution (Å)	41.54–2.50	23.93–2.40	19.87–2.30
R (%)	27.1	29.7	25.9
R_{free} (%)	29.5	30.2	27.3
Avg. B factor (Å^2)	30.2	45.1	46.9
RMSD			
Bonds (Å)	0.004	0.009	0.004
Angles (°)	0.88	1.46	0.97

3.0 Results & Discussion

3.1 System Design and Solution Characterization

3.1.1 *De novo* Tetrameric Coiled Coils

Peptide **1** was designed by Tavenor, *et al*. to fold as a tetrameric coiled coil and coordinate Cu^{2+} in a bis-Tpy fashion, however the resulting lattice only involved Tpy-Cu^{2+}-$Glu^{1/7}$ coordination.[82] Reducing the number of Glu residues in the primary sequence should impart control over the Tpy-Cu^{2+}-Glu coordination, and therefore control over the assembly. To probe this hypothesis, peptide **1** was redesigned yielding peptides **2** and **3**, which each contain only one Tpy and one Glu (Figure 17).

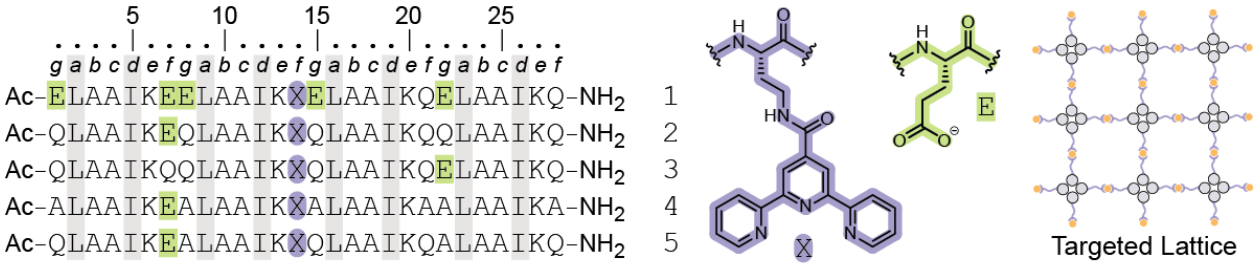

Figure 17. Sequences Peptides 1-5
Sequences of peptides 1-5 (left) which were designed to fold as tetrameric coiled coils and coordinate copper (X-Cu^{2+}-E) to form a tetragonal lattice (right).

To ensure that the *de novo* peptides folded as intended, and measure stability of the fold, circular dichroism (CD) experiments were performed. CD scans of peptides **2** and **3** display roughly equally intense minima at 208 nm and 220 nm, indicating that the coiled-coil fold was

retained after redesign,[93] however, a significant reduction in thermal stability was observed, as indicated by decreased melting temperatures of peptides **2** and **3** compared to peptide **1**. The numerous Glu residues in positions *g* of peptide **1** were originally intended to promote quaternary fold stability through favorable *e*-*g*′ salt bridges between Lys and Glu′ but the relatively high number of Glu residues allowed them to unintentionally participate in the coordination of copper. The purposeful Glu→Gln mutations introduced in the redesign to control copper coordination likely resulted in contacts between Lys and Gln′, both of which are H-bond donors. Repelling interactions between Lys (*e*) and Gln′ (*g*′) were hypothesized to be the cause of the reduced thermal stability of peptides **2** and **3**. To test this hypothesis, peptide **2** was redesigned to yield peptide **4** which contains only Ala residues in position *g* of the α-helix. CD results for this peptide indicate that the coiled-coil fold was retained, and thermal stability was restored (no measurable melting temperature) (Figure 18).

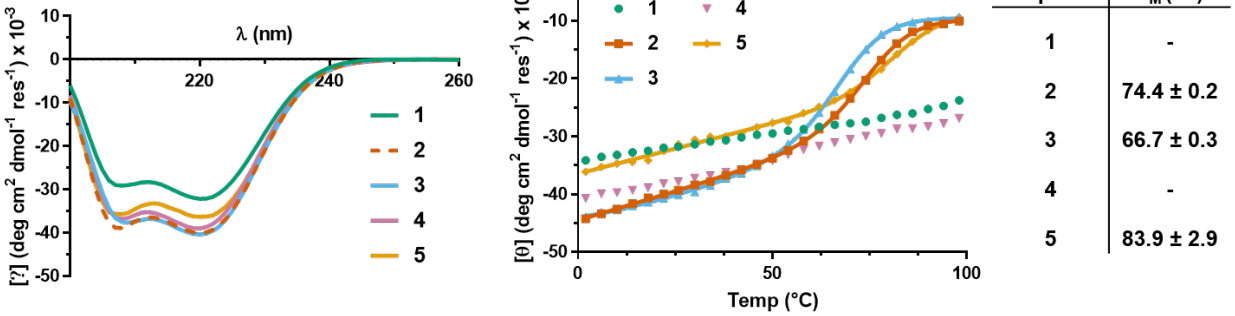

Peptide	T_M (°C)
1	-
2	74.4 ± 0.2
3	66.7 ± 0.3
4	-
5	83.9 ± 2.9

Figure 18. CD Peptides 1-5
CD scans (left) of peptides **1-5** show intense minima at 208 nm and 220 nm, indicating coiled-coil character. Thermal denaturation experiments (right) were used to determine the thermal stability of each peptide quaternary structure.

Increased incorporation of solvent-exposed Ala side chains in peptide **4** caused a significant reduction in aqueous solubility, and study of peptide **4** was abandoned. Finally, peptide

5 was designed as the "middle ground" between the solubility of peptide **2** and the stability of peptide **4**. Thus, it contains a mixture of Ala and Gln residues in position *g* of the coil (Figure 17), and as a result, has a melting temperature between those of peptides **2** and **4** (Figure 18).

3.1.2 *De novo* Trimeric Coiled Coils

Peptide **6** was designed by Tavenor, *et al*. to fold as a coiled-coil trimer and coordinate in an offset parallel fashion (hypothetical lattice not shown), but was also hindered by extraneous Glu residues, resulting in an unexpected crystalline assembly.[82] Similarly, peptide **7** was designed to self-assemble into an open hexagonal lattice, but crystals grown of this peptide were too fragile to yield conclusive diffraction data.[85] In a renewed effort to target the open hexagonal lattice, peptides **8** and **9** were generated with Tpy-Cu^{2+}-Glu coordination, thermal stability, and aqueous solubility in mind (Figure 19). The design of these peptides applied results from the tetramer series which indicated that incorporation of Gln in two *g*-positions, and Ala in the remaining *g*-positions imparted thermal stability on the coiled-coil quaternary structure without sacrificing aqueous solubility. These peptides were designed to self-assemble through two orthogonal driving forces: 1. The hydrophobic packing of *a* and *d* residues that causes the formation of a parallel coiled coil, and 2. The heteroligand coordination of copper by Tpy and Glu that results in the antiparallel arrangement of coils to yield a hexagonal lattice (Figure 20).

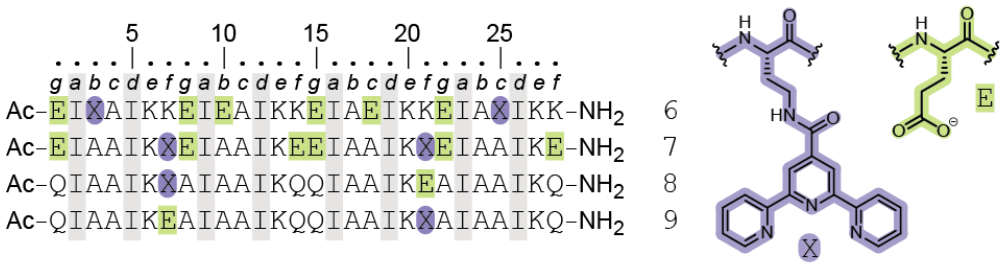

Figure 19. Sequences Peptides 6-9

Sequences of peptides **6-9** (left). Peptides **6** and **7** were the inspiration for the design of peptides **8** and **9**, which target the self-assembly of an open hexagonal lattice (right) via antiparallel X-Cu^{2+}-E coordination.

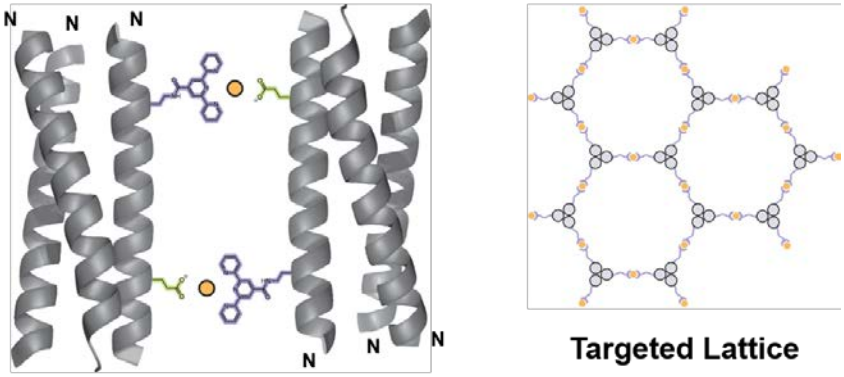

Figure 20. Antiparallel Coordination of Parallel Trimers

Peptides **8** and **9** were designed to fold as parallel coiled-coil trimers which self-assemble in an antiparallel fashion when coordinating copper (II) ion.

CD scans and thermal denaturation experiments for peptides **7-9** were performed in parallel and equally intense minima at 208 nm and 220 nm indicate the presence of a coiled-coil fold in all cases (Figure 21). The high thermal unfolding cooperativity of peptide **7** was unexpected since this peptide was based on a published prototype that did not show such cooperativity (CC-Tri).[17] Changes made to CC-Tri to generate peptide **7** seem to have induced a cooperative fold. However, the cooperative fold was absent in subsequent peptides **8** and **9**. This may indicate that the induced cooperative fold of peptide **7** was the result of incorporating two Glu residues in *f* positions, where peptides **8**, **9**, and CC-Tri have no carboxylate bearing side chains in any position *f*. Furthermore,

the difference in melting temperature for peptides **8** and **9** may be explained by the presence and location of the Tpy residue as precedented by two studies.

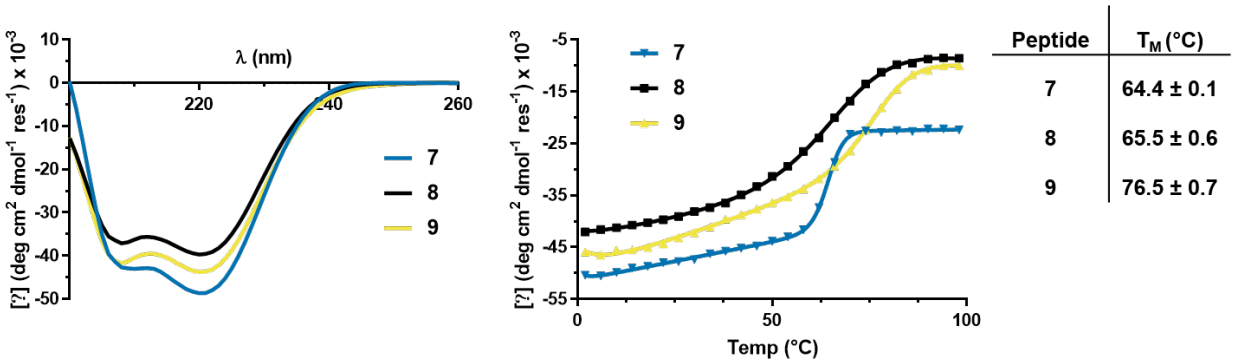

Figure 21. CD Peptides 7-9

CD scans (left) of peptides **7-9** indicate the presence of a coiled-coil fold via intense minima at 208 nm and 220 nm. Thermal denaturation experiments (right) indicate that all peptides melted, however, peptide **9** is the most thermally stable. Furthermore, peptide **7** shows an unexpected coorperative fold. For data concerning peptide **6**, please see Tavenor, N. A.; Murnin, M. J.; Horne, W. S. *J. Am. Chem. Soc.* **2017**, *139* (6), 2212-2215.[82]

In the first, Baldwin and co-workers probed the effect of polar side chain length on coiled coil stability with a series of peptides containing only Ala and R, where R was Lys, L-ornithine (Orn), 2,4-diamino-L-butyric acid (Dab), or 2,3-diamino-L-propionic acid (Dpr). They found that the length of the polar side chains affected helix propensity such that Lys-containing peptides were the most helical, and incorporation of shorter (Dab, Dpr, Orn) side chains significantly reduced helicity. As the Tpy residue used in our work is a functionalized Dab monomer, it follows that incorporation of Tpy residues would decrease the helicity of the secondary structure.[94]

Second, N-terminal residues of the α-helix are known to play a significant role in the folding of the secondary structure, and Hughes, *et al*. found that N-terminal Gln side chains participate in *i-i* and *i-i+3* hydrogen bonding with the backbone at the start of folding.[95] Once folded, the helix is stabilized by *i-i+4* backbone hydrogen bonding. However, peptide **8** contains a Tpy^7 residue with an amide at C_ε within range to disrupt the hydrogen bonding of Ala^3 during

and after folding. The coupled effect of Tpy helix destabilization and H-bond disruption thereby causes a more significant destabilizing effect in peptide **8** than in peptide **9**, since Tpy is closer to the N-terminus in peptide **8**.

3.2 Preliminary Crystallization Trials

The primary goal of this study was to control the morphology of the self-assembling lattice when these coiled-coil peptides are introduced to copper (II) ion. Thus, we performed X-ray crystallography for direct characterization of the resulting lattice and to obtain data bearing on the design hypotheses of metal coordination and peptide oligomer state.

In prior work, peptide **1** was crystallized to diffraction quality (2.1 Å) in 0.095 M BIS-TRIS pH 6.5, 5 mM sodium citrate pH 5.6, 0.125 M 1,6-hexanediol, and 9.5 mM copper (II) chloride.[82] While this peptide was structurally the most similar to peptides **2-5**, it was noted by the authors that the presence of terepthalic acid in the crystallization buffer generally improved the crystallization of their coiled-coil peptides. They posited that the ligand exchange of the carboxylic acid moieties of terepthalic acid and Glu coordinating to the copper ion facilitated the formation of the lattice. This trend was observed in newly performed crystallization trials of peptides **2** and **3**, where most of the crystals obtained grew in the presence of succinate, acetate, formate or citrate. Interestingly, no crystals of peptides **2** or **3** grew in the presence of terepthalic acid.

Crystallization screens of peptide **3** (15 mg/mL) with a commercial buffer kit (Index Screen, Hampton Research) in the absence of metal yielded aggregation in most wells. Crystals were observed in four conditions (Index 36, 73, 81 and 85), each containing 0.1 M Tris pH 8.5, PEG 3,350 or 1,500, and a chloride salt or carboxylic acid. Two of the four wells contained crystals

that were not amenable to X-ray data collection. Of the remaining wells containing crystals in this screen, one of them appeared to be peptidic (Index 81). However, this crystal appeared badly twinned and thus no diffraction data were collected. This screen was repeated for peptide **3** with added copper (II) chloride (10 mM, ~2 eq) in the drop. None of the aforementioned buffers yielded crystals in the presence of $CuCl_2$, but crystals were observed in five new conditions (Index 15, 19, 22, 27, and 89), most containing a carboxylic acid component. One of the five wells may have contained peptidic crystals (Index 27), but they grew in a large cluster and obtaining a single crystal for diffraction analysis proved impossible. At this point in crystallization trials, no more peptide **3** was available, so subsequent experiments were aimed at peptide **2**.

The quantity of peptide **2** available was not sufficient to perform a full screen, so an optimization around Index 81 (0.1 M Tris pH 8.5, 0.1-0.25 M ammonium acetate, 15-40% PEG 3,350) which grew crystals of peptide **3** in the absence of copper, was carried out in the presence of 10 mM $CuCl_2$. This experiment resulted in many single crystals which were observed to be peptidic but diffracted weakly (14-8 Å). Replicates of these crystals were sent to the APS synchrotron radiation source from which four datasets were collected, some to ~3.5 Å. However, none of the acquired datasets were amenable to processing, and all peptide stocks were depleted.

Ultimately, the low quality of crystals obtained for peptides **2** and **3** is likely the result of poorly ordered lattices. However, the fact that these lattices formed at all is a positive indication that, in these systems, metal coordination drives assembly into higher ordered structures. This conclusion is supported by those crystals which grew in the copper-containing formulations but not in the analogous metal-free buffers. Furthermore, it is possible that the targeted open tetragonal lattice had formed but resulted in a crystal that was less mechanically robust than a one of a packed

lattice would have been, facilitating the decomposition of the crystal upon freezing and/or exposure to a high-powered X-ray beam.

Interestingly, crystals of peptide **3** grew in the absence of copper in Index 81, but not with copper present. However, peptide **2** was the opposite, growing crystals only in the presence of copper. Crystallization of peptide **2** sans copper may have been hindered by the length and electron density of the Tpy residue, which may have prevented surface-level interactions between coils, while failing to facilitate Tpy-Tpy stacking interactions. It is possible that peptides **2** and **3** would have more readily crystallized sans copper if they had more than one solvent-exposed Tpy residue, since Tpy-Tpy stacking interactions are well precedented in these systems. Therefore, crystals of peptide **2** grown in the presence of copper likely coordinated in the expected fashion.

No crystallization trials for peptide **4** were performed, as it was not soluble to 15 mg/mL used for previous crystallization experiments. Index Screen (1-48) was performed for peptides **5**, **8**, and **9** (10 mg/mL) in the presence of 5 mM $CuCl_2$ (~1.5 eq). The concentrations of $CuCl_2$ and peptide were reduced from 15 mg/mL and 10 mM, respectively, in order to ameliorate the high percentage of aggregated drops observed in Index Screen for peptides **2** and **3**. A large majority of peptide **5** drops aggregated anyway, while drops of peptides **8** and **9** showed significantly less aggregation upon drop completion and resulted in multiple useful hits within a few days for optimization and diffraction analysis.

High propensity for aggregation and low likelihood of crystallization of tetrameric peptides **2-5** compared to low instances of aggregation and a high number of crystal-yielding conditions for trimeric peptides **8** and **9** led us to focus our efforts on the trimer series.

3.3 Coiled-Coil Assemblies Observed for the Trimer Series

3.3.1 Crystal Form 9*a*

The first solvable crystal form (**9***a*) for peptide **9** was found to be in space group P 2_1 2_1 2. This crystal grew in modified Index #43 (0.1 M BIS-TRIS pH 6.5; 25% w/v PEG 3,350; 5 mM $CuCl_2$) with no optimization. The structure was solved to 2.5 Å and had six unique chains forming two unique trimers in the asymmetric unit (Figure 22).

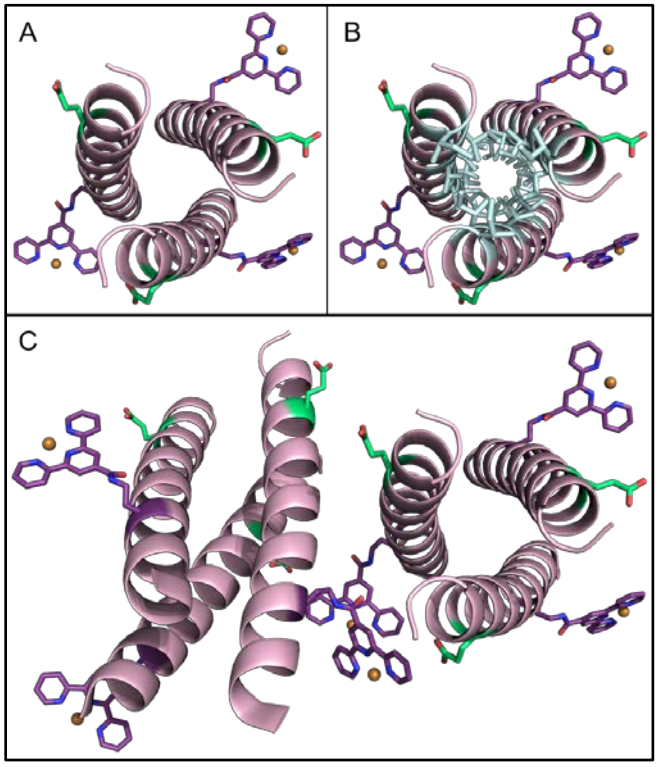

Figure 22. Crystal Form 9*a*: Parallel Trimeric Coiled Coil
A) Single left-handed, parallel trimer formed by three unique chains (N-termini in the foreground). B) Ile hydrophobic core highlighted in light blue C) Asymmetric unit composed of six unique chains, and two trimers. Glu residues highlighted in green, Tpy residues highlighted in violet.

The trimers in the asymmetric unit were associated via a polar contact (3.2 Å) between the amide oxygen of the Tpy residue from one trimer and a Lys^{13} from the other trimer (Figure 23). The nearby Glu residue of the same trimer as Lys^{13} was too far to have participated in the polar contact (6.6 Å). Out of six Tpy side chains in the asymmetric unit, two of them were found participating in only the designed Tpy-Cu^{2+}-Glu coordination mode. These coordination events had a crisscrossed arrangement, so that trimers which coordinated the same copper ion were arranged in an antiparallel fashion (Figure 24).

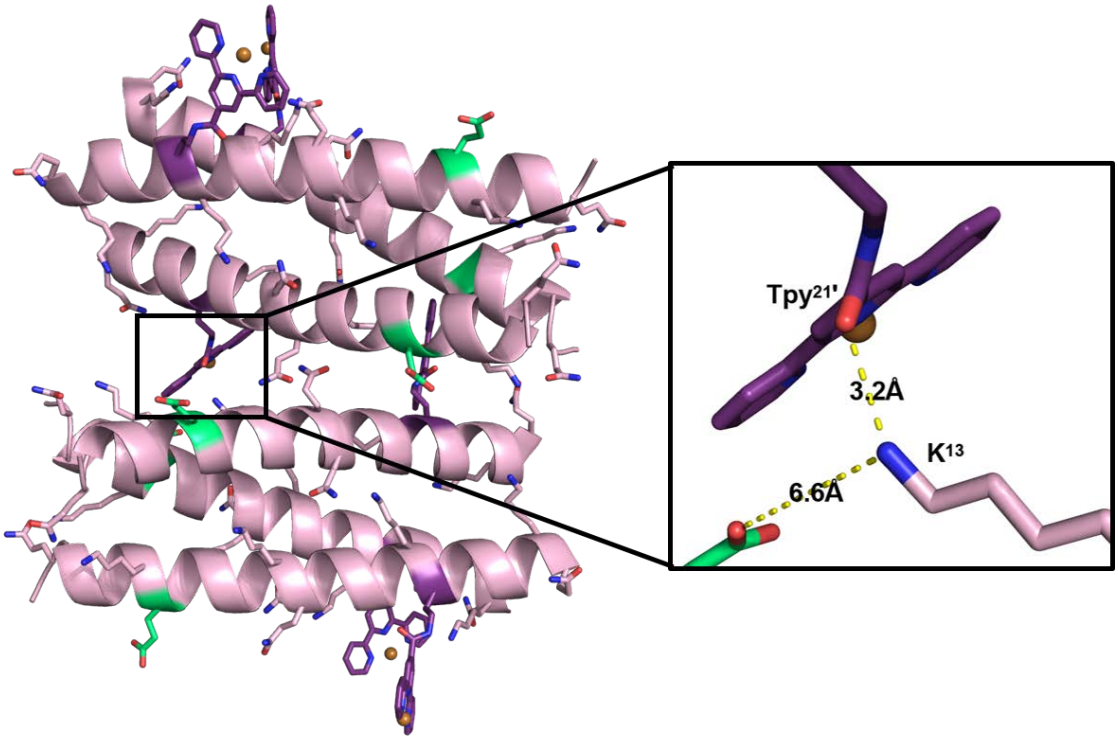

Figure 23. Lys^{13}-$Tpy^{21\prime}$ Polar Contact in Crystal Form 9*a*
Side view of asymmetric unit which is associated via a polar contact between Lys^{13} and Tpy^{21} on opposite coils. Distance between Lys^{13} and nearby Glu is too long to be considered an effective salt bridge.

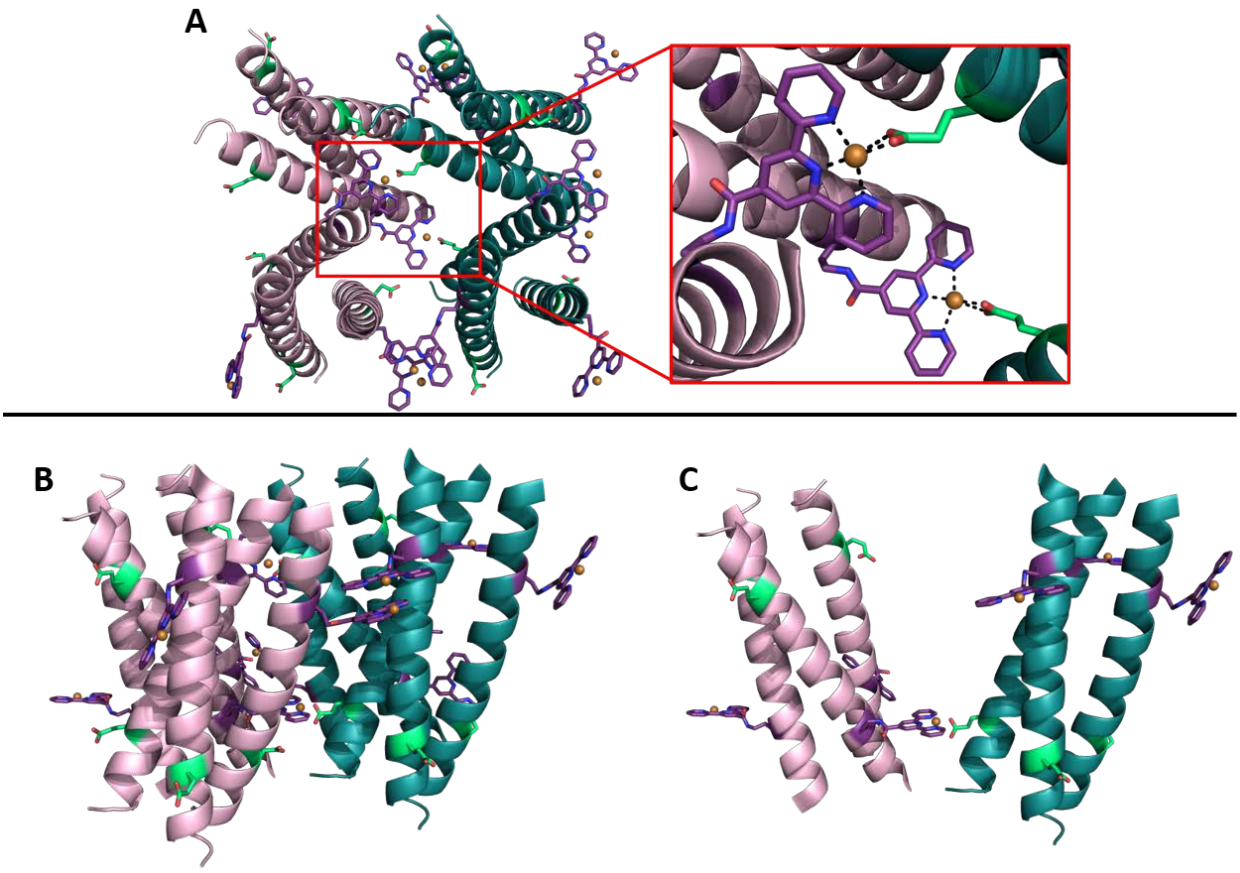

Figure 24. Discrete Copper Coordination Observed in Crystal Form 9*a*

(A) Two asymmetric units (top view) designated by different colored backbones found to coordinate two unique copper ions in an under-over (crisscrossed) fashion. (B) Side view of (A). (C) Trimers found on opposite sides of the same copper ion coordinated copper in an antiparallel fashion (Glu residues located near N-terminii).

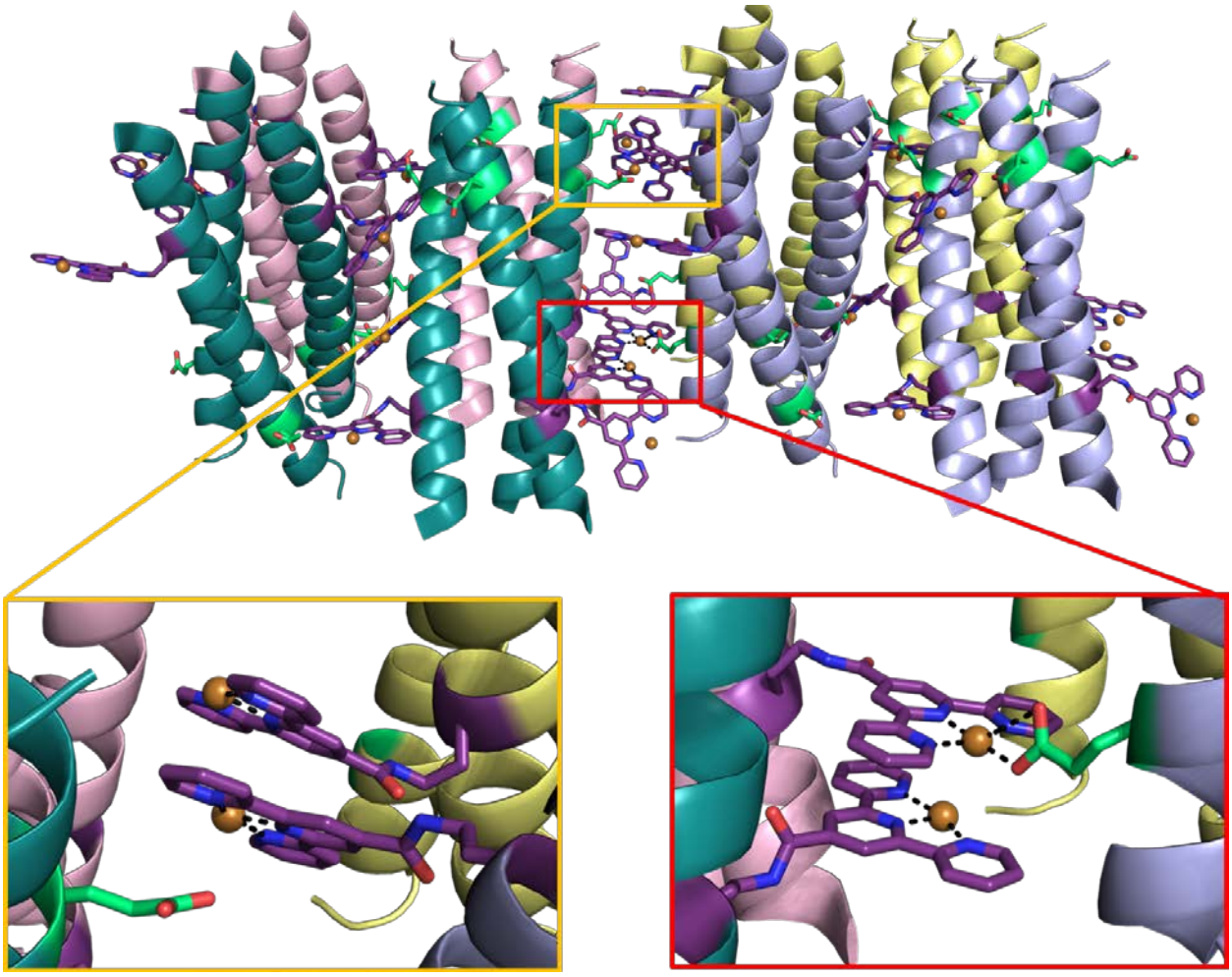

Figure 25. Interface Between Four Asymmetric Units of Crystal Form 9*a*
Generation of four symmetry mates gives a clear view of an example of Tpy-Tpy stacking interactions present with (right) and without (left) accompaniement by Tpy-Cu^{2+}-Glu coordination.

Three of six Tpy residues in the asymmetric unit were found to exclusively participate in Tpy-Tpy stacking interactions, an example of which is shown in Figure 25. The remaining Tpy residue participated in both Tpy-Cu^{2+}-Glu coordination and Tpy-Tpy stacking interactions (Figure 25). Thus, the apparent driving forces for self-assembly of this supramolecular structure are hydrophobic interactions (forming each trimer), Tpy-Tpy stacking interactions, polar contacts, and the intended coordination of copper (II) ion. This crystal form supports some of the coordination assembly design principles, as the supramolecular architecture was driven by metal-directed self-assembly of the peptides, and coils coordinated copper in an antiparallel fashion.

3.3.2 Crystal Form 9*b*

The second crystal form (**9***b*) found for peptide **9** resulted from a single crystal that grew in modified Index #1 (0.1 M citric acid pH 3.5; 2.0 M ammonium sulfate; 5 mM $CuCl_2$) with no optimization. With space group P 6_4 2 2, this crystal form had a single chain in the asymmetric unit which formed an antiparallel tetrameric coiled coil through two two-fold rotation operators (Figure 26) which associated end-to-end through a six-four screw axis (Figure 27). The tetrameric coils propagate through 60° rotations, giving the Tpy side chains a crisscross appearance (Figure 28).

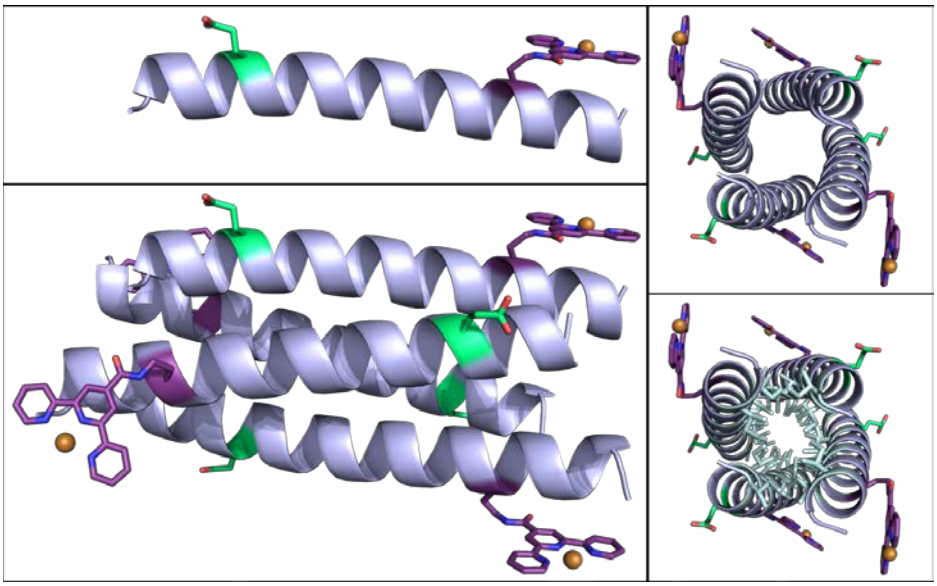

Figure 26. Crystal Form 9*b*: Antiparallel Tetrameric Coiled Coil
(Top left) Asymmetric unit of crystal form 9*b* contains a single α-helixal chain which forms an antiparallel tetrameric coiled coil through symmetry operators (bottom left). (Top right) Top view of a single tetramer and (bottom right) top view with hydrophobic core highlighted in light blue.

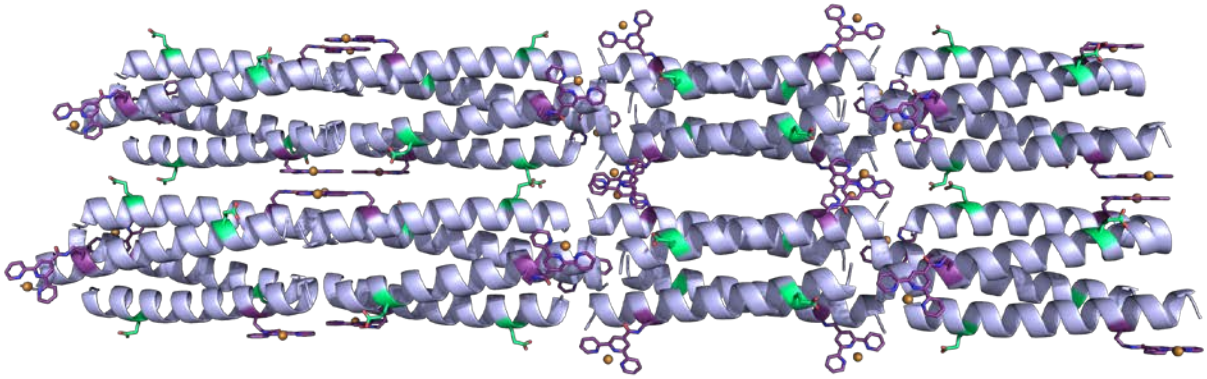

Figure 27. Side View of Crystal Form 9*b* Lattice
Side view of P 6_4 2 2 lattice shows Glu residues (green) are not involved in contacts between tetramers. Instead, they point outward. Tetramers are primarily associated through Tpy-Tpy stacking interactions.

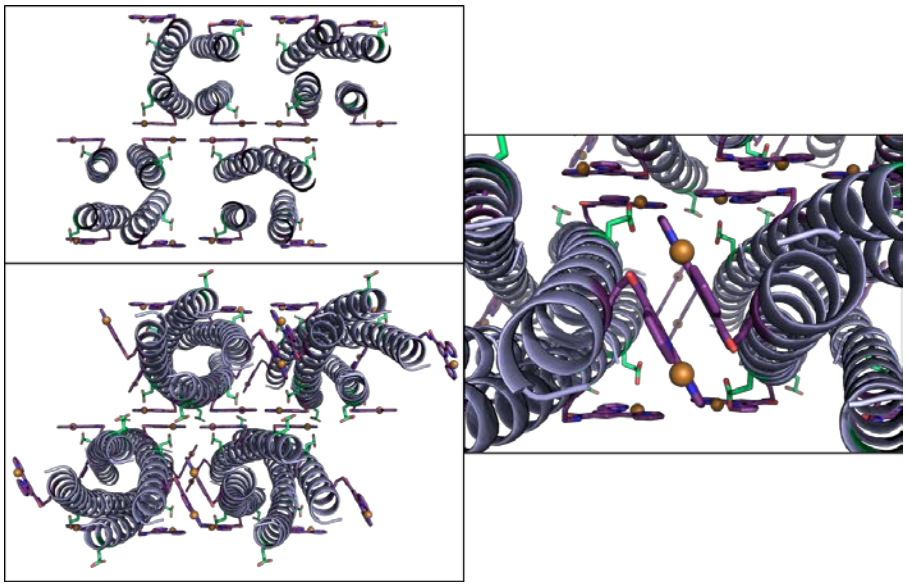

Figure 28. Top View of Crystal Form 9*b* Lattice
(Top left) Cross sectional image of four tetramers show discrete Tpy-Tpy stacking interactions. (Bottom left) Propagation in z-direction with 60° rotation gives Tpy residues a criss-cross appearance. Each tetramer interacts with four different coils to form the lattice. (Right) Closeup of Tpy stacking in the foreground. Each tetramer has rotated 60° to build bundles with crisscrossing Tpy residues.

While the elucidation of an ideal antiparallel homotetrameric coiled-coil structure is fascinating, we were surprised to see such a high-symmetry lattice resulting from a tetrameric coiled coil, since peptide **9** was expressly designed to fold as a trimer. The oligomerization state

of peptide coiled coils is specified by the side chains which form the hydrophobic core. Peptide **9** was designed based on a prototype trimer (CC-pII) which contained only Ile residues in positions *a* and *d* of the helix heptad and was confirmed to fold as a trimer by analytical ultracentrifugation and X-ray crystallography.[17] Thus, an obligatory exploration of the literature surrounding antiparallel tetramers followed.

Some work has been conducted by Ghadiri, *et al*. to determine what single mutations could drive a parallel homotetramer to fold in an antiparallel fashion.[96] In this work, it was found that a single substitution of Ser for Glu in helix position *e* was enough to change the oligomerization mode, and crystals of parallel and antiparallel bundles were obtained in the same crystallization condition. Furthermore, one of the designed parallel homotetramers was found to fold in antiparallel and parallel modes in different crystallization conditions. The authors concluded that both oligomers exist in solution, albeit the antiparallel at low concentration, and that the transition energy between antiparallel and parallel coils was surprisingly low.

An earlier work by Alberti and co-workers determined that uncharged residues at positions *g* and *e* may contribute to the antiparallel homotetramer fold of a *lac* repressor protein.[97] Another, more recent, study by Deng, *et al*. probed the formation of an antiparallel homotetramer defined by a 3-3-1 heptad of nonpolar residues by mutating some charged residues in position *g* to Ala, and concluded that not only does the placement of oppositely charged residues at positions *g* and *e* facilitate favorable salt bridges in the parallel coil, they also reduce the propensity to fold in an antiparallel fashion.[98]

In examining these precedented studies of antiparallel homotetramers, some conclusions regarding crystal form **9***b* can be drawn, as peptide **9** fits a few of the published criteria. First, salt bridges at the interface between *g* and *e* positions were intentionally removed from the sequence

to exert control over the coordination of copper (II) ion, effectively removing the protection from antiparallel coiling they may have imparted.[98] Likewise, uncharged residues were used in position *g*: Gln and Ala.[97-98] Originally, these positions were occupied by Gln exclusively (peptides **2** and **3**), but half of them were changed to Ala in the subsequent designs (peptides **8** and **9**) since the number of Gln residues was suspected of reducing the stability of the quaternary structure. Substituting Ala in some positions *g* then opened the possibility of extending the hydrophobic core as was seen by Deng, *et al*.[98]

While literature precedent may offer some insight into driving forces behind the formation of an antiparallel homotetramer, these insights are offered only as possibilities. Notably, the asymmetric unit of crystal form **9***b* contained a solvent model composed of two water molecules, one citrate ion, and one sulfate ion, whereas the solvent model for crystal form **9***a* contained 119 water molecules and six chloride ions. The significant difference in solvent content between these two crystal forms may indicate that crystal form **9***b* is a result of the crystallization buffer condition. This condition contained a high concentration of ammonium sulfate (2.0 M), which may have disrupted the trimeric fold. Furthermore, crystal form **9***b* grew in a pH of 3.5, a value below the pK_a of the γ-carboxylate of the Glu residue (4.25). This highly acidic environment likely resulted in the protonation of the Glu side chain which may have prevented the Tpy-Cu^{2+}-Glu coordination we desired. Thus, we believe that the antiparallel homotetramer is not an accurate representation of peptide **9** in a solvated model, and that the peptide likely folds as a parallel trimer in solution, as indicated by crystal form **9***a*.

3.3.3 Crystal Form 8

The final crystal form obtained in this study was of peptide **8** in space group H 3. This crystal grew in an optimized modified Index #45 (0.1 M Tris pH 8.5; 25% PEG 3,350; 5 mM $CuCl_2$) and represents the structure which most closely supports our central hypotheses of controlling metal-directed coiled coil assembly. The peptide adopted a parallel coiled-coil trimer fold formed by a 3-fold crystallographic rotation and the structure was solved to 2.3 Å (Figure 29).

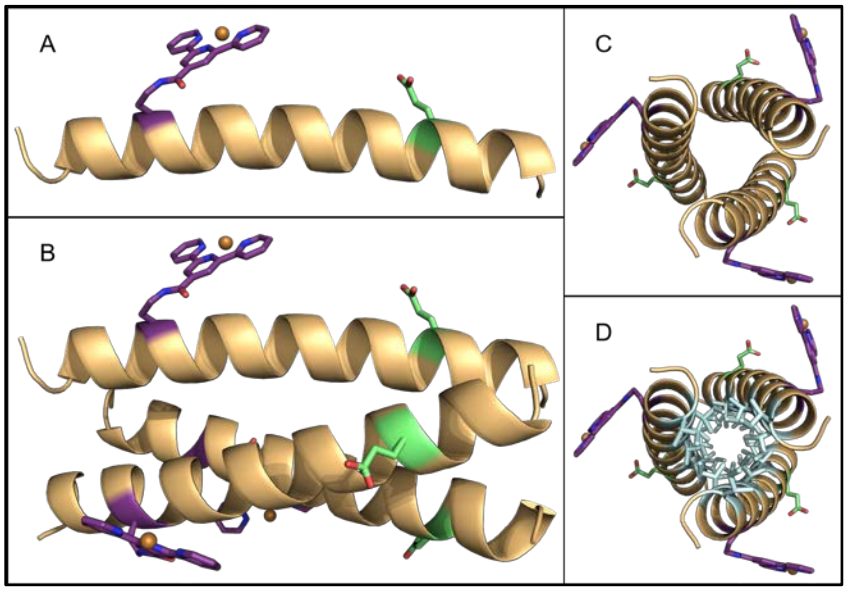

Figure 29. Crystal Form 8: Parallel Trimeric Coiled Coil
(A) Asymmetric unit of crystal form **8**. (B) Left-handed parallel rimer formed by 3-fold crystallographic rotation of asymmetric unit (N-terminus on the left). (C) View of trimer from top (N-terminus in foreground). (D) Highlighted hydrophobic core in light blue.

All Tpy and Glu residues participate in the desired coordination mode of copper, and no π-stacking between Tpy residues was observed (Figure 30).

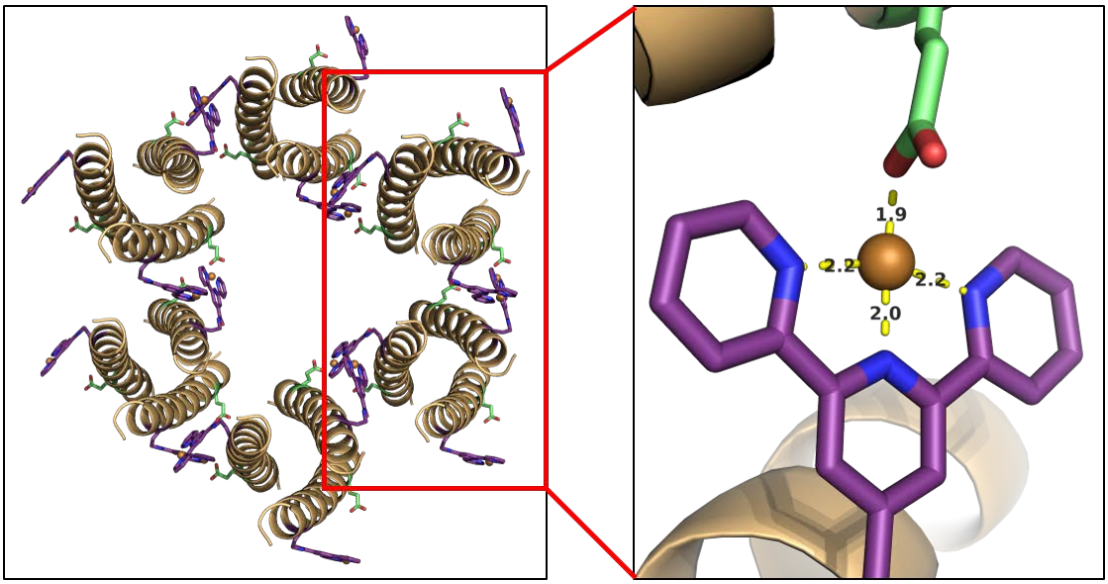

Figure 30. Intercoil Association via Intended Coordination Mode in Crystal Form 8
Trimers associate via only the intended Glu-Cu^{2+}-Tpy coordination to form a hexagonal lattice. Each Tpy of one trimer coordinates with a Glu from three different nearby trimers. Polar contact distances measured in Ångstroms.

The coordination of copper in this fashion resulted in a packed hexagonal lattice in which each trimer is the vertex of multiple unique hexagons (Figure 31).

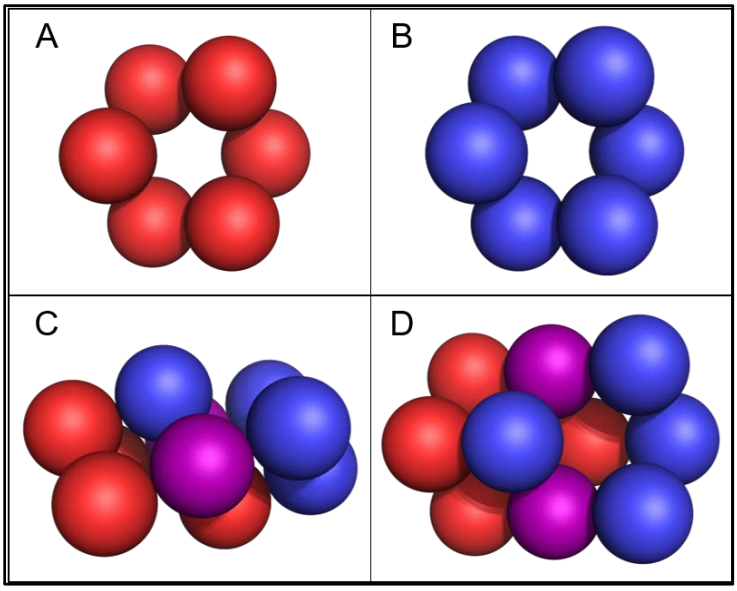

Figure 31. Trimer Packing Observed in Crystal Form 8
Packing arrangement of coiled-coil trimers as represented by their Van der Waals radii (spheres). (A) and (B) left and right, and top and bottom hexagons, respectively, which share two verticies (highlighted in purple) to pack together. (C) Side view of the two packed together. (D) Top view.

Crystal form **8** represents a perfect coiled-coil trimer as it is formed via symmetry operators. This trimer was compared to its predecessor (peptide **6**), and C_α alignment gave an RMSD of 1.220 Å (Figure 32).

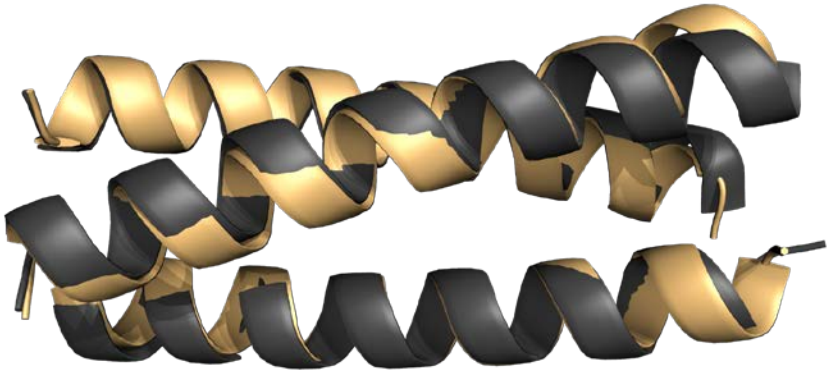

Figure 32. C_α Alignment of Peptides 6 and 8
Crystal form **8** (gold) aligned with published structure for peptide **6** (black) by C_α, with no correction to yield RMSD of 1.220 Å. Trimers are positioned with N-terminus to the left. Peptide **6** PDB ID: 5U5B[82]

Peptide **6** deviates from the ideal 3-fold symmetry near its termini. Upon further investigation, this deviation was revealed to be caused by Tpy-Tpy stacking. Specifically, each terminus in the structure of peptide **6** was moved slightly outwards to accommodate a noncovalent interaction with another nearby Tpy residue in the previously reported lattice (Figure 33).

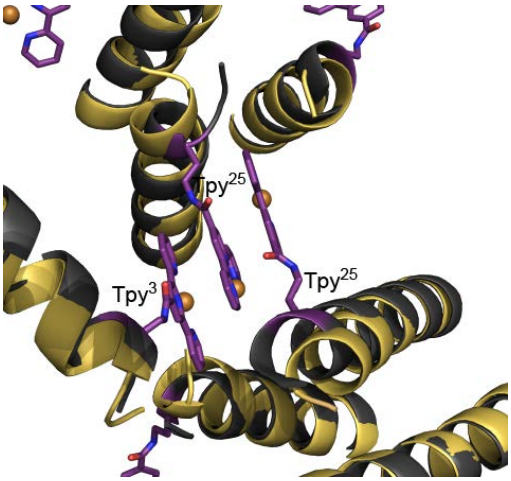

Figure 33. Tpy Stacking in Peptide 6 Structure Causes Deviation from Ideal Trimer
Representative Tpy stacking interactions between three different Tpy residues near the termini of peptide **6** (black) which cause backbone deviation from an ideal trimer, peptide **8** (overlaid in gold). Peptide **6** PDB ID: 5U5B[82]

Crystal form **8** is thus far the closest result to the desired open hexagonal net. This lattice self-assembled via two orthogonal driving forces: hydrophobic interactions forming each coiled-coil, and metal coordination of copper (II) ions. Intercoil interactions are present only as the intended coordination of copper, therefore, control over the assembly mode was effectively exerted.

4.0 Conclusion

Protein-based materials have been studied for decades, but the field of nanoscale peptide-based materials is still relatively new. In nature, many proteins self-associate through interfacial noncovalent interactions to form protein complexes with specific function, whether they be catalytic, structural, or otherwise. Similarly, organic and inorganic chemists have worked to develop functional, self-assembling scaffolds amenable to fine tuning at the molecular level, and the field of nanomaterials has flourished. Our research lies at the intersection of these two schools of thought, attempting to build novel nanomaterials out of large synthetic molecules which assemble through the union two orthogonal mechanisms: one reminiscent of natural protein complexes, and one developed by materials scientists.

At the start of this study, we intended to exert control over the assembly of synthetic coiled-coil tetramers which had arisen from a recent serendipitous observation. At the time, redesign of peptide **1** seemed as though it would be a promptly fruitful endeavor, as diffraction quality crystals were obtained showing that the coils had assembled in a packed fashion,[82] and thus was thought to be close to the targeted lattice. We sought to control the assembly by removing extraneous Glu residues thereby restraining the coils to one possible mode with which to coordinate copper. After a nontrivial amount of work toward this goal, no obtained data could bear on the hypothesized lattice, and the exploration of the tetramers was abandoned. However, some data collected on the tetramer series allowed for optimization of design principles which were applied to the trimers.

The presented trimeric coiled coils represent a thought experiment made real. This series of peptides was not expected to work as well as it did, since no useable crystals of the parent sequence, peptide **7** were ever obtained. Nonetheless, we applied the improved design principles

from the tetramer series to the trimers in an attempt to build an open hexagonal net with the caveat that the change in Tpy position caused some unexpected effects on fold stability. Nonetheless, we succeeded in producing a hexagonal assembly as we intended.

Arguably the presented hexagonal self-assembly of peptide **8** is a big step toward the understanding of how to design such a lattice with these building blocks. Some interesting future directions of this study might include redesign of the termini of peptide **8** to prevent the formation of a packed lattice. Perhaps symmetrical incorporation of Lys at the termini would achieve this goal, or else larger, unnatural residues may be considered. It is also possible that the assembly of peptide **8** in solution phase is an open net as was intended. This may be elucidated through dynamic light scattering (DLS), atomic force microscopy (AFM), or transmission electron microscopy (TEM) experiments.

Furthermore, the observed ideal antiparallel homotetramer adds to a small but growing body of work surrounding this oligomer state. An analysis of the solution phase oligomer states of peptides **8** and **9** would likely offer deeper insight into whether the antiparallel homotetramer was an artifact of the crystallization components, or whether the hydrophobic core allowed for real oligomerization ambiguity. Gel-permeation chromatography may be able to answer this question.

Considering the results of this study as a whole, it may be worthwhile to explore Tpy and Glu placement in subsequent design principle optimization. In the tetramer series, a single solvent-exposed Tpy was displayed in the middle of the chain, while the trimers had Tpy near either the N-terminus or the C-terminus. It was suggested that the presence of Tpy near the N-terminus of a trimeric coiled coil decreased the stability of the fold, and one could argue that the presence of Gln near the N-terminus in tetrameric peptide **2** had the same effect. Peptide **5** was the most stable of all peptides that melted, and it included an N-terminal Glu. It would be interesting to focus further

study on the differences between peptides **5** and **9**, since they only differ in hydrophobic core and Tpy placement and one folded as an antiparallel homotetramer (**9**). Study of these two peptides in depth may shed some light on the interplay between parallel and antiparallel homotetramers.

For now, the collective results of this study validate our design principles and represent a shift from serendipity to rational design previously absent from these metal-driven *de novo* synthetic peptide coiled-coil supramolecular assemblies.

Appendix A NMR Spectra of 4-Carboxy Tpy

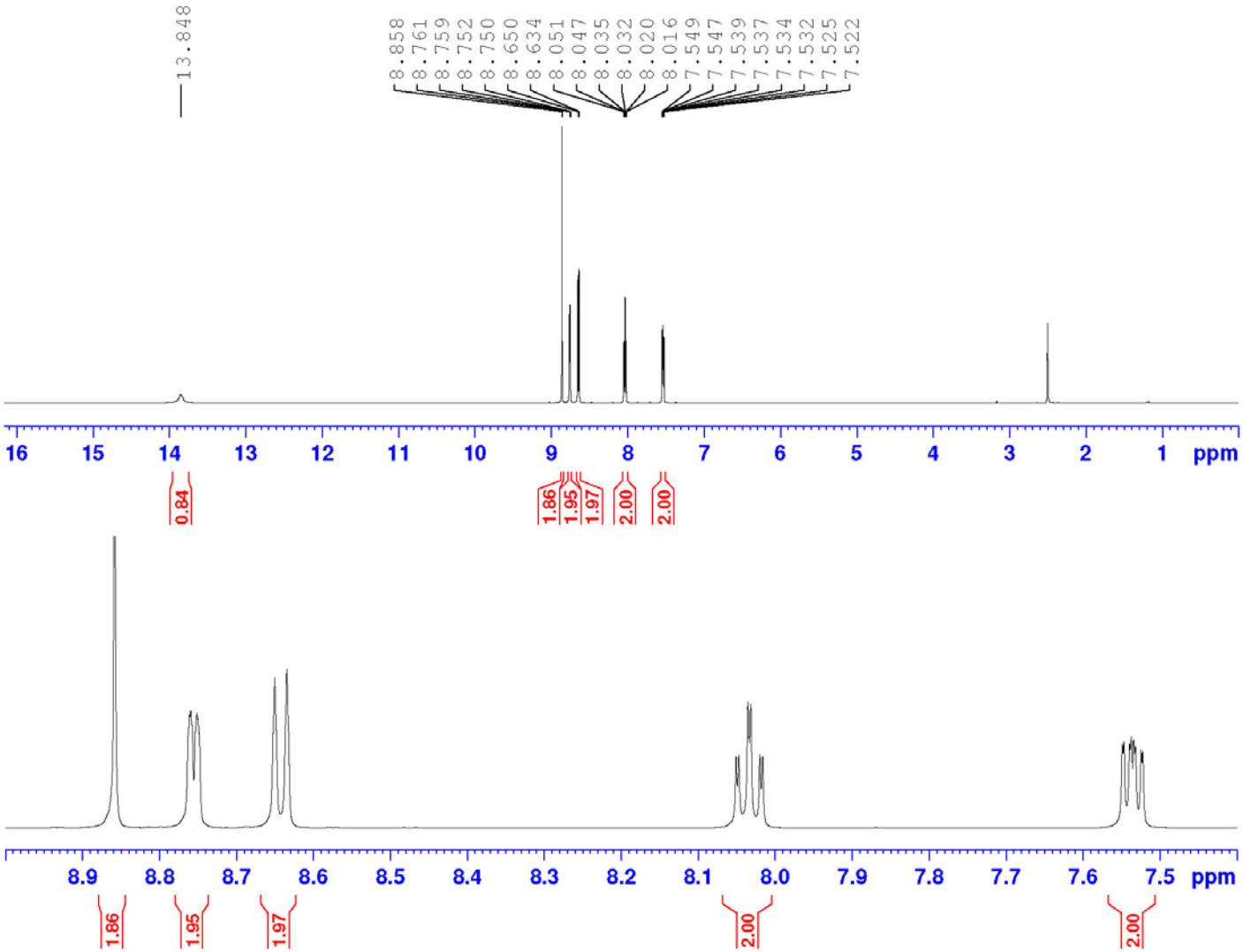

Figure 34. ^{1}H NMR Spectrum of 4-Carboxy Tpy

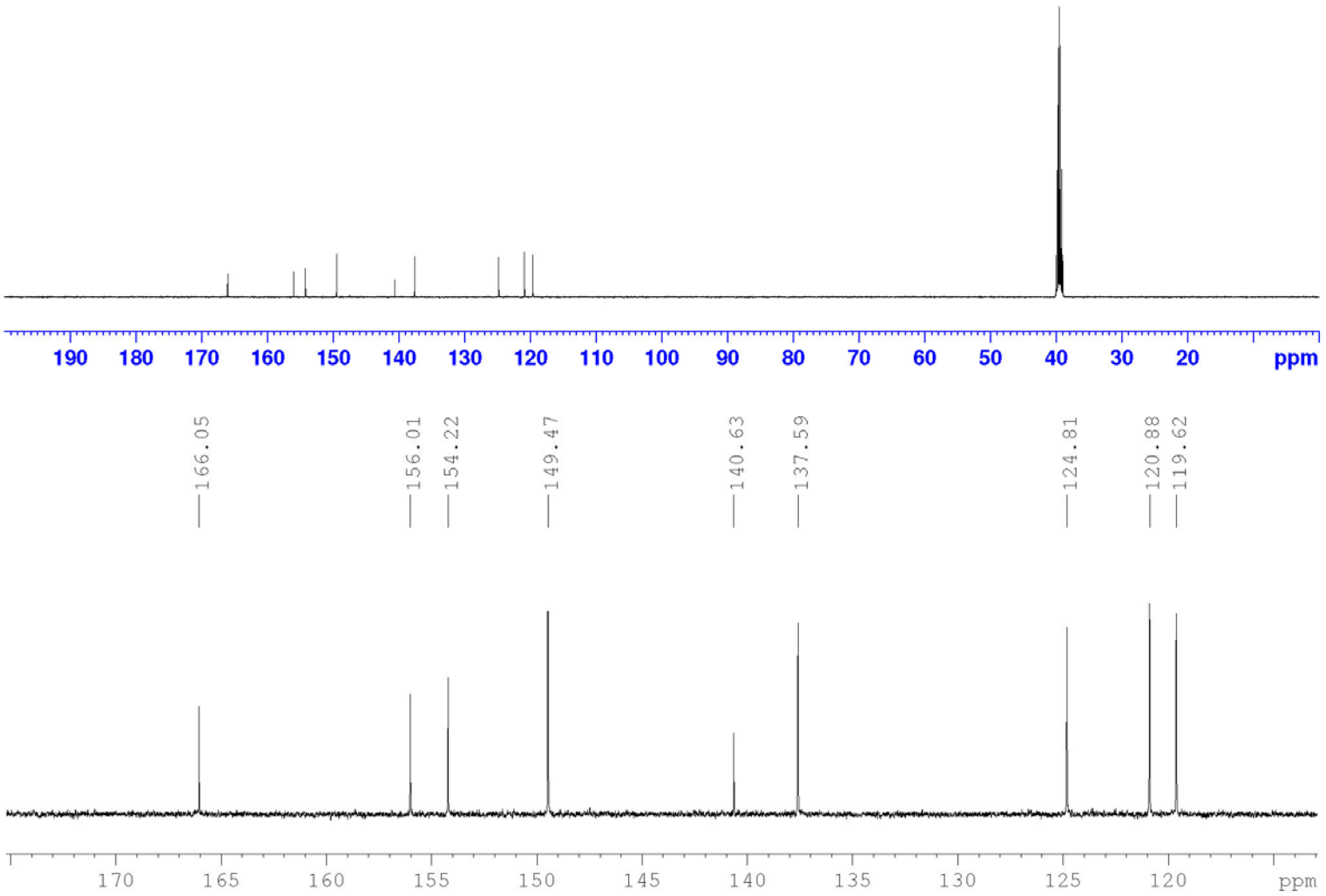

Figure 35. ^{13}C NMR Spectrum of 4-Carboxy Tpy

Appendix B Mass Spectrum of 4-Carboxy Tpy

C:\Xcalibur\data\Horne\78110ESIN 08/09/17 15:40:07 KAS-1-080
DMF+ACN

78110ESIN#30-63 RT: 0.13-0.28 AV: 34
T: FTMS - p ESI Full ms [100.00-500.00]
m/z= 276.00000-277.00000

m/z	Intensity	Relative	Theo. Mass	Delta (ppm)	Composition
276.07688	616549824.0	100.00	276.07730	-1.54	$C_{16}H_{10}O_2N_3$

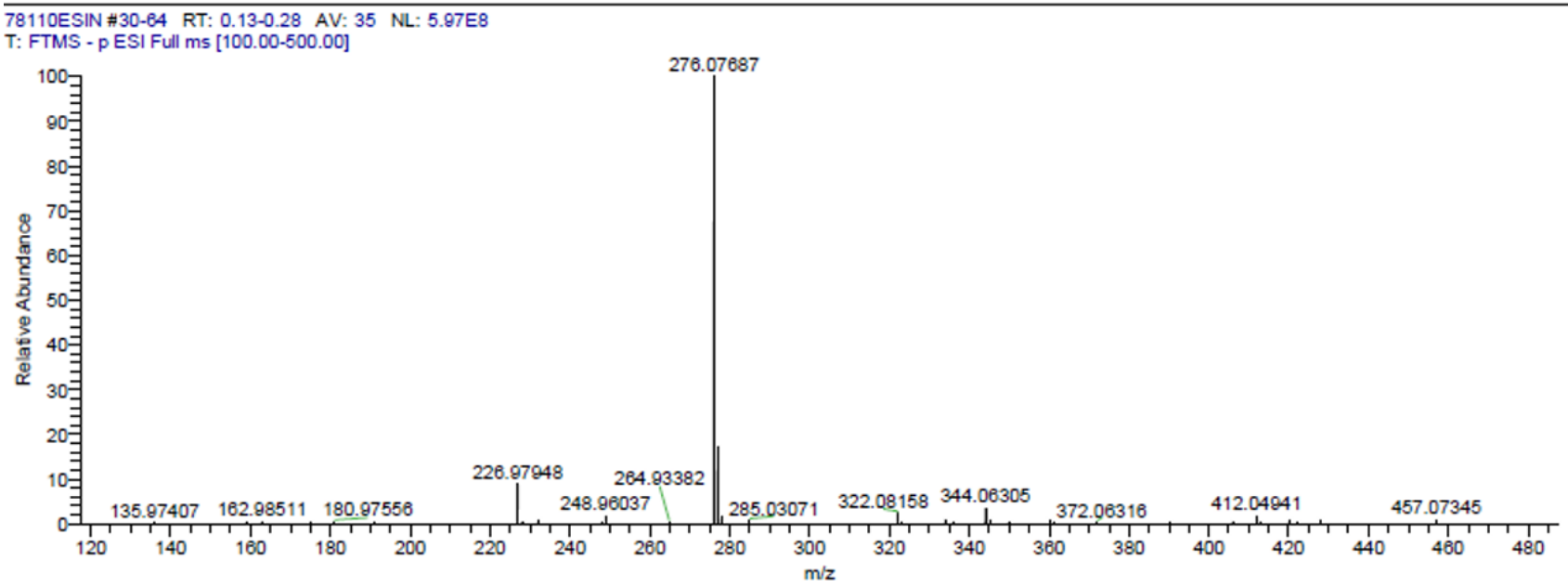

Figure 36. Elemental Composition and HRMS of 4-Carboxy Tpy

Appendix C Peptide MALDI-TOF Spectra

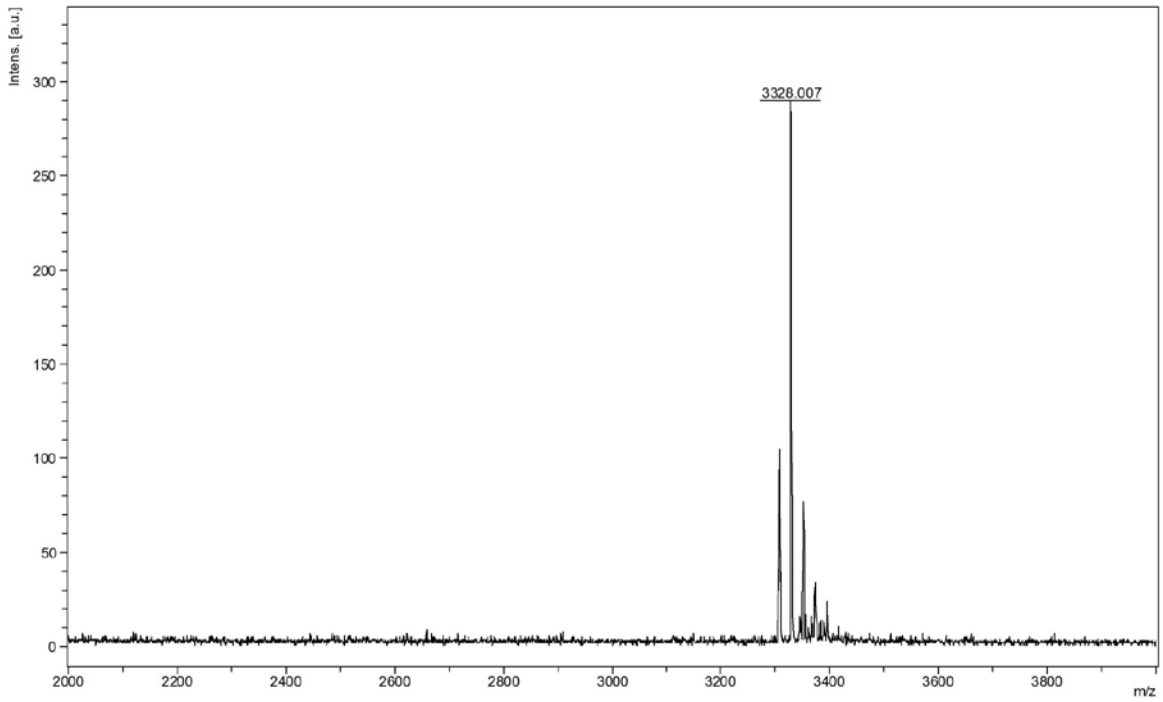

Figure 37. Peptide 1 Full Spectrum

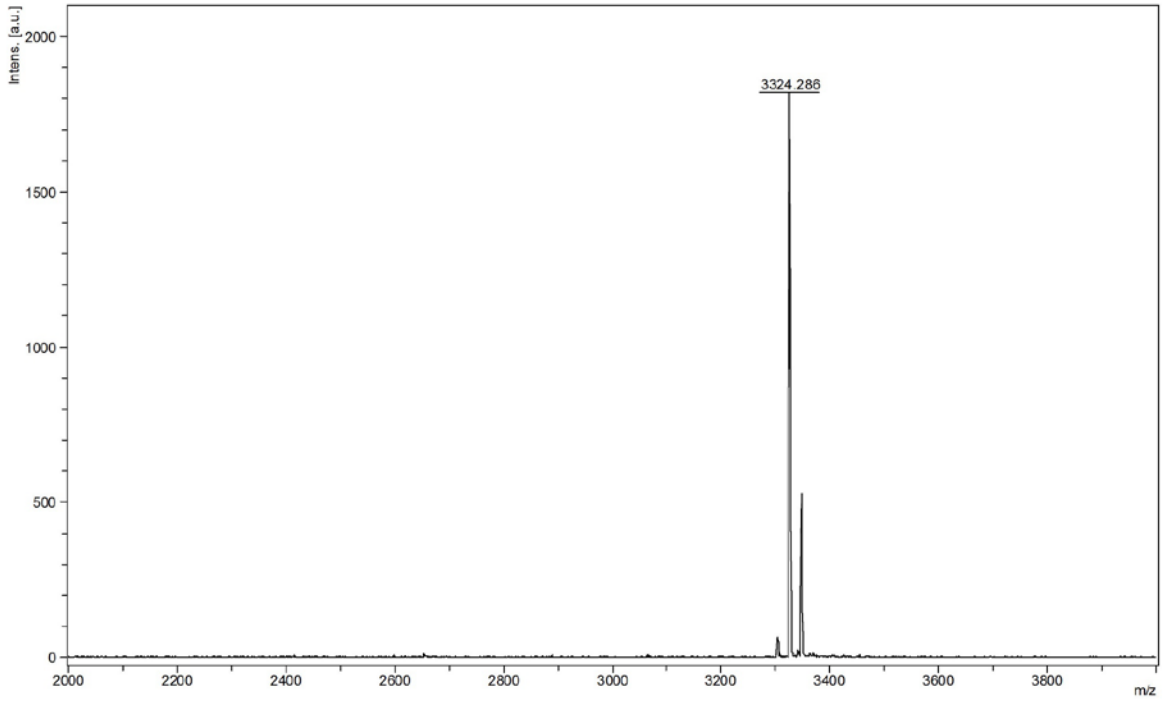

Figure 38. Peptide 2 Full Spectrum

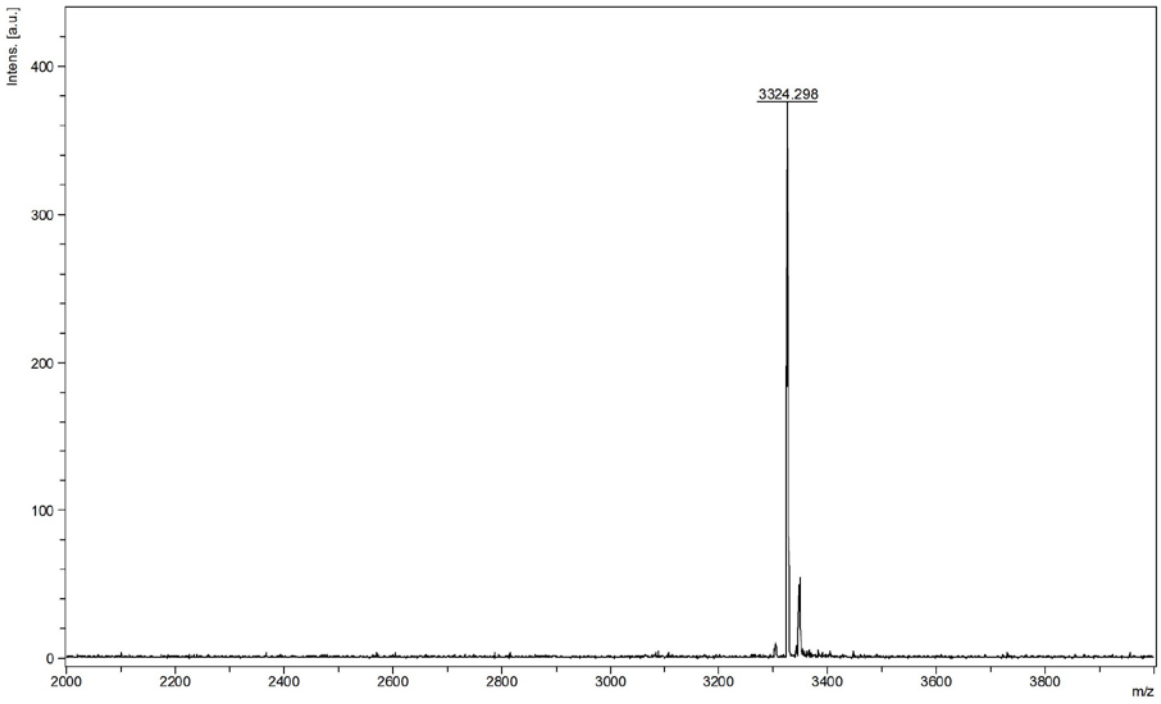

Figure 39. Peptide 3 Full Spectrum

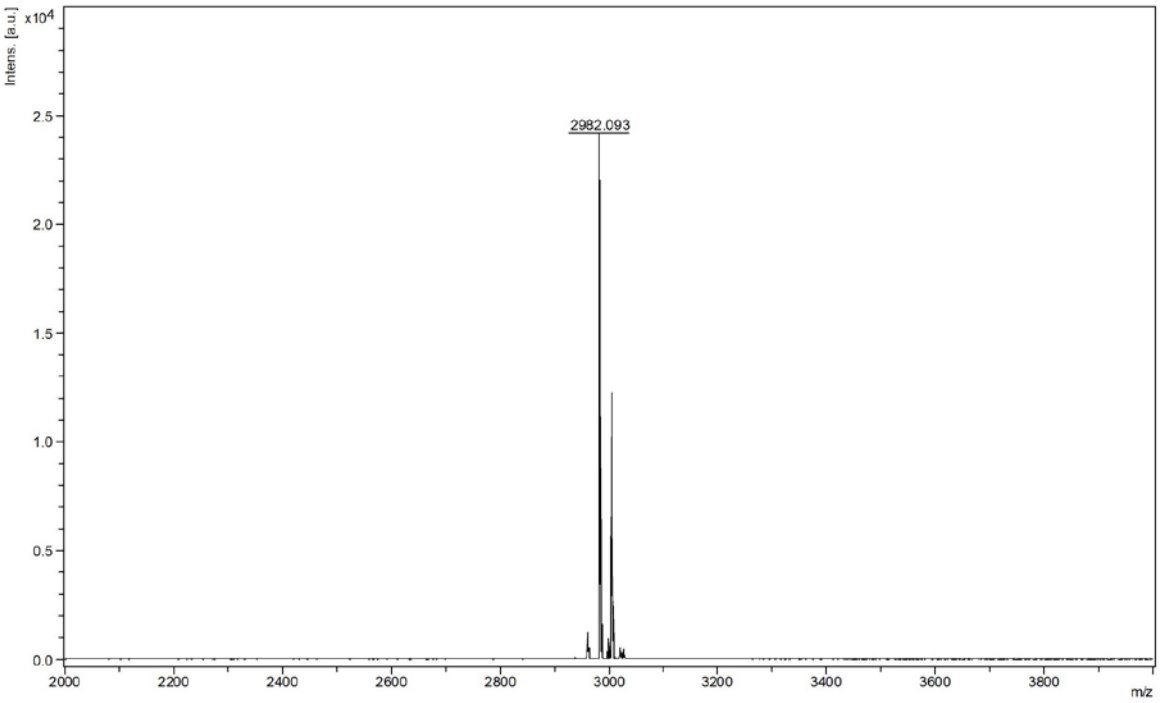

Figure 40. Peptide 4 Full Spectrum

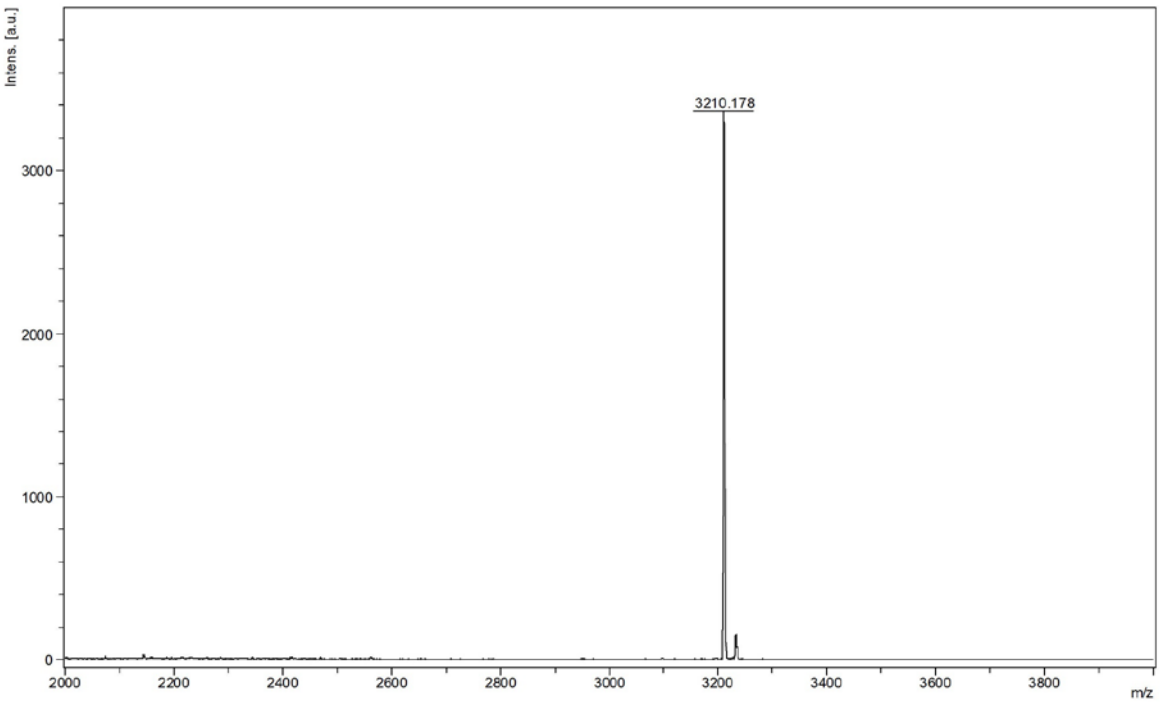

Figure 41. Peptide 5 Full Spectrum

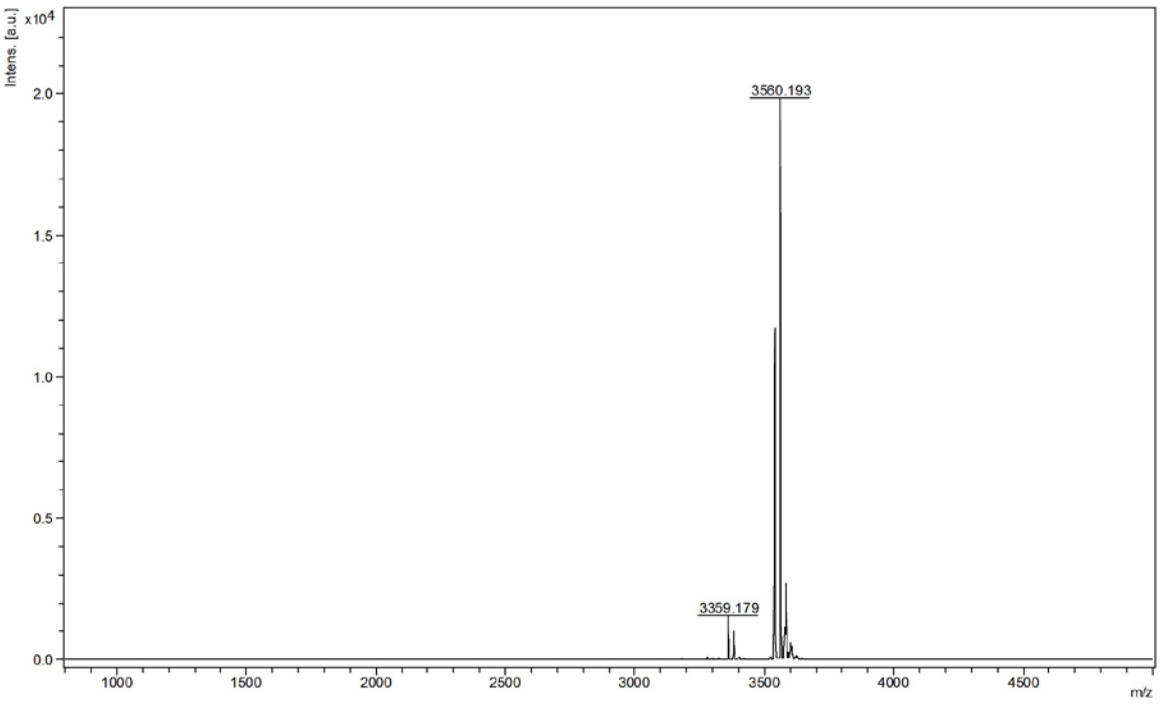

Figure 42. Peptide 7 Full Spectrum

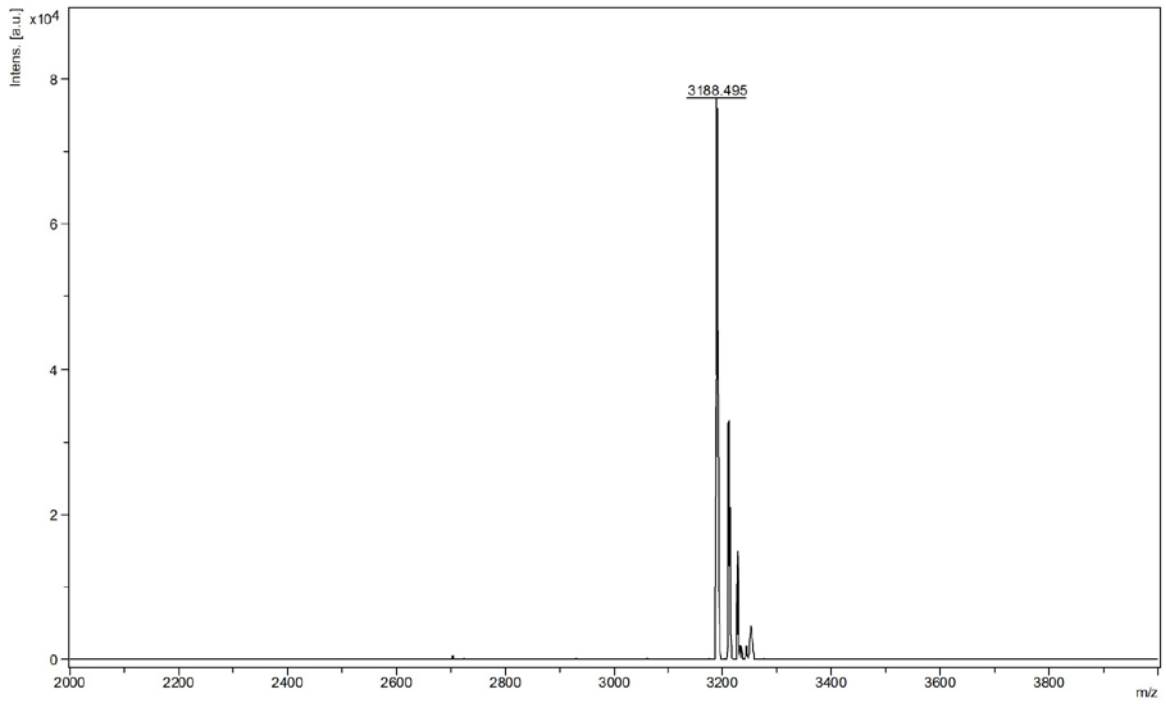

Figure 43. Peptide 8 Full Spectrum

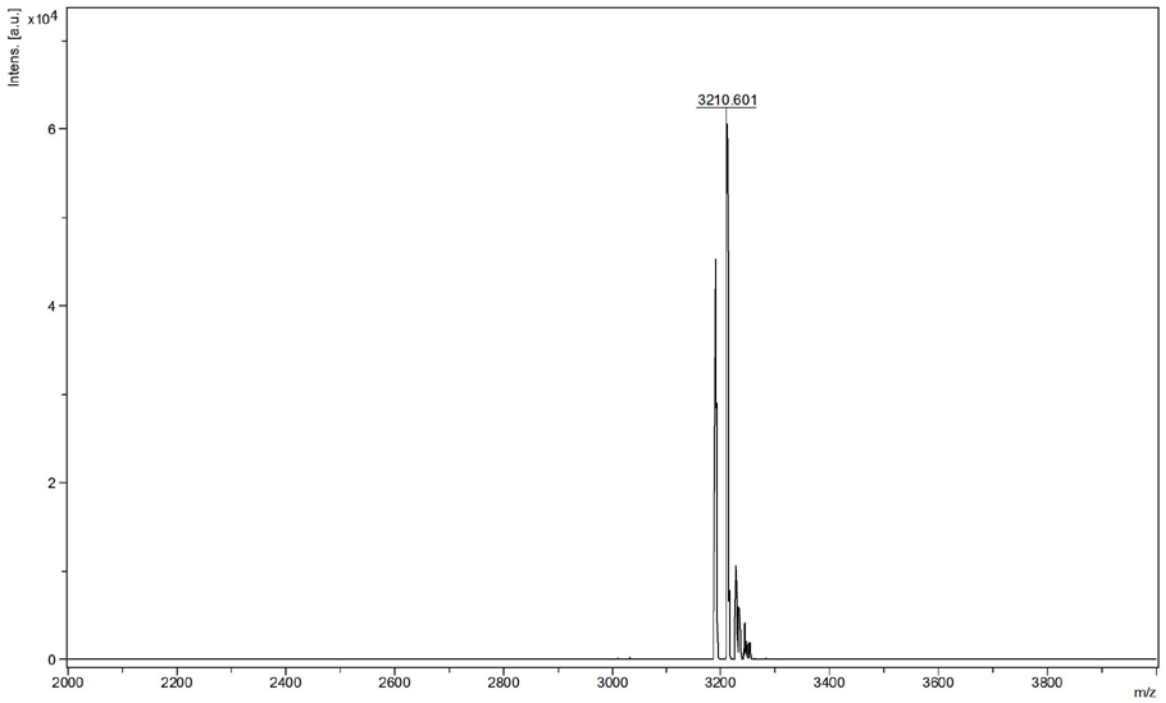

Figure 44. Peptide 9 Full Spectrum

Appendix D Crystallization Score Sheets

Crystallization score sheets for Index Screen are reproduced with permission from Hampton Research Corp. Initial observations are recorded in column 1 using the scores described by the manufacturer. Subsequent observations of the trays were recorded only when a change had been noted (columns 2 and 3). Only conditions 1-48 were set for peptide **5**. In all experiments which contained $CuCl_2$ as an additive, the drop was set with equal volumes of each component in the following order: 1. Well buffer; 2. $CuCl_2$; 3. Peptide. This order was favored to allow for copper ions and buffer components an equal chance to interact with peptide to facilitate even crystal growth and prevent aggregation of peptide stock.

Sample: Peptide 3 (KAS-1-084) Sample Concentration: 15mg/mL
Sample Buffer: 18MΩ H_2O Date: 05/11/2018
Reservoir Volume: 500µL Temperature:
Drop Volume: Total 1.0 µl Sample 0.5 µl Reservoir 0.5 µl Additive ____ µl

1 Clear Drop
2 Phase Separation
3 Regular Granular Precipitate
4 Birefringent Precipitate or Microcrystals
5 Posettes or Spherulites
6 Needles (1D Growth)
7 Plates (2D Growth)
8 Single Crystals (3D Growth < 0.2 mm)
9 Single Crystals (3D Growth > 0.2 mm)

HAMPTON RESEARCH
Solutions for Crystal Growth

Index™ - HR2-144 Scoring Sheet	Date: 05/11/2018	Date: 05/15/2018	Date: 05/29/2018
1. 0.1 M Citric acid pH 3.5, 2.0 M Ammonium sulfate	3		
2. 0.1 M Sodium acetate trihydrate pH 4.5, 2.0 M Ammonium sulfate	3		
3. 0.1 M BIS-TRIS pH 5.5, 2.0 M Ammonium sulfate	3		
4. 0.1 M BIS-TRIS pH 6.5, 2.0 M Ammonium sulfate	3		
5. 0.1 M HEPES pH 7.5, 2.0 M Ammonium sulfate	3		
6. 0.1 M Tris pH 8.5, 2.0 M Ammonium sulfate	3		
7. 0.1 M Citric acid pH 3.5, 3.0 M Sodium chloride	3		
8. 0.1 M Sodium acetate trihydrate pH 4.5, 3.0 M Sodium chloride	3		
9. 0.1 M BIS-TRIS pH 5.5, 3.0 M Sodium chloride	3		
10. 0.1 M BIS-TRIS pH 6.5, 3.0 M Sodium chloride	3		
11. 0.1 M HEPES pH 7.5, 3.0 M Sodium chloride	3		
12. 0.1 M Tris pH 8.5, 3.0 M Sodium chloride	3		
13. 0.1 M BIS-TRIS pH 5.5, 0.3 M Magnesium formate dihydrate	3		
14. 0.1 M BIS-TRIS pH 6.5, 0.5 M Magnesium formate dihydrate	3		
15. 0.1 M HEPES pH 7.5, 0.5 M Magnesium formate dihydrate	3		
16. 0.1 M TRIS pH 8.5, 0.3 M Magnesium formate dihydrate	3		
17. 1.26 M Sodium phosphate monobasic monohydrate, 0.14 M Potassium phosphate dibasic, pH 5.6	3		
18. 0.49 M Sodium phosphate monobasic monohydrate, 0.91 M Potassium phosphate dibasic, pH 6.9	3		
19. 0.056 M Sodium phosphate monobasic monohydrate, 1.344 M Potassium phosphate dibasic, pH 8.2	3		
20. 0.1 M HEPES pH 7.5, 1.4 M Sodium citrate tribasic dihydrate	3		
21. 1.8 M Ammonium citrate tribasic pH 7.0	3		
22. 0.8 M Succinic acid pH 7.0	3		
23. 2.1 M DL-Malic acid pH 7.0	3		
24. 2.8 M Sodium acetate trihydrate pH 7.0	3		
25. 3.5 M Sodium formate pH 7.0	3		
26. 1.1 M Ammonium tartrate dibasic pH 7.0	3		
27. 2.4 M Sodium malonate pH 7.0	3		
28. 35% v/v Tacsimate™ pH 7.0	3		
29. 60% v/v Tacsimate™ pH 7.0	3		
30. 0.1 M Sodium chloride, 0.1 M BIS-TRIS pH 6.5, 1.5 M Ammonium sulfate	3		
31. 0.8 M Potassium sodium tartrate tetrahydrate, 0.1 M Tris pH 8.5,	3		
0.5% w/v Polyethylene glycol monomethyl ether 5,000	—		
32. 1.0 M Ammonium sulfate, 0.1 M BIS-TRIS pH 5.5, 1% w/v Polyethylene glycol 3,350	3		
33. 1.1 M Sodium malonate pH 7.0, 0.1 M HEPES pH 7.0, 0.5% v/v Jeffamine® ED-2001 pH 7.0	3		
34. 1.0 M Succinic acid pH 7.0, 0.1 M HEPES pH 7.0, 1% w/v Polyethylene glycol monomethyl ether 2,000	3		
35. 1.0 M Ammonium sulfate, 0.1 M HEPES pH 7.0, 0.5% w/v Polyethylene glycol 8,000	3		
36. 15% v/v Tacsimate™ pH 7.0, 0.1 M HEPES pH 7.0, 2% w/v Polyethylene glycol 3,350	3	4	
37. 25% w/v Polyethylene glycol 1,500	1		
38. 0.1 M HEPES pH 7.0, 30% v/v Jeffamine® M-600® pH 7.0	1		
39. 0.1 M HEPES pH 7.0, 30% v/v Jeffamine® ED-2001 pH 7.0	1		
40. 0.1 M Citric acid pH 3.5, 25% w/v Polyethylene glycol 3,350	3		
41. 0.1 M Sodium acetate trihydrate pH 4.5, 25% w/v Polyethylene glycol 3,350	1		
42. 0.1 M BIS-TRIS pH 5.5, 25% w/v Polyethylene glycol 3,350	1		
43. 0.1 M BIS-TRIS pH 6.5, 25% w/v Polyethylene glycol 3,350	1		
44. 0.1 M HEPES pH 7.5, 25% w/v Polyethylene glycol 3,350	1		
45. 0.1 M Tris pH 8.5, 25% w/v Polyethylene glycol 3,350	1		
46. 0.1 M BIS-TRIS pH 6.5, 20% w/v Polyethylene glycol monomethyl ether 5,000	1		
47. 0.1 M BIS-TRIS pH 6.5, 28% w/v Polyethylene glycol monomethyl ether 2,000	1		
48. 0.2 M Calcium chloride dihydrate, 0.1 M BIS-TRIS pH 5.5, 45% v/v (+/-)-2-Methyl-2,4-pentanediol	1		

Sample: Peptide 3 (KAS-1-084) Sample Concentration: 15mg/mL
Sample Buffer: 18MΩ H_2O Date: 05/11/2018
Reservoir Volume: 500µL Temperature: ambient
Drop Volume: Total 1µl Sample 0.5 µl Reservoir 0.5 µl Additive ____ µl

1 Clear Drop
2 Phase Separation
3 Regular Granular Precipitate
4 Birefringent Precipitate or Microcrystals
5 Posettes or Spherulites
6 Needles (1D Growth)
7 Plates (2D Growth)
8 Single Crystals (3D Growth < 0.2 mm)
9 Single Crystals (3D Growth > 0.2 mm)

HAMPTON RESEARCH
Solutions for Crystal Growth

Index™ - HR2-144 Scoring Sheet	Date: 05/11/2018	Date: 05/15/2018	Date: 05/29/2018
49. 0.2 M Calcium chloride dihydrate, 0.1 M BIS-TRIS pH 6.5, 45% v/v (+/-)-2-Methyl-2,4-pentanediol	1		
50. 0.2 M Ammonium acetate, 0.1 M BIS-TRIS pH 5.5, 45% v/v (+/-)-2-Methyl-2,4-pentanediol	1		
51. 0.2 M Ammonium acetate, 0.1 M BIS-TRIS pH 6.5, 45% v/v (+/-)-2-Methyl-2,4-pentanediol	1		
52. 0.2 M Ammonium acetate, 0.1 M HEPES pH 7.5, 45% v/v (+/-)-2-Methyl-2,4-pentanediol	1		
53. 0.2 M Ammonium acetate, 0.1 M Tris pH 8.5, 45% v/v (+/-)-2-Methyl-2,4-pentanediol	1		
54. 0.05 M Calcium chloride dihydrate, 0.1 M BIS-TRIS pH 6.5, 30% v/v Polyethylene glycol monomethyl ether 550	1		
55. 0.05 M Magnesium chloride hexahydrate, 0.1 M HEPES pH 7.5, 30% v/v Polyethylene glycol monomethyl ether 550	1		
56. 0.2 M Potassium chloride, 0.05 M HEPES pH 7.5, 35% v/v Pentaerythritol propoxylate (5/4 PO/OH)	1		
57. 0.05 M Ammonium sulfate, 0.05 M BIS-TRIS pH 6.5, 30% v/v Pentaerythritol ethoxylate (15/4 EO/OH)	3		
58. 0.1 M BIS-TRIS pH 6.5, 45% v/v Polypropylene glycol P 400	1		
59. 0.02 M Magnesium chloride hexahydrate, 0.1 M HEPES pH 7.5, 22% w/v Poly(acrylic acid sodium salt) 5,100	3		
60. 0.01 M Cobalt(II) chloride hexahydrate, 0.1 M Tris pH 8.5, 20% w/v Polyvinylpyrrolidone K 15	1		
61. 0.2 M L-Proline, 0.1 M HEPES pH 7.5, 10% w/v Polyethylene glycol 3,350	1		
62. 0.2 M Trimethylamine N-oxide dihydrate, 0.1 M Tris pH 8.5, 20% w/v Polyethylene glycol monomethyl ether 2,000	3		
63. 5% v/v Tacsimate™ pH 7.0, 0.1 M HEPES pH 7.0, 10% w/v Polyethylene glycol monomethyl ether 5,000	3		
64. 0.005 M Cobalt(II) chloride hexahydrate, 0.005 M Nickel(II) chloride hexahydrate, 0.005 M Cadmium chloride hydrate, 0.005 M Magnesium chloride hexahydrate, 0.1 M HEPES pH 7.5, 12% w/v Polyethylene glycol 3,350	1		
65. 0.1 M Ammonium acetate, 0.1 M BIS-TRIS pH 5.5, 17% w/v Polyethylene glycol 10,000	1		
66. 0.2 M Ammonium sulfate, 0.1 M BIS-TRIS pH 5.5, 25% w/v Polyethylene glycol 3,350	3		
67. 0.2 M Ammonium sulfate, 0.1 M BIS-TRIS pH 6.5, 25% w/v Polyethylene glycol 3,350	3		
68. 0.2 M Ammonium sulfate, 0.1 M HEPES pH 7.5, 25% w/v Polyethylene glycol 3,350	3		
69. 0.2 M Ammonium sulfate, 0.1 M Tris pH 8.5, 25% w/v Polyethylene glycol 3,350	3		
70. 0.2 M Sodium chloride, 0.1 M BIS-TRIS pH 5.5, 25% w/v Polyethylene glycol 3,350	1		
71. 0.2 M Sodium chloride, 0.1 M BIS-TRIS pH 6.5, 25% w/v Polyethylene glycol 3,350	3		
72. 0.2 M Sodium chloride, 0.1 M HEPES pH 7.5, 25% w/v Polyethylene glycol 3,350	3		
73. 0.2 M Sodium chloride, 0.1 M Tris pH 8.5, 25% w/v Polyethylene glycol 3,350	3	8	
74. 0.2 M Lithium sulfate monohydrate, 0.1 M BIS-TRIS pH 5.5, 25% w/v Polyethylene glycol 3,350	3		
75. 0.2 M Lithium sulfate monohydrate, 0.1 M BIS-TRIS pH 6.5, 25% w/v Polyethylene glycol 3,350	3		
76. 0.2 M Lithium sulfate monohydrate, 0.1 M HEPES pH 7.5, 25% w/v Polyethylene glycol 3,350	3		
77. 0.2 M Lithium sulfate monohydrate, 0.1 M Tris pH 8.5, 25% w/v Polyethylene glycol 3,350	3		
78. 0.2 M Ammonium acetate, 0.1 M BIS-TRIS pH 5.5, 25% w/v Polyethylene glycol 3,350	1		
79. 0.2 M Ammonium acetate, 0.1 M BIS-TRIS pH 6.5, 25% w/v Polyethylene glycol 3,350	3		
80. 0.2 M Ammonium acetate, 0.1 M HEPES pH 7.5, 25% w/v Polyethylene glycol 3,350	3		
81. 0.2 M Ammonium acetate, 0.1 M Tris pH 8.5, 25% w/v Polyethylene glycol 3,350	3	6	6+8
82. 0.2 M Magnesium chloride hexahydrate, 0.1 M BIS-TRIS pH 5.5, 25% w/v Polyethylene glycol 3,350	3		
83. 0.2 M Magnesium chloride hexahydrate, 0.1 M BIS-TRIS pH 6.5, 25% w/v Polyethylene glycol 3,350	3		
84. 0.2 M Magnesium chloride hexahydrate, 0.1 M HEPES pH 7.5, 25% w/v Polyethylene glycol 3,350	3		
85. 0.2 M Magnesium chloride hexahydrate, 0.1 M Tris pH 8.5, 25% w/v Polyethylene glycol 3,350	3	5	
86. 0.2 M Potassium sodium tartrate tetrahydrate, 20% w/v Polyethylene glycol 3,350	3		
87. 0.2 M Sodium malonate pH 7.0, 20% w/v Polyethylene glycol 3,350	3		
88. 0.2 M Ammonium citrate tribasic pH 7.0, 20% w/v Polyethylene glycol 3,350	3		
89. 0.1 M Succinic acid pH 7.0, 15% w/v Polyethylene glycol 3,350	3		
90. 0.2 M Sodium formate, 20% w/v Polyethylene glycol 3,350	1		
91. 0.15 M DL-Malic acid pH 7.0, 20% w/v Polyethylene glycol 3,350	3		
92. 0.1 M Magnesium formate dihydrate, 15% w/v Polyethylene glycol 3,350	1		
93. 0.05 M Zinc acetate dihydrate, 20% w/v Polyethylene glycol 3,350	1		
94. 0.2 M Sodium citrate tribasic dihydrate, 20% w/v Polyethylene glycol 3,350	3		
95. 0.1 M Potassium thiocyanate, 30% w/v Polyethylene glycol monomethyl ether 2,000	1		
96. 0.15 M Potassium bromide, 30% w/v Polyethylene glycol monomethyl ether 2,000	1		

34 Journey
Aliso Viejo, CA 92656-5317 U.S.A.
Tel: (949) 425-1321 • Fax: (949) 425-1611
e-mail: rech@hrmail.com
Website: www.hamptonresearch.com

Sample: Peptide 3 (KAS-1-084) Sample Concentration: 15 mg/mL
Sample Buffer: 18MΩ H_2O Date: 05/28/2018
Reservoir Volume: 500 mL Temperature: ambient
Drop Volume: Total 1.5 µl Sample 0.5 µl Reservoir 0.5 µl Additive 0.5 µl 30 mM $CaCl_2$

1 Clear Drop
2 Phase Separation
3 Regular Granular Precipitate
4 Birefringent Precipitate or Microcrystals
5 Posettes or Spherulites
6 Needles (1D Growth)
7 Plates (2D Growth)
8 Single Crystals (3D Growth < 0.2 mm)
9 Single Crystals (3D Growth > 0.2 mm)

HAMPTON RESEARCH
Solutions for Crystal Growth

Index™ - HR2-144 Scoring Sheet	Date: 05/28/18	Date: 05/29	Date:
1. 0.1 M Citric acid pH 3.5, 2.0 M Ammonium sulfate	1		
2. 0.1 M Sodium acetate trihydrate pH 4.5, 2.0 M Ammonium sulfate	1		
3. 0.1 M BIS-TRIS pH 5.5, 2.0 M Ammonium sulfate	1		
4. 0.1 M BIS-TRIS pH 6.5, 2.0 M Ammonium sulfate	3		
5. 0.1 M HEPES pH 7.5, 2.0 M Ammonium sulfate	3		
6. 0.1 M Tris pH 8.5, 2.0 M Ammonium sulfate	3		
7. 0.1 M Citric acid pH 3.5, 3.0 M Sodium chloride	3		
8. 0.1 M Sodium acetate trihydrate pH 4.5, 3.0 M Sodium chloride	3		
9. 0.1 M BIS-TRIS pH 5.5, 3.0 M Sodium chloride	3		
10. 0.1 M BIS-TRIS pH 6.5, 3.0 M Sodium chloride	3		
11. 0.1 M HEPES pH 7.5, 3.0 M Sodium chloride	3		
12. 0.1 M Tris pH 8.5, 3.0 M Sodium chloride	3		
13. 0.1 M BIS-TRIS pH 5.5, 0.3 M Magnesium formate dihydrate	3		
14. 0.1 M BIS-TRIS pH 6.5, 0.5 M Magnesium formate dihydrate	1		
15. 0.1 M HEPES pH 7.5, 0.5 M Magnesium formate dihydrate	3	8	
16. 0.1 M TRIS pH 8.5, 0.3 M Magnesium formate dihydrate	1		
17. 1.26 M Sodium phosphate monobasic monohydrate, 0.14 M Potassium phosphate dibasic, pH 5.6	3		
18. 0.49 M Sodium phosphate monobasic monohydrate, 0.91 M Potassium phosphate dibasic, pH 6.9	3		
19. 0.056 M Sodium phosphate monobasic monohydrate, 1.344 M Potassium phosphate dibasic, pH 8.2	3	5	
20. 0.1 M HEPES pH 7.5, 1.4 M Sodium citrate tribasic dihydrate	1		
21. 1.8 M Ammonium citrate tribasic pH 7.0	1		
22. 0.8 M Succinic acid pH 7.0	1	7	
23. 2.1 M DL-Malic acid pH 7.0	1		
24. 2.8 M Sodium acetate trihydrate pH 7.0	1		
25. 3.5 M Sodium formate pH 7.0	1	4?	
26. 1.1 M Ammonium tartrate dibasic pH 7.0	1		
27. 2.4 M Sodium malonate pH 7.0	1	8	
28. 35% v/v Tacsimate™ pH 7.0	1		
29. 60% v/v Tacsimate™ pH 7.0	1		
30. 0.1 M Sodium chloride, 0.1 M BIS-TRIS pH 6.5, 1.5 M Ammonium sulfate	1		
31. 0.8 M Potassium sodium tartrate tetrahydrate, 0.1 M Tris pH 8.5, 0.5% w/v Polyethylene glycol monomethyl ether 5,000	3 —		
32. 1.0 M Ammonium sulfate, 0.1 M BIS-TRIS pH 5.5, 1% w/v Polyethylene glycol 3,350	1		
33. 1.1 M Sodium malonate pH 7.0, 0.1 M HEPES pH 7.0, 0.5% v/v Jeffamine® ED-2001 pH 7.0	1		
34. 1.0 M Succinic acid pH 7.0, 0.1 M HEPES pH 7.0, 1% w/v Polyethylene glycol monomethyl ether 2,000	1		
35. 1.0 M Ammonium sulfate, 0.1 M HEPES pH 7.0, 0.5% w/v Polyethylene glycol 8,000	1		
36. 15% v/v Tacsimate™ pH 7.0, 0.1 M HEPES pH 7.0, 2% w/v Polyethylene glycol 3,350	1		
37. 25% w/v Polyethylene glycol 1,500	1		
38. 0.1 M HEPES pH 7.0, 30% v/v Jeffamine® M-600® pH 7.0	1		
39. 0.1 M HEPES pH 7.0, 30% v/v Jeffamine® ED-2001 pH 7.0	1		
40. 0.1 M Citric acid pH 3.5, 25% w/v Polyethylene glycol 3,350	1		
41. 0.1 M Sodium acetate trihydrate pH 4.5, 25% w/v Polyethylene glycol 3,350	1		
42. 0.1 M BIS-TRIS pH 5.5, 25% w/v Polyethylene glycol 3,350	1		
43. 0.1 M BIS-TRIS pH 6.5, 25% w/v Polyethylene glycol 3,350	1		
44. 0.1 M HEPES pH 7.5, 25% w/v Polyethylene glycol 3,350	3		
45. 0.1 M Tris pH 8.5, 25% w/v Polyethylene glycol 3,350	1		
46. 0.1 M BIS-TRIS pH 6.5, 20% w/v Polyethylene glycol monomethyl ether 5,000	1		
47. 0.1 M BIS-TRIS pH 6.5, 28% w/v Polyethylene glycol monomethyl ether 2,000	1		
48. 0.2 M Calcium chloride dihydrate, 0.1 M BIS-TRIS pH 5.5, 45% v/v (+/-)-2-Methyl-2,4-pentanediol	1		

Sample: Peptide 3 (KAS-1-084) Sample Concentration: 15 mg/mL
Sample Buffer: 18MΩ H_2O Date: 05/28/2018
Reservoir Volume: 500 µL Temperature: ambient
Drop Volume: Total 1.5 µl Sample 0.5 µl Reservoir 0.5 µl Additive 0.5 µl 30 mM $CaCl_2$

1 Clear Drop
2 Phase Separation
3 Regular Granular Precipitate
4 Birefringent Precipitate or Microcrystals
5 Posettes or Spherulites
6 Needles (1D Growth)
7 Plates (2D Growth)
8 Single Crystals (3D Growth < 0.2 mm)
9 Single Crystals (3D Growth > 0.2 mm)

HAMPTON RESEARCH
Solutions for Crystal Growth

Index™ - HR2-144 Scoring Sheet	Date: 05/28	Date: 05/29	Date:
49. 0.2 M Calcium chloride dihydrate, 0.1 M BIS-TRIS pH 6.5, 45% v/v (+/-)-2-Methyl-2,4-pentanediol	1		
50. 0.2 M Ammonium acetate, 0.1 M BIS-TRIS pH 5.5, 45% v/v (+/-)-2-Methyl-2,4-pentanediol	1		
51. 0.2 M Ammonium acetate, 0.1 M BIS-TRIS pH 6.5, 45% v/v (+/-)-2-Methyl-2,4-pentanediol	1		
52. 0.2 M Ammonium acetate, 0.1 M HEPES pH 7.5, 45% v/v (+/-)-2-Methyl-2,4-pentanediol	3		
53. 0.2 M Ammonium acetate, 0.1 M Tris pH 8.5, 45% v/v (+/-)-2-Methyl-2,4-pentanediol	1		
54. 0.05 M Calcium chloride dihydrate, 0.1 M BIS-TRIS pH 6.5, 30% v/v Polyethylene glycol monomethyl ether 550	1		
55. 0.05 M Magnesium chloride hexahydrate, 0.1 M HEPES pH 7.5, 30% v/v Polyethylene glycol monomethyl ether 550	1		
56. 0.2 M Potassium chloride, 0.05 M HEPES pH 7.5, 35% v/v Pentaerythritol propoxylate (5/4 PO/OH)	1		
57. 0.05 M Ammonium sulfate, 0.05 M BIS-TRIS pH 6.5, 30% v/v Pentaerythritol ethoxylate (15/4 EO/OH)	1		
58. 0.1 M BIS-TRIS pH 6.5, 45% v/v Polypropylene glycol P 400	1		
59. 0.02 M Magnesium chloride hexahydrate, 0.1 M HEPES pH 7.5, 22% w/v Poly(acrylic acid sodium salt) 5,100	3		
60. 0.01 M Cobalt(II) chloride hexahydrate, 0.1 M Tris pH 8.5, 20% w/v Polyvinylpyrrolidone K 15	1		
61. 0.2 M L-Proline, 0.1 M HEPES pH 7.5, 10% w/v Polyethylene glycol 3,350	1		
62. 0.2 M Trimethylamine N-oxide dihydrate, 0.1 M Tris pH 8.5, 20% w/v Polyethylene glycol monomethyl ether 2,000	1		
63. 5% v/v Tacsimate™ pH 7.0, 0.1 M HEPES pH 7.0, 10% w/v Polyethylene glycol monomethyl ether 5,000	3		
64. 0.005 M Cobalt(II) chloride hexahydrate, 0.005 M Nickel(II) chloride hexahydrate, 0.005 M Cadmium chloride hydrate, 0.005 M Magnesium chloride hexahydrate, 0.1 M HEPES pH 7.5, 12% w/v Polyethylene glycol 3,350	1		
65. 0.1 M Ammonium acetate, 0.1 M BIS-TRIS pH 5.5, 17% w/v Polyethylene glycol 10,000	1		
66. 0.2 M Ammonium sulfate, 0.1 M BIS-TRIS pH 5.5, 25% w/v Polyethylene glycol 3,350	1		
67. 0.2 M Ammonium sulfate, 0.1 M BIS-TRIS pH 6.5, 25% w/v Polyethylene glycol 3,350	3		
68. 0.2 M Ammonium sulfate, 0.1 M HEPES pH 7.5, 25% w/v Polyethylene glycol 3,350	3		
69. 0.2 M Ammonium sulfate, 0.1 M Tris pH 8.5, 25% w/v Polyethylene glycol 3,350	3		
70. 0.2 M Sodium chloride, 0.1 M BIS-TRIS pH 5.5, 25% w/v Polyethylene glycol 3,350	1		
71. 0.2 M Sodium chloride, 0.1 M BIS-TRIS pH 6.5, 25% w/v Polyethylene glycol 3,350	1		
72. 0.2 M Sodium chloride, 0.1 M HEPES pH 7.5, 25% w/v Polyethylene glycol 3,350	3		
73. 0.2 M Sodium chloride, 0.1 M Tris pH 8.5, 25% w/v Polyethylene glycol 3,350	1		
74. 0.2 M Lithium sulfate monohydrate, 0.1 M BIS-TRIS pH 5.5, 25% w/v Polyethylene glycol 3,350	1		
75. 0.2 M Lithium sulfate monohydrate, 0.1 M BIS-TRIS pH 6.5, 25% w/v Polyethylene glycol 3,350	3		
76. 0.2 M Lithium sulfate monohydrate, 0.1 M HEPES pH 7.5, 25% w/v Polyethylene glycol 3,350	3		
77. 0.2 M Lithium sulfate monohydrate, 0.1 M Tris pH 8.5, 25% w/v Polyethylene glycol 3,350	3		
78. 0.2 M Ammonium acetate, 0.1 M BIS-TRIS pH 5.5, 25% w/v Polyethylene glycol 3,350	1		
79. 0.2 M Ammonium acetate, 0.1 M BIS-TRIS pH 6.5, 25% w/v Polyethylene glycol 3,350	4 3		
80. 0.2 M Ammonium acetate, 0.1 M HEPES pH 7.5, 25% w/v Polyethylene glycol 3,350	1		
81. 0.2 M Ammonium acetate, 0.1 M Tris pH 8.5, 25% w/v Polyethylene glycol 3,350	3		
82. 0.2 M Magnesium chloride hexahydrate, 0.1 M BIS-TRIS pH 5.5, 25% w/v Polyethylene glycol 3,350	1		
83. 0.2 M Magnesium chloride hexahydrate, 0.1 M BIS-TRIS pH 6.5, 25% w/v Polyethylene glycol 3,350	1		
84. 0.2 M Magnesium chloride hexahydrate, 0.1 M HEPES pH 7.5, 25% w/v Polyethylene glycol 3,350	3		
85. 0.2 M Magnesium chloride hexahydrate, 0.1 M Tris pH 8.5, 25% w/v Polyethylene glycol 3,350	3		
86. 0.2 M Potassium sodium tartrate tetrahydrate, 20% w/v Polyethylene glycol 3,350	3		
87. 0.2 M Sodium malonate pH 7.0, 20% w/v Polyethylene glycol 3,350	3		
88. 0.2 M Ammonium citrate tribasic pH 7.0, 20% w/v Polyethylene glycol 3,350	3		
89. 0.1 M Succinic acid pH 7.0, 15% w/v Polyethylene glycol 3,350	—		
90. 0.2 M Sodium formate, 20% w/v Polyethylene glycol 3,350	1		
91. 0.15 M DL-Malic acid pH 7.0, 20% w/v Polyethylene glycol 3,350	3	2	
92. 0.1 M Magnesium formate dihydrate, 15% w/v Polyethylene glycol 3,350	1		
93. 0.05 M Zinc acetate dihydrate, 20% w/v Polyethylene glycol 3,350	1		
94. 0.2 M Sodium citrate tribasic dihydrate, 20% w/v Polyethylene glycol 3,350	3	2	
95. 0.1 M Potassium thiocyanate, 30% w/v Polyethylene glycol monomethyl ether 2,000	3		
96. 0.15 M Potassium bromide, 30% w/v Polyethylene glycol monomethyl ether 2,000	—		

34 Journey
Aliso Viejo, CA 92656-3317 U.S.A.
Tel: (949) 425-1321 • Fax: (949) 425-1611
e-mail: tech@hrmail.com
Website: www.hamptonresearch.com

Sample: Peptide 5 (KAS-1-161) Sample Concentration: 10mg/mL
Sample Buffer: 18MΩ H_2O Date: 10/02/2018
Reservoir Volume: — Temperature: —
Drop Volume: Total — µl Sample ____ µl Reservoir ____ µl Additive ____ µl

1 Clear Drop
2 Phase Separation
3 Regular Granular Precipitate
4 Birefringent Precipitate or Microcrystals
5 Posettes or Spherulites
6 Needles (1D Growth)
7 Plates (2D Growth)
8 Single Crystals (3D Growth < 0.2mm)
9 Single Crystals (3D Growth > 0.2mm)

Index™ - HR2-144 Scoring Sheet 49-96 never set for Peptide 5	Date:	Date:	Date:
49. 0.2 M Calcium chloride dihydrate, 0.1 M BIS-TRIS pH 6.5, 45% v/v (+/-)-2-Methyl-2,4-pentanediol			
50. 0.2 M Ammonium acetate, 0.1 M BIS-TRIS pH 5.5, 45% v/v (+/-)-2-Methyl-2,4-pentanediol			
51. 0.2 M Ammonium acetate, 0.1 M BIS-TRIS pH 6.5, 45% v/v (+/-)-2-Methyl-2,4-pentanediol			
52. 0.2 M Ammonium acetate, 0.1 M HEPES pH 7.5, 45% v/v (+/-)-2-Methyl-2,4-pentanediol			
53. 0.2 M Ammonium acetate, 0.1 M Tris pH 8.5, 45% v/v (+/-)-2-Methyl-2,4-pentanediol			
54. 0.05 M Calcium chloride dihydrate, 0.1 M BIS-TRIS pH 6.5, 30% v/v Polyethylene glycol monomethyl ether 550			
55. 0.05 M Magnesium chloride hexahydrate, 0.1 M HEPES pH 7.5, 30% v/v Polyethylene glycol monomethyl ether 550			
56. 0.2 M Potassium chloride, 0.05 M HEPES pH 7.5, 35% v/v Pentaerythritol propoxylate (5/4 PO/OH)			
57. 0.05 M Ammonium sulfate, 0.05 M BIS-TRIS pH 6.5, 30% v/v Pentaerythritol ethoxylate (15/4 EO/OH)			
58. 0.1 M BIS-TRIS pH 6.5, 45% v/v Polypropylene glycol P 400			
59. 0.02 M Magnesium chloride hexahydrate, 0.1 M HEPES pH 7.5, 22% w/v Poly(acrylic acid sodium salt) 5,100			
60. 0.01 M Cobalt(II) chloride hexahydrate, 0.1 M Tris pH 8.5, 20% w/v Polyvinylpyrrolidone K 15			
61. 0.2 M L-Proline, 0.1 M HEPES pH 7.5, 10% w/v Polyethylene glycol 3,350			
62. 0.2 M Trimethylamine N-oxide dihydrate, 0.1 M Tris pH 8.5, 20% w/v Polyethylene glycol monomethyl ether 2,000			
63. 5% v/v Tacsimate™ pH 7.0, 0.1 M HEPES pH 7.0, 10% w/v Polyethylene glycol monomethyl ether 5,000			
64. 0.005 M Cobalt(II) chloride hexahydrate, 0.005 M Nickel(II) chloride hexahydrate, 0.005 M Cadmium chloride hydrate, 0.005 M Magnesium chloride hexahydrate, 0.1 M HEPES pH 7.5, 12% w/v Polyethylene glycol 3,350			
65. 0.1 M Ammonium acetate, 0.1 M BIS-TRIS pH 5.5, 17% w/v Polyethylene glycol 10,000			
66. 0.2 M Ammonium sulfate, 0.1 M BIS-TRIS pH 5.5, 25% w/v Polyethylene glycol 3,350			
67. 0.2 M Ammonium sulfate, 0.1 M BIS-TRIS pH 6.5, 25% w/v Polyethylene glycol 3,350			
68. 0.2 M Ammonium sulfate, 0.1 M HEPES pH 7.5, 25% w/v Polyethylene glycol 3,350			
69. 0.2 M Ammonium sulfate, 0.1 M Tris pH 8.5, 25% w/v Polyethylene glycol 3,350			
70. 0.2 M Sodium chloride, 0.1 M BIS-TRIS pH 5.5, 25% w/v Polyethylene glycol 3,350			
71. 0.2 M Sodium chloride, 0.1 M BIS-TRIS pH 6.5, 25% w/v Polyethylene glycol 3,350			
72. 0.2 M Sodium chloride, 0.1 M HEPES pH 7.5, 25% w/v Polyethylene glycol 3,350			
73. 0.2 M Sodium chloride, 0.1 M Tris pH 8.5, 25% w/v Polyethylene glycol 3,350			
74. 0.2 M Lithium sulfate monohydrate, 0.1 M BIS-TRIS pH 5.5, 25% w/v Polyethylene glycol 3,350			
75. 0.2 M Lithium sulfate monohydrate, 0.1 M BIS-TRIS pH 6.5, 25% w/v Polyethylene glycol 3,350			
76. 0.2 M Lithium sulfate monohydrate, 0.1 M HEPES pH 7.5, 25% w/v Polyethylene glycol 3,350			
77. 0.2 M Lithium sulfate monohydrate, 0.1 M Tris pH 8.5, 25% w/v Polyethylene glycol 3,350			
78. 0.2 M Ammonium acetate, 0.1 M BIS-TRIS pH 5.5, 25% w/v Polyethylene glycol 3,350			
79. 0.2 M Ammonium acetate, 0.1 M BIS-TRIS pH 6.5, 25% w/v Polyethylene glycol 3,350			
80. 0.2 M Ammonium acetate, 0.1 M HEPES pH 7.5, 25% w/v Polyethylene glycol 3,350			
81. 0.2 M Ammonium acetate, 0.1 M Tris pH 8.5, 25% w/v Polyethylene glycol 3,350			
82. 0.2 M Magnesium chloride hexahydrate, 0.1 M BIS-TRIS pH 5.5, 25% w/v Polyethylene glycol 3,350			
83. 0.2 M Magnesium chloride hexahydrate, 0.1 M BIS-TRIS pH 6.5, 25% w/v Polyethylene glycol 3,350			
84. 0.2 M Magnesium chloride hexahydrate, 0.1 M HEPES pH 7.5, 25% w/v Polyethylene glycol 3,350			
85. 0.2 M Magnesium chloride hexahydrate, 0.1 M Tris pH 8.5, 25% w/v Polyethylene glycol 3,350			
86. 0.2 M Potassium sodium tartrate tetrahydrate, 20% w/v Polyethylene glycol 3,350			
87. 0.2 M Sodium malonate pH 7.0, 20% w/v Polyethylene glycol 3,350			
88. 0.2 M Ammonium citrate tribasic pH 7.0, 20% w/v Polyethylene glycol 3,350			
89. 0.1 M Succinic acid pH 7.0, 15% w/v Polyethylene glycol 3,350			
90. 0.2 M Sodium formate, 20% w/v Polyethylene glycol 3,350			
91. 0.15 M DL-Malic acid pH 7.0, 20% w/v Polyethylene glycol 3,350			
92. 0.1 M Magnesium formate dihydrate, 15% w/v Polyethylene glycol 3,350			
93. 0.05 M Zinc acetate dihydrate, 20% w/v Polyethylene glycol 3,350			
94. 0.2 M Sodium citrate tribasic dihydrate, 20% w/v Polyethylene glycol 3,350			
95. 0.1 M Potassium thiocyanate, 30% w/v Polyethylene glycol monomethyl ether 2,000			
96. 0.15 M Potassium bromide, 30% w/v Polyethylene glycol monomethyl ether 2,000			

HAMPTON RESEARCH
Solutions for Crystal Growth

34 Journey
Aliso Viejo, CA 92656-3317 U.S.A.
Tel: (949) 425-1321 • Fax: (949) 425-1611
e-mail: tech@hrmail.com
Website: www.hamptonresearch.com

Sample: Peptide 8 (KAS-1-192) Sample Concentration: 10mg/mL
Sample Buffer: 18MΩ H_2O Date: 10/02/2018
Reservoir Volume: 700µL Temperature: ambient
Drop Volume: Total 1.5 µl Sample 0.5 µl Reservoir 0.5 µl Additive 0.5 µl 15mM $CaCl_2$

1 Clear Drop
2 Phase Separation
3 Regular Granular Precipitate
4 Birefringent Precipitate or Microcrystals
5 Posettes or Spherulites
6 Needles (1D Growth)
7 Plates (2D Growth)
8 Single Crystals (3D Growth < 0.2 mm)
9 Single Crystals (3D Growth > 0.2 mm)

HAMPTON RESEARCH
Solutions for Crystal Growth

Index™ - HR2-144 Scoring Sheet	Date: 10/02	Date: 10/10	Date: 12/3
1. 0.1 M Citric acid pH 3.5, 2.0 M Ammonium sulfate	1		
2. 0.1 M Sodium acetate trihydrate pH 4.5, 2.0 M Ammonium sulfate	1		
3. 0.1 M BIS-TRIS pH 5.5, 2.0 M Ammonium sulfate	1		
4. 0.1 M BIS-TRIS pH 6.5, 2.0 M Ammonium sulfate	1		
5. 0.1 M HEPES pH 7.5, 2.0 M Ammonium sulfate	1		
6. 0.1 M Tris pH 8.5, 2.0 M Ammonium sulfate	1		
7. 0.1 M Citric acid pH 3.5, 3.0 M Sodium chloride	1		
8. 0.1 M Sodium acetate trihydrate pH 4.5, 3.0 M Sodium chloride	1		
9. 0.1 M BIS-TRIS pH 5.5, 3.0 M Sodium chloride	1		
10. 0.1 M BIS-TRIS pH 6.5, 3.0 M Sodium chloride	2+3		
11. 0.1 M HEPES pH 7.5, 3.0 M Sodium chloride	3		
12. 0.1 M Tris pH 8.5, 3.0 M Sodium chloride	2+3		
13. 0.1 M BIS-TRIS pH 5.5, 0.3 M Magnesium formate dihydrate	1		
14. 0.1 M BIS-TRIS pH 6.5, 0.5 M Magnesium formate dihydrate	1		
15. 0.1 M HEPES pH 7.5, 0.5 M Magnesium formate dihydrate	3		
16. 0.1 M TRIS pH 8.5, 0.3 M Magnesium formate dihydrate	1		
17. 1.26 M Sodium phosphate monobasic monohydrate, 0.14 M Potassium phosphate dibasic, pH 5.6	3		
18. 0.49 M Sodium phosphate monobasic monohydrate, 0.91 M Potassium phosphate dibasic, pH 6.9	3		
19. 0.056 M Sodium phosphate monobasic monohydrate, 1.344 M Potassium phosphate dibasic, pH 8.2	3		
20. 0.1 M HEPES pH 7.5, 1.4 M Sodium citrate tribasic dihydrate	1		
21. 1.8 M Ammonium citrate tribasic pH 7.0	1		
22. 0.8 M Succinic acid pH 7.0	1		
23. 2.1 M DL-Malic acid pH 7.0	1		
24. 2.8 M Sodium acetate trihydrate pH 7.0	1		
25. 3.5 M Sodium formate pH 7.0	1	5/8	
26. 1.1 M Ammonium tartrate dibasic pH 7.0	1		
27. 2.4 M Sodium malonate pH 7.0	1	7	
28. 35% v/v Tacsimate™ pH 7.0	1		
29. 60% v/v Tacsimate™ pH 7.0	1		
30. 0.1 M Sodium chloride, 0.1 M BIS-TRIS pH 6.5, 1.5 M Ammonium sulfate	1		
31. 0.8 M Potassium sodium tartrate tetrahydrate, 0.1 M Tris pH 8.5, 0.5% w/v Polyethylene glycol monomethyl ether 5,000	1		
32. 1.0 M Ammonium sulfate, 0.1 M BIS-TRIS pH 5.5, 1% w/v Polyethylene glycol 3,350	1		
33. 1.1 M Sodium malonate pH 7.0, 0.1 M HEPES pH 7.0, 0.5% v/v Jeffamine® ED-2001 pH 7.0	1		
34. 1.0 M Succinic acid pH 7.0, 0.1 M HEPES pH 7.0, 1% w/v Polyethylene glycol monomethyl ether 2,000	1		
35. 1.0 M Ammonium sulfate, 0.1 M HEPES pH 7.0, 0.5% w/v Polyethylene glycol 8,000	1		
36. 15% v/v Tacsimate™ pH 7.0, 0.1 M HEPES pH 7.0, 2% w/v Polyethylene glycol 3,350	1		
37. 25% w/v Polyethylene glycol 1,500	1		
38. 0.1 M HEPES pH 7.0, 30% v/v Jeffamine® M-600® pH 7.0	3		
39. 0.1 M HEPES pH 7.0, 30% v/v Jeffamine® ED-2001 pH 7.0	3	5	
40. 0.1 M Citric acid pH 3.5, 25% w/v Polyethylene glycol 3,350	1	5/6	
41. 0.1 M Sodium acetate trihydrate pH 4.5, 25% w/v Polyethylene glycol 3,350	1		
42. 0.1 M BIS-TRIS pH 5.5, 25% w/v Polyethylene glycol 3,350	1		
43. 0.1 M BIS-TRIS pH 6.5, 25% w/v Polyethylene glycol 3,350	1		
44. 0.1 M HEPES pH 7.5, 25% w/v Polyethylene glycol 3,350	1		
45. 0.1 M Tris pH 8.5, 25% w/v Polyethylene glycol 3,350	1		8/9
46. 0.1 M BIS-TRIS pH 6.5, 20% w/v Polyethylene glycol monomethyl ether 5,000	1	8/9	
47. 0.1 M BIS-TRIS pH 6.5, 28% w/v Polyethylene glycol monomethyl ether 2,000	1	8/9	
48. 0.2 M Calcium chloride dihydrate, 0.1 M BIS-TRIS pH 5.5, 45% v/v (+/-)-2-Methyl-2,4-pentanediol	1		

Sample: Peptide 8 (KAS-1-192) Sample Concentration: 10mg/mL
Sample Buffer: 18MΩ H_2O Date: 11/20/2018
Reservoir Volume: 700 µL Temperature: ambient
Drop Volume: Total 1.5 µl Sample 0.5 µl Reservoir 0.5 µl Additive 0.5 µl 15 mM $CaCl_2$

1 Clear Drop
2 Phase Separation
3 Regular Granular Precipitate
4 Birefringent Precipitate or Microcrystals
5 Rosettes or Spherulites
6 Needles (1D Growth)
7 Plates (2D Growth)
8 Single Crystals (3D Growth < 0.2 mm)
9 Single Crystals (3D Growth > 0.2 mm)

HAMPTON RESEARCH
Solutions for Crystal Growth

Index™ - HR2-144 Scoring Sheet	Date: 11/20	Date: 12/3	Date: 01/14/19
49. 0.2 M Calcium chloride dihydrate, 0.1 M BIS-TRIS pH 6.5, 45% v/v (+/-)-2-Methyl-2,4-pentanediol	1		
50. 0.2 M Ammonium acetate, 0.1 M BIS-TRIS pH 5.5, 45% v/v (+/-)-2-Methyl-2,4-pentanediol	1		
51. 0.2 M Ammonium acetate, 0.1 M BIS-TRIS pH 6.5, 45% v/v (+/-)-2-Methyl-2,4-pentanediol	1		
52. 0.2 M Ammonium acetate, 0.1 M HEPES pH 7.5, 45% v/v (+/-)-2-Methyl-2,4-pentanediol	1		
53. 0.2 M Ammonium acetate, 0.1 M Tris pH 8.5, 45% v/v (+/-)-2-Methyl-2,4-pentanediol	1		
54. 0.05 M Calcium chloride dihydrate, 0.1 M BIS-TRIS pH 6.5, 30% v/v Polyethylene glycol monomethyl ether 550	1		
55. 0.05 M Magnesium chloride hexahydrate, 0.1 M HEPES pH 7.5, 30% v/v Polyethylene glycol monomethyl ether 550	3	3	
56. 0.2 M Potassium chloride, 0.05 M HEPES pH 7.5, 35% v/v Pentaerythritol propoxylate (5/4 PO/OH)	1	6	
57. 0.05 M Ammonium sulfate, 0.05 M BIS-TRIS pH 6.5, 30% v/v Pentaerythritol ethoxylate (15/4 EO/OH)	3		
58. 0.1 M BIS-TRIS pH 6.5, 45% v/v Polypropylene glycol P 400	1	6	
59. 0.02 M Magnesium chloride hexahydrate, 0.1 M HEPES pH 7.5, 22% w/v Poly(acrylic acid sodium salt) 5,100	3		
60. 0.01 M Cobalt(II) chloride hexahydrate, 0.1 M Tris pH 8.5, 20% w/v Polyvinylpyrrolidone K 15	1		
61. 0.2 M L-Proline, 0.1 M HEPES pH 7.5, 10% w/v Polyethylene glycol 3,350	1		
62. 0.2 M Trimethylamine N-oxide dihydrate, 0.1 M Tris pH 8.5, 20% w/v Polyethylene glycol monomethyl ether 2,000	1		
63. 5% v/v Tacsimate™ pH 7.0, 0.1 M HEPES pH 7.0, 10% w/v Polyethylene glycol monomethyl ether 5,000	1	2	
64. 0.005 M Cobalt(II) chloride hexahydrate, 0.005 M Nickel(II) chloride hexahydrate, 0.005 M Cadmium chloride hydrate,	3	2/3	
0.005 M Magnesium chloride hexahydrate, 0.1 M HEPES pH 7.5, 12% w/v Polyethylene glycol 3,350	—	—	
65. 0.1 M Ammonium acetate, 0.1 M BIS-TRIS pH 5.5, 17% w/v Polyethylene glycol 10,000	1	2	
66. 0.2 M Ammonium sulfate, 0.1 M BIS-TRIS pH 5.5, 25% w/v Polyethylene glycol 3,350	3	3	
67. 0.2 M Ammonium sulfate, 0.1 M BIS-TRIS pH 6.5, 25% w/v Polyethylene glycol 3,350	3	3	
68. 0.2 M Ammonium sulfate, 0.1 M HEPES pH 7.5, 25% w/v Polyethylene glycol 3,350	3	3	
69. 0.2 M Ammonium sulfate, 0.1 M Tris pH 8.5, 25% w/v Polyethylene glycol 3,350	2	2/3	
70. 0.2 M Sodium chloride, 0.1 M BIS-TRIS pH 5.5, 25% w/v Polyethylene glycol 3,350	1		5/6
71. 0.2 M Sodium chloride, 0.1 M BIS-TRIS pH 6.5, 25% w/v Polyethylene glycol 3,350	1	8	8/9
72. 0.2 M Sodium chloride, 0.1 M HEPES pH 7.5, 25% w/v Polyethylene glycol 3,350	3	5	
73. 0.2 M Sodium chloride, 0.1 M Tris pH 8.5, 25% w/v Polyethylene glycol 3,350	1	5	
74. 0.2 M Lithium sulfate monohydrate, 0.1 M BIS-TRIS pH 5.5, 25% w/v Polyethylene glycol 3,350	1	2	
75. 0.2 M Lithium sulfate monohydrate, 0.1 M BIS-TRIS pH 6.5, 25% w/v Polyethylene glycol 3,350	3	3/4	
76. 0.2 M Lithium sulfate monohydrate, 0.1 M HEPES pH 7.5, 25% w/v Polyethylene glycol 3,350	3	3/4	
77. 0.2 M Lithium sulfate monohydrate, 0.1 M Tris pH 8.5, 25% w/v Polyethylene glycol 3,350	2/3		
78. 0.2 M Ammonium acetate, 0.1 M BIS-TRIS pH 5.5, 25% w/v Polyethylene glycol 3,350	1		
79. 0.2 M Ammonium acetate, 0.1 M BIS-TRIS pH 6.5, 25% w/v Polyethylene glycol 3,350	1		
80. 0.2 M Ammonium acetate, 0.1 M HEPES pH 7.5, 25% w/v Polyethylene glycol 3,350	1		
81. 0.2 M Ammonium acetate, 0.1 M Tris pH 8.5, 25% w/v Polyethylene glycol 3,350	1		
82. 0.2 M Magnesium chloride hexahydrate, 0.1 M BIS-TRIS pH 5.5, 25% w/v Polyethylene glycol 3,350	1		8
83. 0.2 M Magnesium chloride hexahydrate, 0.1 M BIS-TRIS pH 6.5, 25% w/v Polyethylene glycol 3,350	1	5	
84. 0.2 M Magnesium chloride hexahydrate, 0.1 M HEPES pH 7.5, 25% w/v Polyethylene glycol 3,350	2/3	5	
85. 0.2 M Magnesium chloride hexahydrate, 0.1 M Tris pH 8.5, 25% w/v Polyethylene glycol 3,350	1	5	
86. 0.2 M Potassium sodium tartrate tetrahydrate, 20% w/v Polyethylene glycol 3,350	1	2	
87. 0.2 M Sodium malonate pH 7.0, 20% w/v Polyethylene glycol 3,350	1		
88. 0.2 M Ammonium citrate tribasic pH 7.0, 20% w/v Polyethylene glycol 3,350	1		
89. 0.1 M Succinic acid pH 7.0, 15% w/v Polyethylene glycol 3,350	1	4	
90. 0.2 M Sodium formate, 20% w/v Polyethylene glycol 3,350	1	8/9	8/9
91. 0.15 M DL-Malic acid pH 7.0, 20% w/v Polyethylene glycol 3,350	1		
92. 0.1 M Magnesium formate dihydrate, 15% w/v Polyethylene glycol 3,350	1	2/8	
93. 0.05 M Zinc acetate dihydrate, 20% w/v Polyethylene glycol 3,350	1		
94. 0.2 M Sodium citrate tribasic dihydrate, 20% w/v Polyethylene glycol 3,350	1		
95. 0.1 M Potassium thiocyanate, 30% w/v Polyethylene glycol monomethyl ether 2,000	2/3	3	-3 + 9
96. 0.15 M Potassium bromide, 30% w/v Polyethylene glycol monomethyl ether 2,000	1	5	

34 Journey
Aliso Viejo, CA 92656-3317 U.S.A.
Tel: (949) 425-1321 • Fax: (949) 425-1611
e-mail: tech@hamptonresearch.com
Website: www.hamptonresearch.com

Sample: Peptide 9 (KAS-1-193) Sample Concentration: 10mg/mL
Sample Buffer: 18MΩ H_2O Date: 10/02/2018
Reservoir Volume: 700µL Temperature: ambient
Drop Volume: Total 1.5 µl Sample 0.5 µl Reservoir 0.5 µl Additive 0.5 µl

1 Clear Drop
2 Phase Separation
3 Regular Granular Precipitate
4 Birefringent Precipitate or Microcrystals
5 Rosettes or Spherulites
6 Needles (1D Growth)
7 Plates (2D Growth)
8 Single Crystals (3D Growth < 0.2 mm)
9 Single Crystals (3D Growth > 0.2 mm)

HAMPTON RESEARCH
Solutions for Crystal Growth

Index™ - HR2-144 Scoring Sheet	Date: 10/02	Date: 10/03	Date: 10/10
1. 0.1 M Citric acid pH 3.5, 2.0 M Ammonium sulfate	1	6/8	6/+8
2. 0.1 M Sodium acetate trihydrate pH 4.5, 2.0 M Ammonium sulfate	1	~~1~~	
3. 0.1 M BIS-TRIS pH 5.5, 2.0 M Ammonium sulfate	1		8
4. 0.1 M BIS-TRIS pH 6.5, 2.0 M Ammonium sulfate	1		
5. 0.1 M HEPES pH 7.5, 2.0 M Ammonium sulfate	1		
6. 0.1 M Tris pH 8.5, 2.0 M Ammonium sulfate	1	8	
7. 0.1 M Citric acid pH 3.5, 3.0 M Sodium chloride	3/6	2/3/6	
8. 0.1 M Sodium acetate trihydrate pH 4.5, 3.0 M Sodium chloride	3/6	2/3/6	
9. 0.1 M BIS-TRIS pH 5.5, 3.0 M Sodium chloride	3/6	2/3/6	+6
10. 0.1 M BIS-TRIS pH 6.5, 3.0 M Sodium chloride	3/6	2/3/+6	
11. 0.1 M HEPES pH 7.5, 3.0 M Sodium chloride	3/6	2/3/+6	+5
12. 0.1 M Tris pH 8.5, 3.0 M Sodium chloride	3/6	2/3/+6	+5
13. 0.1 M BIS-TRIS pH 5.5, 0.3 M Magnesium formate dihydrate	1		
14. 0.1 M BIS-TRIS pH 6.5, 0.5 M Magnesium formate dihydrate	1		
15. 0.1 M HEPES pH 7.5, 0.5 M Magnesium formate dihydrate	3		
16. 0.1 M TRIS pH 8.5, 0.3 M Magnesium formate dihydrate	1		
17. 1.26 M Sodium phosphate monobasic monohydrate, 0.14 M Potassium phosphate dibasic, pH 5.6	3		
18. 0.49 M Sodium phosphate monobasic monohydrate, 0.91 M Potassium phosphate dibasic, pH 6.9	3		
19. 0.056 M Sodium phosphate monobasic monohydrate, 1.344 M Potassium phosphate dibasic, pH 8.2	1	5	
20. 0.1 M HEPES pH 7.5, 1.4 M Sodium citrate tribasic dihydrate	1	3	
21. 1.8 M Ammonium citrate tribasic pH 7.0	1	3	
22. 0.8 M Succinic acid pH 7.0	1		
23. 2.1 M DL-Malic acid pH 7.0	1		
24. 2.8 M Sodium acetate trihydrate pH 7.0	1		
25. 3.5 M Sodium formate pH 7.0	1		
26. 1.1 M Ammonium tartrate dibasic pH 7.0	1		
27. 2.4 M Sodium malonate pH 7.0	1		3/8
28. 35% v/v Tacsimate™ pH 7.0	1		
29. 60% v/v Tacsimate™ pH 7.0	1		5/6
30. 0.1 M Sodium chloride, 0.1 M BIS-TRIS pH 6.5, 1.5 M Ammonium sulfate	1		
31. 0.8 M Potassium sodium tartrate tetrahydrate, 0.1 M Tris pH 8.5,	1		
0.5% w/v Polyethylene glycol monomethyl ether 5,000	—		
32. 1.0 M Ammonium sulfate, 0.1 M BIS-TRIS pH 5.5, 1% w/v Polyethylene glycol 3,350	1		9
33. 1.1 M Sodium malonate pH 7.0, 0.1 M HEPES pH 7.0, 0.5% v/v Jeffamine® ED-2001 pH 7.0	1		
34. 1.0 M Succinic acid pH 7.0, 0.1 M HEPES pH 7.0, 1% w/v Polyethylene glycol monomethyl ether 2,000	1		
35. 1.0 M Ammonium sulfate, 0.1 M HEPES pH 7.0, 0.5% w/v Polyethylene glycol 8,000	1		
36. 15% v/v Tacsimate™ pH 7.0, 0.1 M HEPES pH 7.0, 2% w/v Polyethylene glycol 3,350	1		
37. 25% w/v Polyethylene glycol 1,500	1		
38. 0.1 M HEPES pH 7.0, 30% v/v Jeffamine® M-600® pH 7.0	3		
39. 0.1 M HEPES pH 7.0, 30% v/v Jeffamine® ED-2001 pH 7.0	3	5	8
40. 0.1 M Citric acid pH 3.5, 25% w/v Polyethylene glycol 3,350	1	2	
41. 0.1 M Sodium acetate trihydrate pH 4.5, 25% w/v Polyethylene glycol 3,350	1		
42. 0.1 M BIS-TRIS pH 5.5, 25% w/v Polyethylene glycol 3,350	1		
43. 0.1 M BIS-TRIS pH 6.5, 25% w/v Polyethylene glycol 3,350	1		7
44. 0.1 M HEPES pH 7.5, 25% w/v Polyethylene glycol 3,350	1		
45. 0.1 M Tris pH 8.5, 25% w/v Polyethylene glycol 3,350	1		
46. 0.1 M BIS-TRIS pH 6.5, 20% w/v Polyethylene glycol monomethyl ether 5,000	1		
47. 0.1 M BIS-TRIS pH 6.5, 28% w/v Polyethylene glycol monomethyl ether 2,000	1		
48. 0.2 M Calcium chloride dihydrate, 0.1 M BIS-TRIS pH 5.5, 45% v/v (+/-)-2-Methyl-2,4-pentanediol	1		

Sample: Peptide 9 (KAS-1-193) Sample Concentration: 10mg/mL
Sample Buffer: 18MΩ H_2O Date: 11/20/2018
Reservoir Volume: 700uL Temperature: ambient
Drop Volume: Total 1.5 µl Sample 0.5 µl Reservoir 0.5 µl Additive 0.5 µl 15mM $CaCl_2$

1 Clear Drop
2 Phase Separation
3 Regular Granular Precipitate
4 Birefringent Precipitate or Microcrystals
5 Posettes or Spherulites
6 Needles (1D Growth)
7 Plates (2D Growth)
8 Single Crystals (3D Growth < 0.2mm)
9 Single Crystals (3D Growth > 0.2mm)

HAMPTON RESEARCH
Solutions for Crystal Growth

Index™ - HR2-144 Scoring Sheet	Date: 11/20	Date: 12/05	Date: 01/14/19
49. 0.2 M Calcium chloride dihydrate, 0.1 M BIS-TRIS pH 6.5, 45% v/v (+/-)-2-Methyl-2,4-pentanediol	1		
50. 0.2 M Ammonium acetate, 0.1 M BIS-TRIS pH 5.5, 45% v/v (+/-)-2-Methyl-2,4-pentanediol	1		
51. 0.2 M Ammonium acetate, 0.1 M BIS-TRIS pH 6.5, 45% v/v (+/-)-2-Methyl-2,4-pentanediol	1		
52. 0.2 M Ammonium acetate, 0.1 M HEPES pH 7.5, 45% v/v (+/-)-2-Methyl-2,4-pentanediol	1		
53. 0.2 M Ammonium acetate, 0.1 M Tris pH 8.5, 45% v/v (+/-)-2-Methyl-2,4-pentanediol	1		
54. 0.05 M Calcium chloride dihydrate, 0.1 M BIS-TRIS pH 6.5, 30% v/v Polyethylene glycol monomethyl ether 550	1		
55. 0.05 M Magnesium chloride hexahydrate, 0.1 M HEPES pH 7.5, 30% v/v Polyethylene glycol monomethyl ether 550	3	+3	
56. 0.2 M Potassium chloride, 0.05 M HEPES pH 7.5, 35% v/v Pentaerythritol propoxylate (5/4 PO/OH)	3	+3	
57. 0.05 M Ammonium sulfate, 0.05 M BIS-TRIS pH 6.5, 30% v/v Pentaerythritol ethoxylate (15/4 EO/OH)	1	7	8/9
58. 0.1 M BIS-TRIS pH 6.5, 45% v/v Polypropylene glycol P 400	1		
59. 0.02 M Magnesium chloride hexahydrate, 0.1 M HEPES pH 7.5, 22% w/v Poly(acrylic acid sodium salt) 5,100	1		
60. 0.01 M Cobalt(II) chloride hexahydrate, 0.1 M Tris pH 8.5, 20% w/v Polyvinylpyrrolidone K 15	1		
61. 0.2 M L-Proline, 0.1 M HEPES pH 7.5, 10% w/v Polyethylene glycol 3,350	1		
62. 0.2 M Trimethylamine N-oxide dihydrate, 0.1 M Tris pH 8.5, 20% w/v Polyethylene glycol monomethyl ether 2,000	1		
63. 5% v/v Tacsimate™ pH 7.0, 0.1 M HEPES pH 7.0, 10% w/v Polyethylene glycol monomethyl ether 5,000	1	2	
64. 0.005 M Cobalt(II) chloride hexahydrate, 0.005 M Nickel(II) chloride hexahydrate, 0.005 M Cadmium chloride hydrate,	3	+2	
0.005 M Magnesium chloride hexahydrate, 0.1 M HEPES pH 7.5, 12% w/v Polyethylene glycol 3,350	—	—	
65. 0.1 M Ammonium acetate, 0.1 M BIS-TRIS pH 5.5, 17% w/v Polyethylene glycol 10,000	1	2	
66. 0.2 M Ammonium sulfate, 0.1 M BIS-TRIS pH 5.5, 25% w/v Polyethylene glycol 3,350	3		
67. 0.2 M Ammonium sulfate, 0.1 M BIS-TRIS pH 6.5, 25% w/v Polyethylene glycol 3,350	3	+3	
68. 0.2 M Ammonium sulfate, 0.1 M HEPES pH 7.5, 25% w/v Polyethylene glycol 3,350	3	+3	
69. 0.2 M Ammonium sulfate, 0.1 M Tris pH 8.5, 25% w/v Polyethylene glycol 3,350	1	2/3	
70. 0.2 M Sodium chloride, 0.1 M BIS-TRIS pH 5.5, 25% w/v Polyethylene glycol 3,350	1	2/3	
71. 0.2 M Sodium chloride, 0.1 M BIS-TRIS pH 6.5, 25% w/v Polyethylene glycol 3,350	1	6/8	+8
72. 0.2 M Sodium chloride, 0.1 M HEPES pH 7.5, 25% w/v Polyethylene glycol 3,350	3	5/6	
73. 0.2 M Sodium chloride, 0.1 M Tris pH 8.5, 25% w/v Polyethylene glycol 3,350	1	4	
74. 0.2 M Lithium sulfate monohydrate, 0.1 M BIS-TRIS pH 5.5, 25% w/v Polyethylene glycol 3,350	1	7/8	+6 +8
75. 0.2 M Lithium sulfate monohydrate, 0.1 M BIS-TRIS pH 6.5, 25% w/v Polyethylene glycol 3,350	3	+3	
76. 0.2 M Lithium sulfate monohydrate, 0.1 M HEPES pH 7.5, 25% w/v Polyethylene glycol 3,350	2/3	+3/4	
77. 0.2 M Lithium sulfate monohydrate, 0.1 M Tris pH 8.5, 25% w/v Polyethylene glycol 3,350	2/3		
78. 0.2 M Ammonium acetate, 0.1 M BIS-TRIS pH 5.5, 25% w/v Polyethylene glycol 3,350	1		
79. 0.2 M Ammonium acetate, 0.1 M BIS-TRIS pH 6.5, 25% w/v Polyethylene glycol 3,350	1		
80. 0.2 M Ammonium acetate, 0.1 M HEPES pH 7.5, 25% w/v Polyethylene glycol 3,350	1		
81. 0.2 M Ammonium acetate, 0.1 M Tris pH 8.5, 25% w/v Polyethylene glycol 3,350	1		
82. 0.2 M Magnesium chloride hexahydrate, 0.1 M BIS-TRIS pH 5.5, 25% w/v Polyethylene glycol 3,350	1	5/6	
83. 0.2 M Magnesium chloride hexahydrate, 0.1 M BIS-TRIS pH 6.5, 25% w/v Polyethylene glycol 3,350	1	8	
84. 0.2 M Magnesium chloride hexahydrate, 0.1 M HEPES pH 7.5, 25% w/v Polyethylene glycol 3,350	2/3	6	
85. 0.2 M Magnesium chloride hexahydrate, 0.1 M Tris pH 8.5, 25% w/v Polyethylene glycol 3,350	1	5/6	
86. 0.2 M Potassium sodium tartrate tetrahydrate, 20% w/v Polyethylene glycol 3,350	1	2	
87. 0.2 M Sodium malonate pH 7.0, 20% w/v Polyethylene glycol 3,350	1		
88. 0.2 M Ammonium citrate tribasic pH 7.0, 20% w/v Polyethylene glycol 3,350	1		
89. 0.1 M Succinic acid pH 7.0, 15% w/v Polyethylene glycol 3,350	1	4	
90. 0.2 M Sodium formate, 20% w/v Polyethylene glycol 3,350	1		
91. 0.15 M DL-Malic acid pH 7.0, 20% w/v Polyethylene glycol 3,350	1		
92. 0.1 M Magnesium formate dihydrate, 15% w/v Polyethylene glycol 3,350	1	2/6	
93. 0.05 M Zinc acetate dihydrate, 20% w/v Polyethylene glycol 3,350	1		
94. 0.2 M Sodium citrate tribasic dihydrate, 20% w/v Polyethylene glycol 3,350	1		
95. 0.1 M Potassium thiocyanate, 30% w/v Polyethylene glycol monomethyl ether 2,000	—	5	
96. 0.15 M Potassium bromide, 30% w/v Polyethylene glycol monomethyl ether 2,000	—	5	

34 Journey
Aliso Viejo, CA 92656-3317 U.S.A.
Tel: (949) 425-1321 • Fax: (949) 425-1611
e-mail: tech@hrmail.com
Website: www.hamptonresearch.com

Bibliography

1. Fernandez-Lopez, S.; Kim, H.-S.; Choi, E. C.; Delgado, M.; Granja, J. R.; Khasanov, A.; Kraehenbuehl, K.; Long, G.; Weinberger, D. A.; Wilcoxen, K. M.; Ghadiri, M. R., Antibacterial agents based on the cyclic D, L-α-peptide architecture. *Nature* **2001,** *412* (6845), 452.

2. Lustig, W. P.; Mukherjee, S.; Rudd, N. D.; Desai, A. V.; Li, J.; Ghosh, S. K., Metal-organic frameworks: functional luminescent and photonic materials for sensing applications. *Chemical Society Reviews* **2017,** *46* (11), 3242-3285.

3. Abascal, N. C.; Regan, L., The past, present and future of protein-based materials. *Open Biology* **2018,** *8* (10), 180113.

4. Yeates, T. O.; Padilla, J. E., Designing supramolecular protein assemblies. *Current Opinion in Structural Biology* **2002,** *12* (4), 464-470.

5. Hecht, M. H., De novo design of beta-sheet proteins. *Proceedings of the National Academy of Sciences* **1994,** *91* (19), 8729.

6. Richardson, J. S.; Richardson, D. C., Natural β-sheet proteins use negative design to avoid edge-to-edge aggregation. *Proceedings of the National Academy of Sciences* **2002,** *99* (5), 2754-2759.

7. West, M. W.; Wang, W.; Patterson, J.; Mancias, J. D.; Beasley, J. R.; Hecht, M. H., De novo amyloid proteins from designed combinatorial libraries. *Proceedings of the National Academy of Sciences* **1999,** *96* (20), 11211-11216.

8. Wang, W.; Hecht, M. H., Rationally designed mutations convert de novo amyloid-like fibrils into monomeric β-sheet proteins. *Proceedings of the National Academy of Sciences* **2002,** *99* (5), 2760-2765.

9. Li, D.; Jones, E. M.; Sawaya, M. R.; Furukawa, H.; Luo, F.; Ivanova, M.; Sievers, S. A.; Wang, W.; Yaghi, O. M.; Liu, C.; Eisenberg, D. S., Structure-Based Design of Functional Amyloid Materials. *Journal of the American Chemical Society* **2014,** *136* (52), 18044-18051.

10. Knowles, T. P. J.; Buehler, M. J., Nanomechanics of functional and pathological amyloid materials. *Nature Nanotechnology* **2011,** *6*, 469.

11. Knowles, T. P. J.; Mezzenga, R., Amyloid Fibrils as Building Blocks for Natural and Artificial Functional Materials. *Advanced Materials* **2016,** *28* (31), 6546-6561.

12. Pittenger, M. F.; Kazzaz, J. A.; Helfman, D. M., Functional properties of non-muscle tropomyosin isoforms. *Current Opinion in Cell Biology* **1994,** *6* (1), 96-104.

13. Perry, S. V., Vertebrate tropomyosin: distribution, properties and function. *Journal of Muscle Research & Cell Motility* **2001,** *22* (1), 5-49.

14. Hicks, M. R.; Holberton, D. V.; Kowalczyk, C.; Woolfson, D. N., Coiled-coil assembly by peptides with non-heptad sequence motifs. *Folding and Design* **1997,** *2* (3), 149-158.

15. Woolfson, D. N., The design of coiled-coil structures and assemblies. In *Advances in Protein Chemistry*, Elsevier: 2005; Vol. 70, pp 79-112.

16. Woolfson, D. N., Building fibrous biomaterials from α-helical and collagen-like coiled-coil peptides. *Peptide Science* **2010,** *94* (1), 118-127.

17. Fletcher, J. M.; Boyle, A. L.; Bruning, M.; Bartlett, G. J.; Vincent, T. L.; Zaccai, N. R.; Armstrong, C. T.; Bromley, E. H. C.; Booth, P. J.; Brady, R. L.; Thomson, A. R.; Woolfson, D. N., A Basis Set of de Novo Coiled-Coil Peptide Oligomers for Rational Protein Design and Synthetic Biology. *ACS Synthetic Biology* **2012,** *1* (6), 240-250.

18. Pieters, B. J. G. E.; van Eldijk, M. B.; Nolte, R. J. M.; Mecinović, J., Natural supramolecular protein assemblies. *Chemical Society Reviews* **2016,** *45* (1), 24-39.

19. Ogihara, N. L.; Ghirlanda, G.; Bryson, J. W.; Gingery, M.; DeGrado, W. F.; Eisenberg, D., Design of three-dimensional domain-swapped dimers and fibrous oligomers. *Proceedings of the National Academy of Sciences* **2001,** *98* (4), 1404-1409.

20. Padilla, J. E.; Colovos, C.; Yeates, T. O., Nanohedra: using symmetry to design self assembling protein cages, layers, crystals, and filaments. *Proceedings of the National Academy of Sciences* **2001,** *98* (5), 2217-2221.

21. Sun, H.; Luo, Q.; Hou, C.; Liu, J., Nanostructures based on protein self-assembly: From hierarchical construction to bioinspired materials. *Nano Today* **2017,** *14*, 16-41.

22. Sander, C., De novo design of proteins. *Current Opinion in Structural Biology* **1991,** *1* (4), 630-637.

23. Salgado, E. N.; Radford, R. J.; Tezcan, F. A., Metal-directed protein self-assembly. *Accounts of Chemical Research* **2010,** *43* (5), 661-672.

24. Pabo, C. O.; Peisach, E.; Grant, R. A., Design and selection of novel Cys2His2 zinc finger proteins. *Annual Review of Biochemistry* **2001,** *70* (1), 313-340.

25. Salgado, E. N.; Faraone-Mennella, J.; Tezcan, F. A., Controlling Protein− Protein Interactions through Metal Coordination: Assembly of a 16-Helix Bundle Protein. *Journal of the American Chemical Society* **2007,** *129* (44), 13374-13375.

26. Salgado, E. N.; Lewis, R. A.; Mossin, S.; Rheingold, A. L.; Tezcan, F. A., Control of Protein Oligomerization Symmetry by Metal Coordination: C2 and C3 Symmetrical Assemblies through CuII and NiII Coordination. *Inorganic Chemistry* **2009,** *48* (7), 2726-2728.

27. Faraone-Mennella, J.; Tezcan, F. A.; Gray, H. B.; Winkler, J. R., Stability and folding kinetics of structurally characterized cytochrome c-b562. *Biochemistry* **2006,** *45* (35), 10504-11.

28. Salgado, E. N.; Lewis, R. A.; Faraone-Mennella, J.; Tezcan, F. A., Metal-mediated self-assembly of protein superstructures: influence of secondary interactions on protein oligomerization and aggregation. *Journal of the American Chemical Society* **2008,** *130* (19), 6082-6084.

29. Radford, R. J.; Tezcan, F. A., A Superprotein Triangle Driven by Nickel(II) Coordination: Exploiting Non-Natural Metal Ligands in Protein Self-Assembly. *Journal of the American Chemical Society* **2009,** *131* (26), 9136-9137.

30. Salgado, E. N.; Ambroggio, X. I.; Brodin, J. D.; Lewis, R. A.; Kuhlman, B.; Tezcan, F. A., Metal templated design of protein interfaces. *Proceedings of the National Academy of Sciences* **2010,** *107* (5), 1827-1832.

31. Liu, Y.; Kuhlman, B., RosettaDesign server for protein design. *Nucleic Acids Research* **2006,** *34* (suppl_2), W235-W238.

32. Zhang, S.; Marini, D. M.; Hwang, W.; Santoso, S., Design of nanostructured biological materials through self-assembly of peptides and proteins. *Current Opinion in Chemical Biology* **2002,** *6* (6), 865-871.

33. Petka, W. A.; Harden, J. L.; McGrath, K. P.; Wirtz, D.; Tirrell, D. A., Reversible hydrogels from self-assembling artificial proteins. *Science* **1998,** *281* (5375), 389-392.

34. Aggeli, A.; Nyrkova, I. A.; Bell, M.; Harding, R.; Carrick, L.; McLeish, T. C.; Semenov, A. N.; Boden, N., Hierarchical self-assembly of chiral rod-like molecules as a model for peptide β-sheet tapes, ribbons, fibrils, and fibers. *Proceedings of the National Academy of Sciences* **2001,** *98* (21), 11857-11862.

35. An, B.; Lin, Y.-S.; Brodsky, B., Collagen interactions: Drug design and delivery. *Advanced Drug Delivery Reviews* **2016,** *97*, 69-84.

36. Bella, J., Collagen structure: new tricks from a very old dog. *Biochemical Journal* **2016,** *473* (8), 1001.

37. Sionkowska, A.; Skrzyński, S.; Śmiechowski, K.; Kołodziejczak, A., The review of versatile application of collagen. *Polymers for Advanced Technologies* **2017,** *28* (1), 4-9.

38. Manning, M. C.; Illangasekare, M.; Woody, R. W., Circular dichroism studies of distorted alpha-helices, twisted beta-sheets, and beta turns. *Biophysical chemistry* **1988,** *31* (1-2), 77-86.

39. Kumar, S.; Bansal, M., Structural and sequence characteristics of long alpha helices in globular proteins. *Biophysical Journal* **1996,** *71* (3), 1574-1586.

40. Oshaben, K. M.; Salari, R.; McCaslin, D. R.; Chong, L. T.; Horne, W. S., The Native GCN4 Leucine-Zipper Domain Does Not Uniquely Specify a Dimeric Oligomerization State. *Biochemistry* **2012,** *51* (47), 9581-9591.

41. Kohn, W. D.; Kay, C. M.; Hodges, R. S., Orientation, positional, additivity, and oligomerization-state effects of interhelical ion pairs in alpha-helical coiled-coils. *Journal of Molecular Biology* **1998,** *283* (5), 993-1012.

42. O'Shea, E. K.; Rutkowski, R.; Kim, P. S., Mechanism of specificity in the Fos-Jun oncoprotein heterodimer. *Cell* **1992,** *68* (4), 699-708.

43. Vinson, C. R.; Hai, T.; Boyd, S. M., Dimerization specificity of the leucine zipper-containing bZIP motif on DNA binding: prediction and rational design. *Genes & development* **1993,** *7* (6), 1047-58.

44. Walshaw, J.; Woolfson, D. N., SOCKET: a program for identifying and analysing coiled-coil motifs within protein structures11Edited by J. Thornton. *Journal of Molecular Biology* **2001,** *307* (5), 1427-1450.

45. Pandya, M. J.; Spooner, G. M.; Sunde, M.; Thorpe, J. R.; Rodger, A.; Woolfson, D. N., Sticky-End Assembly of a Designed Peptide Fiber Provides Insight into Protein Fibrillogenesis. *Biochemistry* **2000,** *39* (30), 8728-8734.

46. Ryadnov, M. G.; Woolfson, D. N., Introducing branches into a self-assembling peptide fiber. *Angewandte Chemie* **2003,** *115* (26), 3129-3131.

47. Ryadnov, M. G.; Woolfson, D. N., Engineering the morphology of a self-assembling protein fibre. *Nature Materials* **2003,** *2* (5), 329.

48. Ryadnov, M. G.; Woolfson, D. N., Fiber recruiting peptides: noncovalent decoration of an engineered protein scaffold. *Journal of the American Chemical Society* **2004,** *126* (24), 7454-7455.

49. Apostolovic, B.; Danial, M.; Klok, H.-A., Coiled coils: attractive protein folding motifs for the fabrication of self-assembled, responsive and bioactive materials. *Chemical Society Reviews* **2010,** *39* (9), 3541-3575.

50. Staples, J. K.; Oshaben, K. M.; Horne, W. S., A modular synthetic platform for the construction of protein-based supramolecular polymers via coiled-coil self-assembly. *Chemical Science* **2012,** *3* (12), 3387-3392.

51. Adil, K.; Belmabkhout, Y.; Pillai, R. S.; Cadiau, A.; Bhatt, P. M.; Assen, A. H.; Maurin, G.; Eddaoudi, M., Gas/vapour separation using ultra-microporous metal-organic frameworks: insights into the structure/separation relationship. *Chemical Society Reviews* **2017,** *46* (11), 3402-3430.

52. Bobbitt, N. S.; Mendonca, M. L.; Howarth, A. J.; Islamoglu, T.; Hupp, J. T.; Farha, O. K.; Snurr, R. Q., Metal-organic frameworks for the removal of toxic industrial chemicals and chemical warfare agents. *Chemical Society Reviews* **2017,** *46* (11), 3357-3385.

53. Lian, X.; Fang, Y.; Joseph, E.; Wang, Q.; Li, J.; Banerjee, S.; Lollar, C.; Wang, X.; Zhou, H.-C., Enzyme-MOF (metal-organic framework) composites. *Chemical Society Reviews* **2017,** *46* (11), 3386-3401.

54. Rogge, S. M. J.; Bavykina, A.; Hajek, J.; Garcia, H.; Olivos-Suarez, A. I.; Sepulveda-Escribano, A.; Vimont, A.; Clet, G.; Bazin, P.; Kapteijn, F.; Daturi, M.; Ramos-Fernandez, E. V.; Llabres i Xamena, F. X.; Van Speybroeck, V.; Gascon, J., Metal-organic and covalent organic frameworks as single-site catalysts. *Chemical Society Reviews* **2017,** *46* (11), 3134-3184.

55. Tan, L.; Tan, B., Hypercrosslinked porous polymer materials: design, synthesis, and applications. *Chemical Society Reviews* **2017,** *46* (11), 3322-3356.

56. Lan, A.; Li, K.; Wu, H.; Olson, D. H.; Emge, T. J.; Ki, W.; Hong, M.; Li, J., A luminescent microporous metal–organic framework for the fast and reversible detection of high explosives. *Angewandte Chemie* **2009,** *121* (13), 2370-2374.

57. Pramanik, S.; Zheng, C.; Zhang, X.; Emge, T. J.; Li, J., New microporous metal− organic framework demonstrating unique selectivity for detection of high explosives and aromatic compounds. *Journal of the American Chemical Society* **2011,** *133* (12), 4153-4155.

58. Wang, B.; Lv, X.-L.; Feng, D.; Xie, L.-H.; Zhang, J.; Li, M.; Xie, Y.; Li, J.-R.; Zhou, H.-C., Highly Stable Zr(IV)-Based Metal–Organic Frameworks for the Detection and Removal of Antibiotics and Organic Explosives in Water. *Journal of the American Chemical Society* **2016,** *138* (19), 6204-6216.

59. Wanderley, M. M.; Wang, C.; Wu, C.-D.; Lin, W., A chiral porous metal–organic framework for highly sensitive and enantioselective fluorescence sensing of amino alcohols. *Journal of the American Chemical Society* **2012,** *134* (22), 9050-9053.

60. He, J.; Zha, M.; Cui, J.; Zeller, M.; Hunter, A. D.; Yiu, S.-M.; Lee, S.-T.; Xu, Z., Convenient detection of Pd (II) by a metal–organic framework with sulfur and olefin functions. *Journal of the American Chemical Society* **2013,** *135* (21), 7807-7810.

61. Li, G.-B.; Fang, H.-C.; Cai, Y.-P.; Zhou, Z.-Y.; Thallapally, P. K.; Tian, J., Construction of a novel Zn− Ni trinuclear Schiff base and a Ni2+ chemosensor. *Inorganic Chemistry* **2010,** *49* (16), 7241-7243.

62. Liu, J.; Chen, L.; Cui, H.; Zhang, J.; Zhang, L.; Su, C.-Y., Applications of metal–organic frameworks in heterogeneous supramolecular catalysis. *Chemical Society Reviews* **2014,** *43* (16), 6011-6061.

63. Lee, Y.-R.; Chung, Y.-M.; Ahn, W.-S., A new site-isolated acid–base bifunctional metal–organic framework for one-pot tandem reaction. *RSC Advances* **2014,** *4* (44), 23064-23067.

64. To, T. A.; Vo, Y. H.; Nguyen, H. T. T.; Ha, P. T. M.; Doan, S. H.; Doan, T. L. H.; Li, S.; Le, H. V.; Tu, T. N.; Phan, N. T. S., Iron-catalyzed one-pot sequential transformations: Synthesis of quinazolinones via oxidative Csp3H bond activation using a new metal-organic framework as catalyst. *Journal of Catalysis* **2019,** *370*, 11-20.

65. Wei, X.; Wang, Y.; Chen, J.; Xu, P.; Xu, W.; Ni, R.; Meng, J.; Zhou, Y., Poly(deep eutectic solvent)-functionalized magnetic metal-organic framework composites coupled with solid-phase extraction for the selective separation of cationic dyes. *Analytica Chimica Acta* **2019**.

66. Kemper, B.; Zengerling, L.; Spitzer, D.; Otter, R.; Bauer, T.; Besenius, P., Kinetically Controlled Stepwise Self-Assembly of AuI-Metallopeptides in Water. *Journal of the American Chemical Society* **2018,** *140* (2), 534-537.

67. Marqusee, S.; Baldwin, R. L., Helix stabilization by Glu-...Lys+ salt bridges in short peptides of de novo design. *Proceedings of the National Academy of Sciences* **1987,** *84* (24), 8898-902.

68. Ghadiri, M. R.; Choi, C., Secondary structure nucleation in peptides. Transition metal ion stabilized. alpha.-helices. *Journal of the American Chemical Society* **1990,** *112* (4), 1630-1632.

69. Ghadiri, M. R.; Soares, C.; Choi, C., A convergent approach to protein design. Metal ion-assisted spontaneous self-assembly of a polypeptide into a triple-helix bundle protein. *Journal of the American Chemical Society* **1992,** *114* (3), 825-831.

70. Lieberman, M.; Sasaki, T., Iron(II) organizes a synthetic peptide into three-helix bundles. *Journal of the American Chemical Society* **1991,** *113* (4), 1470-1471.

71. Lieberman, M.; Tabet, M.; Sasaki, T., Dynamic Structure and Potential Energy Surface of a Three-Helix Bundle Protein. *Journal of the American Chemical Society* **1994,** *116* (12), 5035-5044.

72. Zou, R.; Wang, Q.; Wu, J.; Wu, J.; Schmuck, C.; Tian, H., Peptide self-assembly triggered by metal ions. *Chemical Society Reviews* **2015,** *44* (15), 5200-5219.

73. Ohr, K.; Gilmartin, B. P.; Williams, M. E., Pyridine-Substituted Oligopeptides as Scaffolds for the Assembly of Multimetallic Complexes: Variation of Chain Length. *Inorganic Chemistry* **2005,** *44* (22), 7876-7885.

74. Gilmartin, B. P.; Ohr, K.; McLaughlin, R. L.; Koerner, R.; Williams, M. E., Artificial Oligopeptide Scaffolds for Stoichiometric Metal Binding. *Journal of the American Chemical Society* **2005,** *127* (26), 9546-9555.

75. Hartgerink, J. D.; Zubarev, E. R.; Stupp, S. I., Supramolecular one-dimensional objects. *Current Opinion in Solid State and Materials Science* **2001,** *5* (4), 355-361.

76. Hartgerink, J. D.; Beniash, E.; Stupp, S. I., Peptide-amphiphile nanofibers: A versatile scaffold for the preparation of self-assembling materials. *Proceedings of the National Academy of Sciences* **2002,** *99* (8), 5133.

77. Beniash, E.; Hartgerink, J. D.; Storrie, H.; Stendahl, J. C.; Stupp, S. I., Self-assembling peptide amphiphile nanofiber matrices for cell entrapment. *Acta Biomaterialia* **2005,** *1* (4), 387-397.

78. Stendahl, J. C.; Rao, M. S.; Guler, M. O.; Stupp, S. I., Intermolecular Forces in the Self-Assembly of Peptide Amphiphile Nanofibers. *Advanced Functional Materials* **2006,** *16* (4), 499-508.

79. Wei, P.; Yan, X.; Huang, F., Supramolecular polymers constructed by orthogonal self-assembly based on host–guest and metal–ligand interactions. *Chemical Society Reviews* **2015,** *44* (3), 815-832.

80. Su, J. Y.; Hodges, R. S.; Kay, C. M., Effect of chain length on the formation and stability of synthetic. alpha.-helical coiled coils. *Biochemistry* **1994,** *33* (51), 15501-15510.

81. Vandermeulen, G. W. M.; Tziatzios, C.; Schubert, D.; Andres, P. R.; Alexeev, A.; Schubert, U. S.; Klok, H.-A., Metal Ion Assisted Folding and Supramolecular Organization of a De Novo Designed Metalloprotein. *Australian Journal of Chemistry* **2004,** *57* (1), 33-39.

82. Tavenor, N. A.; Murnin, M. J.; Horne, W. S., Supramolecular Metal-Coordination Polymers, Nets, and Frameworks from Synthetic Coiled-Coil Peptides. *Journal of the American Chemical Society* **2017,** *139* (6), 2212-2215.

83. Wang, P.; Moorefield, C. N.; Panzer, M.; Newkome, G. R., Terpyridine copperii–polycarboxylic acid architectures: formation of dimeric, helical, and cyclic nanostructures and their included-water molecule motifs. *Chemical Communications* **2005,** (35), 4405-4407.

84. Zhou, W.; Wang, X.; Hu, M.; Guo, Z., Improving nuclease activity of copper (II)–terpyridine complex through solubilizing and charge effects of glycine. *Journal of Inorganic Biochemistry* **2013,** *121*, 114-120.

85. Tavenor, N. A. Supramolecular Architectures and Mimics of Complex Natural Folds Derived from Rationally Designed α-Helical Protein Structures. University of Pittsburgh, 2017.

86. Vougioukalakis, G. C.; Stergiopoulos, T.; Kantonis, G.; Kontos, A. G.; Papadopoulos, K.; Stublla, A.; Potvin, P. G.; Falaras, P., Terpyridine-and 2, 6-dipyrazinylpyridine-coordinated ruthenium (II) complexes: Synthesis, characterization and application in TiO 2-based dye-sensitized solar cells. *Journal of Photochemistry and Photobiology A: Chemistry* **2010,** *214* (1), 22-32.

87. Grieco, P.; Gitu, P.; Hruby, V., Preparation of 'side-chain-to-side-chain'cyclic peptides by Allyl and Alloc strategy: potential for library synthesis. *The Journal of Peptide Research* **2001,** *57* (3), 250-256.

88. Savitzky, A.; Golay, M. J. E., Smoothing and Differentiation of Data by Simplified Least Squares Procedures. *Analytical chemistry* **1964,** *36* (8), 1627-1639.

89. Shortle, D.; Meeker, A. K.; Freire, E., Stability mutants of staphylococcal nuclease: large compensating enthalpy-entropy changes for the reversible denaturation reaction. *Biochemistry* **1988,** *27* (13), 4761-4768.

90. Bunkóczi, G.; Echols, N.; McCoy, A. J.; Oeffner, R. D.; Adams, P. D.; Read, R. J., Phaser. MRage: automated molecular replacement. *Acta Crystallographica Section D: Biological Crystallography* **2013,** *69* (11), 2276-2286.

91. Adams, P. D.; Afonine, P. V.; Bunkóczi, G.; Chen, V. B.; Davis, I. W.; Echols, N.; Headd, J. J.; Hung, L.-W.; Kapral, G. J.; Grosse-Kunstleve, R. W., PHENIX: a comprehensive Python-based system for macromolecular structure solution. *Acta Crystallographica Section D: Biological Crystallography* **2010,** *66* (2), 213-221.

92. Emsley, P.; Lohkamp, B.; Scott, W. G.; Cowtan, K., Features and development of Coot. *Acta Crystallographica Section D: Biological Crystallography* **2010,** *66* (4), 486-501.

93. Zhou, N. E.; Kay, C. M.; Hodges, R. S., Synthetic model proteins: the relative contribution of leucine residues at the nonequivalent positions of the 3-4 hydrophobic repeat to the stability of the two-stranded. alpha.-helical coiled-coil. *Biochemistry* **1992,** *31* (25), 5739-5746.

94. Padmanabhan, S.; York, E. J.; Stewart, J. M.; Baldwin, R. L., Helix propensities of basic amino acids increase with the length of the side-chain. *Journal of Molecular Biology* **1996,** *257* (3), 726-734.

95. Penel, S.; Hughes, E.; Doig, A. J., Side-chain structures in the first turn of the α-helix11Edited by J. M. Thornton. *Journal of Molecular Biology* **1999,** *287* (1), 127-143.

96. Yadav, M. K.; Leman, L. J.; Price, D. J.; Brooks, C. L.; Stout, C. D.; Ghadiri, M. R., Coiled-Coils at the Edge of Configurational Heterogeneity. Structural Analyses of Parallel and Antiparallel Homotetrameric Coiled-Coils Reveal Configurational Sensitivity to a Single Solvent-Exposed Amino Acid Substitution. *Biochemistry* **2006,** *45* (14), 4463-4473.

97. Alberti, S.; Oehler, S.; von Wilcken-Bergmann, B.; Müller-Hill, B., Genetic analysis of the leucine heptad repeats of Lac repressor: evidence for a 4-helical bundle. *The EMBO Journal* **1993,** *12* (8), 3227-3236.

98. Deng, Y.; Liu, J.; Zheng, Q.; Eliezer, D.; Kallenbach, N. R.; Lu, M., Antiparallel Four-Stranded Coiled Coil Specified by a 3-3-1 Hydrophobic Heptad Repeat. *Structure* **2006,** *14* (2), 247-255.